Advanced Ultrasonic Inspection Technologies Applied to the Welded Joints of Hydraulic Turbine Runners

by

Mohammadebrahim BAJGHOLI

MANUSCRIPT-BASED THESIS PRESENTED TO ÉCOLE DE TECHNOLOGIE SUPÉRIEURE IN PARTIAL FULFILLMENT FOR THE DEGREE OF DOCTOR OF PHILOSOPHY
PH.D.

MONTREAL, FEBRUARY 15TH, 2023

ÉCOLE DE TECHNOLOGIE SUPÉRIEURE
UNIVERSITÉ DU QUÉBEC

BOARD OF EXAMINERS

THIS THESIS HAS BEEN EVALUATED

BY THE FOLLOWING BOARD OF EXAMINERS

Mr. Martin Viens, Thesis Supervisor
Department of Mechanical Engineering, École de technologie supérieure

Mr. Gilles Rousseau, External Co-director
Research Institute of Hydro-Québec (IREQ)

Mr. Michel Rioux, President of the Board of Examiners
Department of Systems Engineering, École de technologie supérieure

Mr. Souheil-Antoine Tahan, Member of the jury
Department of Mechanical Engineering, École de technologie supérieure

Mr. Nicolas Giguère, External Evaluator
Department of mining, metallurgy and material Engineering, Laval university

THIS THESIS WAS PRESENTED AND DEFENDED

IN THE PRESENCE OF A BOARD OF EXAMINERS AND PUBLIC

ON FEBRUARY 09TH, 2023

AT ÉCOLE DE TECHNOLOGIE SUPÉRIEURE

Dedicated to

my sincere and generous father and my loving sisters, for their unconditional love

&

to the memories of great and dear soul of my mother and my nephew (Mohammad Amin), whose memories are always alive in my heart and are a motivation for progress and improvement in my life.

ACKNOWLEDGMENT

I would be pleased to thank my supervisor, Prof. Martin Viens, for his patience, kindness, and comments and for the financial and emotional support he has provided throughout my study. During my time with him, he provided tons of freedom to explore the problems that were interesting to me. Also, guided me in the right direction when it was needed.

Throughout my studies, Mr. Gilles Rousseau has always provided me with invaluable advice, and I would like to thank him for his help and support. His kindness and mentorship greatly influenced me, and I cannot thank him enough. He provided me with new perspectives toward my project, and I deeply appreciate his devotion to being a teacher. He has always helped me during my presence at IREQ and after that. He enthusiastically supports me throughout my term with respect to simulation and experiment approaches. This journey would not have been possible to accomplish without his guidance, encouragement, and supports.

I would like to extend my appreciation to my thesis committee members, Professors
Michel Rioux, Souheil-Antoine Tahan, and Nicolas Giguère for accepting to evaluate my thesis and for providing useful suggestions and constructive comments.

Also, I would like to acknowledge oNDuTy! Canada team. The great committee for NDT research and development in Canada for giving me this opportunity and supporting me emotionally and financially during my Ph.D. I wish to acknowledge Dr. Clemente Ibarra, the coordinator, Prof. Xavier Maldague, the program director, and all faculty members and students. Also, I would like to acknowledge our Industrial research partner Hydro Quebec Research Institute (IREQ), and its staff, especially Dr. Denis Thibaut and Dr. Martin Gagnon for providing this opportunity and supporting me technically during the work. This study is financially supported under the MITACS accelerate program in collaboration with the Institute de recherche d'Hydro-Quebec (IREQ), and I have been financially supported by the "oN DuTy!" program.

Moreover, I deeply express my gratitude to Professor Edward Ginzel and Mr.Jeremy Carignan for their kind help and valuable advice during this project. I wish to thank my close friends, Dr. Amir Hossein Baghdadi and Mr. Alireza shalbafzade, who have helped me since the very beginning of my Ph.D., accompanied me throughout my studies, and have been kind and amazing friends. I would like to thank all the individuals who have directly or indirectly contributed to the advancement of my research. Many thanks to all of you.

I owe everything to my family, who encouraged and helped me at every stage of my personal and academic life. Every breath of my life and drop of blood in my body is dedicated to my family. I love you all.

Technologies avancées d'inspection par ultrasons appliquées aux joints soudés des aubes de turbines hydrauliques

Mohammadebrahim BAJGHOLI

RÉSUMÉ

En raison de l'importance des coûts de production d'énergie, il est essentiel de réduire les arrêts inutiles ou imprévus des équipements de production d'énergie. Hydro-Québec, une importante société de production d'énergie, utilise des modèles pour estimer la durée de vie des aubes de turbine afin d'éviter les arrêts susmentionnés. Pour ces modèles, les caractéristiques des défauts dans les aubes sont l'une des données les plus importantes. Les techniques d'essais non destructifs (END) étant utilisées pour caractériser ces défauts, il est important d'évaluer la fiabilité de ces méthodes et d'identifier celles qui pourraient fournir de meilleurs résultats d'inspection. Le projet actuel vise à fournir à l'IREQ des données fiables sur la performance des méthodes END servant à évaluer les défauts (mesurés et simulés) pour leur modèle d'estimation de la durée de vie. En augmentant la précision des estimations de la durée de vie, Hydro-Québec sera en mesure de minimiser le nombre d'arrêts et donc de réduire les coûts de production d'électricité. Malgré toutes les études précédentes, il existe un besoin essentiel d'étendre les connaissances sur la détectabilité des défauts de soudure dans les joints de soudure des roues de turbines hydroélectriques. Cette recherche s'inscrit dans le cadre d'un programme visant à mieux comprendre les performances de la technologie de contrôle par ultrasons pour l'inspection des zones soumises à de fortes contraintes dans les joints soudés de roue Francis.

Dans cette recherche, nous allons d'abord essayer d'étudier en profondeur la capacité des technologies avancées d'inspection par ultrasons pour les aubes de turbines hydrauliques. L'inspection de l'échantillon d'une maquette de joint en T a été effectuée par différentes méthodes de contrôle non destructif (CND), à savoir l'écholocation conventionnelle (UT), le réseau phasé (PAUT) et la méthode de focalisation en tous points (TFM). Avec ces résultats, les taux de détection ont été obtenus afin de comparer l'efficacité de chaque méthode. Dans un deuxième temps, la fiabilité des différentes méthodes de CND (UT, RT- radiographie, PAUT, et TFM) dans la détection des défauts dans les composants soudés a été étudiée à l'aide d'une approche statistique basée sur la probabilité de détection (POD). Les différentes techniques d'inspection ont ainsi pu être comparées sur la base d'une POD de 90% (a_{90}) afin de déterminer quelle est la taille de défaut qui peut être détectée de manière fiable. La première et la deuxième étape traitent de l'efficacité du contrôle par ultrasons appliqué à une maquette constituée de plaques en SS415 et soudée avec les mêmes matériaux et selon la même procédure. Enfin, la démonstration sur une roue de turbine réelle utilisant les techniques permettant d'obtenir les POD les plus élevées a été expérimentée. La conclusion est qu'une stratégie d'inspection double pourrait être mise en œuvre après la fabrication ou pendant l'inspection en service avec des inspections en deux passes pour améliorer l'évaluation de l'aptitude au service des aubes de turbine hydraulique. La première passe consisterait en l'utilisation de PAUT avec un réseau conventionnel alors que la deuxième passe serait basée sur l'utilisation du TFM. La PAUT a

montré une excellente sensibilité aux défauts volumétriques et planaires tandis que la TFM fournit une dimension plus précise des défauts. Cette double stratégie d'inspection vise à augmenter la fiabilité de l'inspection par ultrasons, ce qui permet de réduire les coûts et d'améliorer la fiabilité des roues de turbines hydrauliques. Les données collectées sur la turbine réelle ont ouvert une nouvelle opportunité pour améliorer le développement des procédures de CND.

Cette nouvelle approche démontre comment le TFM peut permettre d'optimiser le processus de qualification d'une procédure d'inspection basé sur la POD. La méthodologie proposée est axée sur une approche non destructive de dimensionnement des défauts basées en grande partie sur les examens TFM comme méthode pour obtenir de l'information sur la taille réelle des défauts. Cela permet de tracer les courbes POD sans avoir recourt aux essais destructifs qui sont couteux à réaliser et qui détruisent de manière irrémédiable les spécimens. Notre travail est centré sur une roue de turbine réelle en utilisant diverses configurations de réseaux ultrasoniques pour caractériser les défauts. Le développement d'une méthodologie d'inspection des aubes de turbines hydrauliques nous aide à mieux mesurer la taille des défauts utilisés dans le modèle d'évaluation de la fatigue. Les résultats de cette recherche seront également utilisés pour améliorer l'évaluation de l'aptitude au service des aubes de turbines hydrauliques après la fabrication ou pendant les opérations d'inspection en cours de vie utile.

Mots-clés: Contrôle non destructif (CND), contrôle par ultrasons (UT), technique ultrasonique à réseau phasé (PAUT), méthode de focalisation en tous points (TFM), défauts, probabilité de détection (POD), roue de turbine hydroélectrique

Advanced ultrasonic inspection technologies applied to the welded joints of hydraulic turbine runners

Mohammadebrahim BAJGHOLI

ABSTRACT

Due to the importance of energy production cost, it is critical to reduce unnecessary or unpredicted halts of power generation equipment. Hydro-Québec, as a major power generation company, uses models to estimate the service life of turbine runners to avoid the aforementioned halts. For these models, the characteristics of flaws in the runners are one of the most influential inputs. Since non-destructive testing (NDT) techniques are used to characterize these flaws, it is important to assess the reliability of these methods and to identify methods that could provide better inspection results. The current project aims to provide IREQ with the performance of NDT methods to supply reliable flaw data (both measured and simulated) for their life estimation model. By increasing the accuracy of life estimations, Hydro-Québec will be able to minimize the number of halts and hence reduce the power generation costs. Despite all the previous studies, there is an essential need to extend the knowledge on the detectability of the welding flaws in weld joints of hydroelectric turbine runners.

This research is part of a program aimed at better understanding the performance of ultrasonic testing technology for the inspection of high-stress areas in Francis runner weld joints. In this research, we will first try to thoroughly study the capability of advanced ultrasonic inspection technologies for hydraulic turbine runners. Inspection of the T-joint mock-up sample was carried out by various NDT methods, namely conventional pulse-echo, phased array, and total focusing method (TFM). With these results, detection rates were obtained in order to compare the effectiveness of each method. In the second step, the reliability of different NDT methods (UT, RT, PAUT, and TFM) in detecting flaws in welded components was investigated using a statistical approach based on the Probability of Detection (POD). The different inspection techniques could thus be compared based on a 90% POD (a_{90}) to determine what is the flaw size that can be reliably detected. The first and second phases deal with the efficiency of ultrasonic inspection as applied to a mock-up sample made of SS415 plates and welded using the same materials and procedure. Finally, the demonstration on a real turbine runner using the highest POD techniques has been experimented. A dual inspection strategy could be implemented after manufacturing or during the in-service inspection with two pass inspections to improve the fitness-for-service assessment of hydraulic turbine runners. The first pass would consist of the use of PAUT with a conventional array while the second pass would be based on the use of TFM. PAUT has shown excellent sensitivity to volumetric and planar defects, while TFM provides more accurate flaw size dimension. This dual inspection strategy aims to increase the reliability of ultrasonic inspection, leading to reduced costs and improved reliability for the hydraulic turbine runner industry. The data collected on the real turbine opened a new opportunity to improve the NDT procedure development.

Demonstrating how TFM has better sizing accuracy is crucial for optimizing the inspection process. This leads to an improvement in the detectability of flaws and improves the process of generating POD curves based largely on TFM examinations as the ground truth method to get the flaw size information. This makes it possible to draw POD curves without using destructive tests which are expensive to perform, and irreparably destroy the specimens. Our work is centered on a real turbine runner using various ultrasonic array configurations to characterize defects. Developing the inspection methodology for hydraulic turbine runners helps us to achieve better sizing measurements of flaws used in the fatigue assessment model. Also, the outcome of this research would be employed to improve the fitness-for-service assessment of hydraulic turbine runners after manufacturing or during inspection operations performed over the useful life of the part.

Keywords: Non-destructive testing (NDT), Ultrasonic testing (UT), Phased Array Ultrasonic Technique (PAUT), total focusing method (TFM), flaws, Probability of Detection (POD), hydroelectric turbine runner

TABLE OF CONTENTS

Page

LIST OF TABLES

LIST OF FIGURES

Page

LIST OF ABREVIATIONS

ASTM	American Society for Testing and Materials
ASME	American Society of Mechanical Engineers
DDF	Dynamic Depth Focusing
EDM	Electrical Discharge Machined
FCAW	Flux-Cored Arc Welding
FMC	Full Matrix Capture
FFS	Fitness-For-Service
HAZ	Heat Affected Zone
IIW	International Institute of Welding
IQI	Image Quality Indicator
IREQ	Institut de Recherche d'Hydro-Québec
LOF	Lack of Fusion
LOP	Lack of Penetration
MAPOD	Model Assisted POD
NDE	Non-Destructive Evaluation
NDT	Non-Destructive Testing
PAUT	Phased-Array Ultrasonic Testing
POD	Probability of Detection
POO	Probability of Occurrence
PFA	Probability of False Alarm
PFP	Probability of False Positive
PAF	Passive Axis Focusing
PWI	Plane Wave Imaging
ROC	Relative Operating Characteristics
ROI	Region of Interest
SNR	Signal-to-Noise Ratio
SDH	Side-Drilled Holes
TOFD	Time-of-Flight Diffraction
TFM	Total Focusing Method

TWI	The Welding Institute
UT	Ultrasonic Testing

LIST OF SYMBOLS

a	Flaw Size
a_{50}	Flaw Size Having 50% Probability of Detection
a_{90}	Flaw Size Having 90% Probability of Detection
$a_{90/95}$	Flaw Size Having 90% Probability of Detection in 95% POD Experiments
$\hat{a}$	Signal Amplitude
$\hat{a}_{dec}$	Value of $\hat{a}$ above which the signal is interpreted as a hit, and below which the signal is interpreted as a miss
Al_2O_3	Alumina oxide
dB	Decibel
Hz	Hertz
L	Longitudinal wave
N	Number of elements
Rx	Receiving transducer
Si_3N_4	Silicon nitride
T	Transverse wave
T_x	Transmitting transducer
ZrO_2	Zirconia

INTRODUCTION

Problem Statement

Power generation equipment suffers from different degradation mechanisms, such as fatigue, that could be initiated by flaws around which dynamic stresses are concentrated. This is why maintenance process of this equipment shall be planned so as to carefully monitor the integrity of its components. At Hydro-Québec, welding flaws induced during the manufacturing of hydraulic turbine runners have been found to be at high risk of instigating fatigue damages. To plan preventive maintenance, Hydro-Québec developed life estimation models base on the Kitagawa diagram that requires flaw severity (flaw size, shape, and location) as critical model inputs (Gagnon et al., 2012). Flaw size and location are generally assessed using non-destructive testing (NDT) methods. Therefore, the NDT method should be reliable enough to be used as the basis for decisions, which allows us to keep a component in service for a specified time without increasing risks beyond a certain threshold. NDT methods are currently used in the industry. Among available NDT methods, ultrasonic inspection is one of the most efficient methods for detecting welded joint flaws in hydraulic turbine runners (Boukani et al., 2018).

In investigation of runners made of martensitic stainless steel by IREQ researcher, either installed or during fabrication, various flaws were found in the high-stress area after the final heat treatment. The area where the highest in-service stress is located is the dubbed zone Z (Figure 0.1), the area of the weld between the blade and band spanning over 250 mm from the trailing edge. Weld defects have initiated the majority of observed in-service cracking in this zone. Additionally, because the peak stress occurs in the zone spanning over 7 mm from the trailing edge (Zone Y), the sub-region should be studied and smaller acceptance criteria should be set for this sub-region. Starting and stopping welding passes are more likely to cause defects in the Y region. The Y region is challenging from an inspection perspective because the curvature of the trailing edge is detrimental to ultrasonic inspection coupling, and good wedge contact is not always maintained.

(a) (b)

Figure 0.1 Francis turbine runner a) Scan inspection plan for blade, and b) View of blades

The main problem with flaws left after fabrication is determining if they pose a risk of developing into a fatigue crack. The degradation model used by Hydro-Québec for flaw assessment requires a precise flaw dimension, i.e., length, height, ligament, and position in order to put the flaw in a stress analysis model that would predict the susceptibility to develop a service crack (Gagnon et al., 2014). The NDT method must thus be reliable enough to find all flaws larger than the critical size and provide a flaw dimension sufficiently accurate for stress calculation. The sizing information provided by conventional ultrasound is inadequate for this purpose. Sizing accuracy improvement shall be investigated using ultrasonic array methods.

According to the facts mentioned above, probability of detection study shall focus on flaws that are more likely to occur in the welds based on the manufacturing processes performed. In addition, the performance of advanced ultrasonic testing methods shall be evaluated with respect to these postulated flaws. The current study aims to identify the best ultrasonic inspection methods to provide reliable flaw data for the life estimation model.

Research Objectives

The general objective of this project is to improve flaw detection and sizing using UT technology for welded joints of hydraulic turbine runners. Currently, the Francis turbine fabrication industry relies on manual ultrasonic testing. There is resistance to new ultrasonic techniques because of the lack of data supporting the merits of these technologies introduced to the NDT market over the past two decades. Studies are thus needed to evaluate the performance of conventional and advanced ultrasonic techniques centered on the inspection capability as applied to a Francis runner.

While a lot of effort has been placed into determining the critical flaw size, not sufficient information has been found in the public domain about the detection capability of NDT in the Francis runner weld joint. Generally speaking, this information is usually produced through a comprehensive qualification program that applies to a specific inspection technique, component geometry, and material. Qualification programs are not widely implemented because of the cost involved and the technical complexity of building samples and executing the testing program.

A good understanding of NDT capability is essential to ascertain that inspection technology can meet the requirements set by fracture mechanic analysis. Meeting this objective would help move one-step closer to quantifying the uncertainty around the flaw size that can be reliably detected, which will thus improve the confidence of the estimated remaining service life of the runners based on the population of flaws left after fabrication. The main objective of the project is to find which NDT techniques have better flaw detection and sizing capability. This objective can be divided into specific objectives to enhance our knowledge about NDT methods concerning the welding flaws in Francis turbine runners. In the following paragraphs, the project's general objective is divided into four sub-objectives with corresponding activities.

1. Evaluation of the capability of ultrasonic inspection methods to detect flaws in a T-joint mock-up mimicking a Francis runner trailing edge.
2. Quantification of the inspection reliability (POD) of various NDT methods applied to a T-joint sample representative of a turbine runner trailing edge.
3. Determination of the probability of detection of advanced ultrasonic inspection using TFM as an accurate non destructive sizing method.

First, it is necessary to compare the detection capability of advanced ultrasonic inspection technologies for hydraulic turbine runners. This step one objective consists of collecting initial data on a simplified T-joint mock-up and then to compare the experimental ultrasonic data with the results of simulations performed by CIVA, a computer simulation package. The sample was inspected by various NDT methods, namely conventional pulse-echo, phased array, and TFM. Inspection procedures used either free probe movement (non-encoded) or linear-encoded scan. The goals were to assess the capability of advanced ultrasonic inspection technologies for detecting flaws in Francis turbine runners, especially near the trailing edge.

Second, Conventional Ultrasonic Testing (UT), Phased Array Ultrasonic Testing (PAUT), Total Focusing Method (TFM), and Radiography testing (RT) were compared in terms of their reliability for the inspection of weld joints in hydraulic turbine runners. The knowledge of the Probability Of Detection (POD) curves, required by Fitness-For-Service (FFS) assessments, is mostly absent for structures such as the hydroelectric turbine industry. The main goal of the study reported here is to evaluate the reliability of NDT methods for the inspection of welded joints in turbine runners. It focuses on determining POD curves for different inspection techniques applied to a T-joint sample representative of a turbine runner trailing edge with artificially induced flaws (ceramic beads inserted during welding).

Finally, as a ground truth method to obtain flaw size information, we propose a new approach to generate POD curves based mainly on TFM examinations. Two case studies are presented to demonstrate the NDT methodology for producing POD curves without relying on destructive analysis. This chapter considers the use of the TFM as a tool to provide accurate

flaw sizing for POD determinations. The proposed methodology offers the flexibility to build POD curves using a real component without destructively analyzing the sample to get flaw size data.

State of the art

As part of a large project, this research focuses on detecting and characterizing flaws in the welded joints of hydroelectric turbine runners, as they are located in the most critical zones in terms of fatigue failure. Loading conditions and fatigue-related material properties have been previously studied in detail as two inputs of life estimation models, while flaw characteristics are still fed into the developed models as assumptive third input values. No publications found regarding inspecting hydraulic turbine runners with TFM. There are few studies about inspecting hydraulic turbine runners with a phased array ultrasonic testing on real turbine runners. This is the first research to use TFM in the hydroelectric industry. To do so, and based on a literature review as a first step, a T-joint sample was manufactured in martensitic stainless steel (UNS S41500) in accordance with the manufacturing requirements of turbine runners. The T-joint geometry often mimics a turbine runner's trailing edge. The base plate provides the same ultrasonic path for an inspection performed from the turbine web. The advantage is that the thickness of the joint components is selected to be on the same scale as the most critical part of real runners.

Moreover, the mock-up sample evaluated the capability of advanced ultrasonic inspection technologies for hydraulic turbine runners. The current study goes further by including TFM and compares conventional, phased array and TFM techniques in order to assess their performance in detecting flaws in the trailing edge of a runner blade. The work focuses on ultrasonic inspection techniques applied directly to the blade because they conform to current fabrication and in-service inspection methods. On the other hand, insufficient research works have been carried out about creating POD curves on hydraulic turbine runners and martensitic stainless steel. This work is the first of its kind to address the reliability of different NDT

methods by POD curves in detecting flaws in welded components using both a mock-up and a real component.

Then, as the second step, inspection of real turbine runners is carried out by advanced ultrasonic testing methods for fitness for service purposes. Optimizing the inspection process with the data from the mock-up T-joint improves the detectability of flaws. A dual inspection strategy could be implemented with two pass inspections to improve the fitness-for-service assessment of hydraulic turbine runners after manufacturing or during the in-service inspection. Also, this research considers the use of TFM as a tool to provide accurate flaw sizing for POD determinations. It is the first research to propose TFM as the basis of flaw sizing for POD study. TFM could be considered to speed up and reduce the cost of the qualification process by avoiding destructive analysis. The destructive analysis is performed to obtain the ground truth flaw size. This could be avoided if TFM could be applied to generate the same information, i.e., the flaw dimension required to produce the POD data set. This approach permitted to develop POD curves based on real components inspection data. Regarding this novelty, TFM aims to increase the reliability of ultrasonic inspection, leading to reduced costs and improved safety for the hydraulic turbine runner industry.

Thesis structure

The thesis content is structured into 4 chapters. The first chapter reviews the related research previously published in the literature. Chapter 2 is devoted to the capability of advanced ultrasonic inspection technologies for hydraulic turbine runners. The goal was to assess capability of advanced ultrasonic inspection technologies to detect flaws in Francis turbine runners. In Chapter 3, the reliability of NDT methods for the inspection of weld joints in hydraulic turbine runners is evaluated. The knowledge of the POD curves required by fitness-for-service assessments is mostly absent for structures such as the hydroelectric turbine industry. The main goal of the study reported in this chapter is to evaluate the reliability of NDT methods for inspecting welded joints in turbine runners. It focuses on determining POD

curves for different inspection techniques of a T-joint sample representative of a turbine runner trailing edge with artificially induced flaws (ceramic beads inserted during welding). Afterward, Chapter 4 presents the motivation and process to generate POD curves based largely on TFM examinations as the ground truth method to extract the flaw size information. Two case studies are presented to demonstrate the NDT methodology for producing POD curves without relying on destructive analysis.

In this thesis, each chapter is dedicated to answering one of the following questions:

• Chapter 2: What are the best NDT method(s) and technique(s) for inspection of the trailing edge of a turbine runner?

• Chapter 3: What is the POD for volumetric flaws located in the trailing edge of a turbine runner?

• Chapter 4: How to demonstrate the efficiency of NDT methods applied to a real turbine runner?

CHAPTER 1

LITERATURE REVIEW

1.1 Introduction

The importance of energy and its corresponding costs is more realized today with the advances in technology, modern life requirements, and energy needs. A significant amount of these costs is incurred in installing and maintaining the power generation plants and equipment. Since this equipment is exposed to various degradation mechanisms such as fatigue, optimization of the maintenance process of this equipment could lead to significant cost savings. In other words, unrequired interruption of the regular electricity production process imposes non-essential costs to the power producers such as Hydro-Québec. Components of power plants are designed for limited-service life; over time, their material properties are degraded, and irreversible damages may occur due to time-dependent in-service stresses, temperatures, and environment. Due to the fact that replacing a turbine runner is relatively expensive, it is necessary to specify the predicted life more precisely during operation of components considering the data on service conditions, deterioration of material, and real evaluation of the damage. The reliability of production equipment must be rigorously estimated and carefully evaluated during extended life to achieve this goal (Paoliello et al., 2005; Boukani et al., 2018).

The runners are the heart of any turbine because this is where the kinetic energy of water is transferred to the rotating machine. The turbine runner weld can be considered as a series of Y-type weld sections with different web thicknesses and angles (J. Zhang et al., 2014). The Flux-cored arc welding (FCAW) is used to join the runner blade to runner crown/band in turbine runners. Therefore, it naturally generates some discontinuities due to thermal cycles, solidification, cooling, distortion, and residual stresses in welding zone after the process. These joints are one of the most critical sections of turbines due to the presence of welding discontinuities and high stress (Boukani et al., 2018). Francis runners are spinning wheels with fixed blades welded on their top and bottom ends to the crown and band, respectively. The flow of water with large kinetic energy is directed toward these blades, which makes the runner

spin. The reaction forces and torques accompany the force applied by the water flow in the joints. The cyclic nature of the forces causes in-service defects to develop through fatigue in highly stressed areas. According to some previous research, the transitional regions welded between the blade and band or crown are identified as the critical areas of stress concentration for high-head Francis runners (Figure 1.1). Huth indicates that once the runner is put in service, fatigue cracks start propagating from undetected flaws and inclusions (Huth; 2005).

Figure 1.1 Overview of Francis turbine runner

For the fatigue process as the main degradation mechanism of hydraulic turbine runners, Hydro-Québec applies a fracture mechanics approach to develop life estimation models. The model inputs need to be defined as accurately as possible to obtain reliable estimations. Initial flaw size is one of the inputs whose uncertainty has a substantial impact on the reliability assessment (Gagnon et al., 2012). Therefore, any improvement in the definition of this input parameter could significantly enhance the accuracy of the estimated service life. Initial flaw size is generally characterized using NDT methods (Boukani et al., 2018).

As part of a large project, this research focuses on detecting and characterizing flaws in the welded joints of hydroelectric turbine runners as they are located in the most critical zones regarding fatigue failure. Loading conditions and fatigue-related material properties have been studied in detail previously as two inputs of life estimation models (Gagnon et al., 2012;

Gagnon et al., 2014), while flaw characteristics are fed into the developed models as assumptive values as the third input (Boukani et al., 2018).

A proven NDT detection size is typically used in life estimation calculations as the initial crack size. Generally, this initial value is considered to be a size of the flaw that is always detected using a particular NDT method. To characterize this size, quantitative studies are carried out on the reliability of the applied NDT methods leading to the generation of POD curves. This research project's main focus is to answer the detection and sizing capability of NDT methods applied to Francis runner welded joints.

1.2 Non- destructive testing (NDT)

According to (ASTM E1316-13, 2004), a flaw is defined as ‘‘an imperfection or discontinuity that may be detectable by non- destructive testing and is not necessarily rejectable”, whilst a defect is defined as ‘‘one or more flaws whose aggregate size, shape, orientation, location, or properties do not meet specified acceptance criteria and are rejectable”. ‘Flaw’ and ‘defect’ are sometimes used interchangeably in some articles and parts in this thesis.

NDT is the development and application of technical methods to examine materials or components such that the pieces are not destroyed and their future usefulness and serviceability remain (Bray & Stanley, 1996). There is a wide range of NDT methods based on the physical principles of electromagnetic radiation, sound and other inherent properties of the materials. The techniques selected should consider safety, economic, efficiency, and time factors (ASTM E1316-13, 2004).

The application of NDT methods in different industries has been increasing as a reliable means of post-manufacturing quality control, structural health monitoring, and in-service maintenance. These methods are supposed to detect mechanical and physical discontinuities in materials and make intelligible indications of them. Because hydraulic turbine runners are generally inspected using different techniques of ultrasonic inspection method (Boukani et al.,

2014; Boukani et al., 2018; Katchadjian, 2004), the principal focus of this research will be on ultrasonic testing.

Ultrasonic waves are mechanical vibrations with the same characteristics as sound waves but with a frequency so high enough that the human ear cannot perceive them, i.e., higher than 20kHz. For weld examination in metals, ultrasonic waves usually have a frequency range of 500 kHz to 10 MHz, and most applications use a frequency between 2 and 5 MHz. It is important to realize that ultrasonic waves are not electromagnetic radiation passing through the specimen but are the result of induced particle vibration in the sample and are feasible because of the elastic properties of the specimen material. For this reason, the wave velocity is different in different materials (ASTM E1316-13, 2004; ASM Handbook Volume 17, 2018; Chaplin, 2017).

Ultrasonic testing is suitable for detecting and sizing flaws embedded or growing from inaccessible surfaces. There are various reasons for its suitability, including the following:
The ultrasonic waves propagate through thick solid parts, so ultrasonic testing can detect flaws beneath the inspection surface, as opposed to methods that can only detect defects close to or on the inspection surface, e.g., eddy current testing or methods that can only detect defects on the inspection surface, like visuals and penetrants. When defect assessment calculations require a value for how far a component of a defect has grown, ultrasonic testing is the main method used. It is used to detect various types of flaws, such as cracks and inclusions and a wide range of materials, compared to methods like magnetic particle testing, which require the component to be ferromagnetic. Ultrasonic waves are inherently safe compared to methods like radiography, which uses ionizing radiation and thus requires multiple types of protection (Felice et al., 2018).

1.3 Advanced ultrasonic testing

1.3.1 Phased array ultrasonic technique (PAUT)

Phased array (PA) transducers can be considered as multiple small conventional transducers (called elements) housed in a single unit. Each transducer can be pulsed individually and by varying the time delay between pulses from the elements, for example, sequentially along a row, such that constructive interference of the individual waves can occur at a desired angle and focus is achieved (Figure 1.2) (Daniel Kass, Michael Moles, 2014; Michael D. C. Moles, 2007; E. Ginzel, 2013).

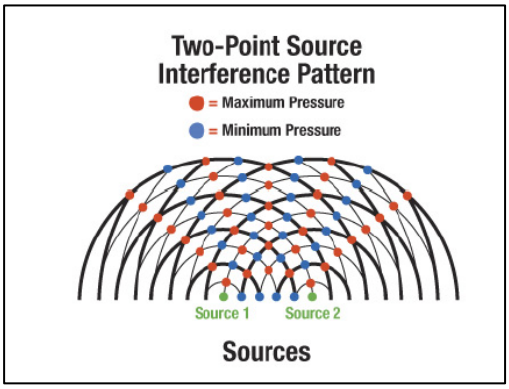

Figure 1.2 Interference patterns
Taken from Daniel Kass,
Michael Moles (2014, p. 6)

The term phased is related to timing and array refers to the multiple elements. Inspection using phased arrays with conventional ultrasonic testing is very common since the physics of wave propagation, reflection, refraction, mode conversion and diffraction remain the same. In this technique, several ultrasonic waves are generated and received. Also, the beam from a phased array transducer can be moved electronically without moving the probe. A wide volume of material can be swept by electronically changing the delay applied to each element in order to steer the beam. Conventional ultrasonic testing uses a single transducer, while the phased array system utilizes up to 256 independent elements (Moles et al., 2007).

The advantages of using PAUT systems over conventional ultrasonic testing are mentioned below:

a. PAUT is capable of sweeping the sound beams through a range of angles without moving the probe. This enables the PAUT probe to be used where mechanical raster scans are impossible.
b. Possibility to inspect defects with different angles increases the POD of defects regardless of their orientation.
c. This method can focus at different depths, thus dynamically improving the ability for sizing critical defects by enhancing the signal-to-noise ratio using focus beams (Ginzel & Johnson, 2008; Ginzel, 2013).

There are a few notable disadvantages of using phased array systems over conventional ultrasonic testing as well:

a. Phased array instruments can be 10-20 times more expensive than conventional ultrasound with costly probes and software upgrades.
b. It requires trained operators with computer, spatial visualization, and ultrasonic skills.
c. Data analysis can be time-consuming.
d. Grating lobes are similar to side lobes, which may interfere with the time base display.
e. Dead elements in an array may inhibit constructive interference and beamforming (Ginzel, 2013).

However, conventional ultrasonic systems do not allow for modification or control of the beam profile generated by a phased-array probe. This leads to three main electronic scanning techniques (shown in Figure 1.3 and described below). Combining these electronic scanning techniques provides far more complicated scans and greater coverage than is possible by conventional methods (Ditchburn & Ibrahim, 2009).

a) Linear scanning

A subset or group of the array elements is pulsed to form the desired beam profile. The focal law giving this beam profile is then multiplexed electronically along with the array length (Figure 1.3(a)). This can be considered as the electronic equivalent of scanning a conventional (single-crystal) probe mechanically along a distance equal to the length of the larger phased-array probe.

b) Dynamic depth focusing (DDF)

DDF is a computer algorithm that focuses on different depths in the reception mode and the axis defined by the transmission law (Figure 1.3(b)).

c) Swept angular (sectorial or azimuthal) scanning

Focal laws are chosen to steer the beam electronically to a fixed incidence angle or sweep the beam through a wide angular range (Figure 1.3(c)).

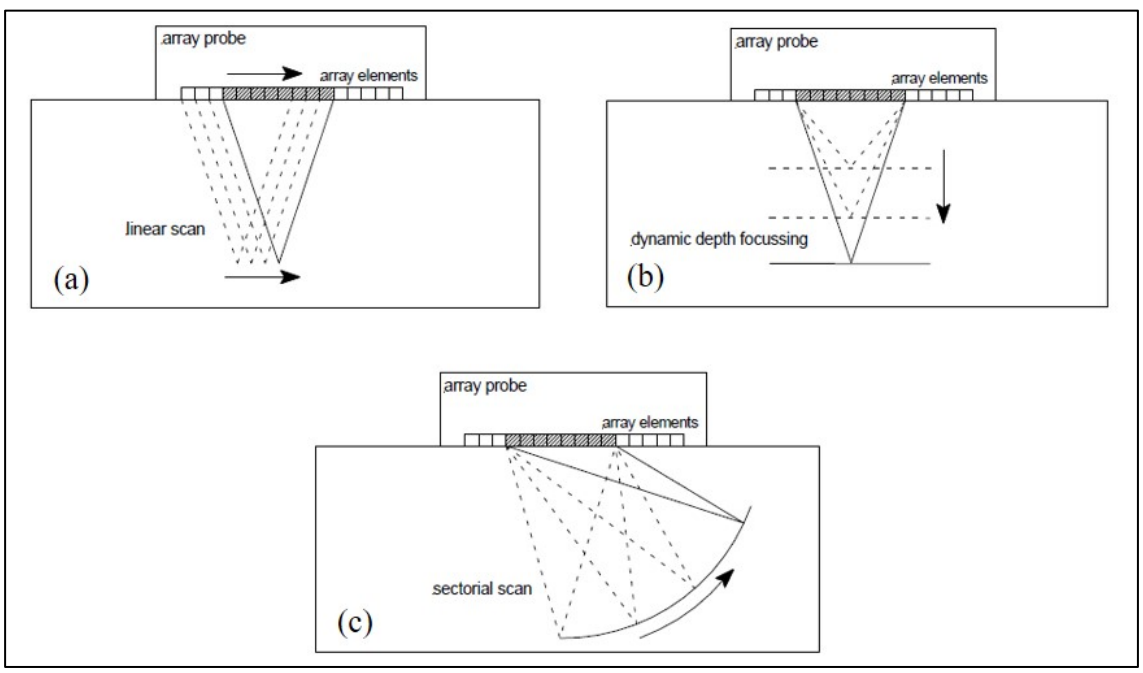

Figure 1.3 Diagrams showing the types of electronic scanning possible with phased-array probes: (a) linear, (b) depth focusing, and (c) swept angular (sectorial)
Taken from Ditchburn & Ibrahim (2009, p.3)

Furthermore, time-of-flight diffraction (TOFD) inspection, a defect-sizing technique that is often more accurate than standard amplitude sizing methods, especially for crack sizing, is possible with some phased-array systems (Ginzel, 2013). It is described in the next section.

1.3.2 Time-of-flight diffraction (TOFD)

Time-of-Flight Diffraction (TOFD) is a very common technique based on time measurements of the signals diffracted by a crack (Figure 1.4), used for sizing cracks, embedded defects, and surface breaking flaws. It is based on diffracted signals from the extremity/extremities of the flaw (Felice et al., 2018). It is supposed that a buried crack is in a plate of some isotropic and homogeneous material. The transmitting transducer (T_x) emits a short burst of ultrasound waves into the component. These waves spread out, propagating into a beam with a wide angular range. Some of this energy impacts the crack and is scattered by it. If the crack face is smooth, there will be a reflection like a mirror from the wave incident to the face just like an optical reflection; this occurs at an angle of reflection equal to the angle of incidence; both angles are measured from the normal to the crack face. In many real situations, the crack grows in a plane perpendicular to the direction of maximum stress (Figure 1.4). For a rough crack, the energy is scattered in all directions. Diffraction is the phenomenon where the edge of a crack or a sharp corner scatters the sounds in all directions. The crack's tip acts like a point source and emits a cylindrical wave front irradiating in all directions which are defined for any crack, whether smooth or rough-faced. The diffraction causes some fraction of the incident energy to travel toward the receiving transducer (R_x). If the crack is big enough, the signals from two extremities of the crack will be separated in time sufficient to be recognized as coming from separate sources. As well for these two signals, some energy will arrive at the receiver directly from the shortest possible path; this is the so-called lateral wave propagating below the surface of the component. A second interface signal may also originate from the back wall. Such a set of actual signals is displayed in the right part of Figure 1.4; this type of time trace is known as an A-scan.

In other words, when an ultrasonic wave encounters a flaw, it undergoes reflection, transmission, and diffraction. Additionally, each flaw tip acts as a point source of diffracted energy over wider angles. This energy is well suited for flaw detection and sizing because it is directly related to the true position of the flaw tip and the corresponding time of flight. These diffracted signals are often of lower amplitude than the reflected signals and depend on several factors, including the crack tip's nature, crack orientation, compressive forces on the crack face, and material noisiness.

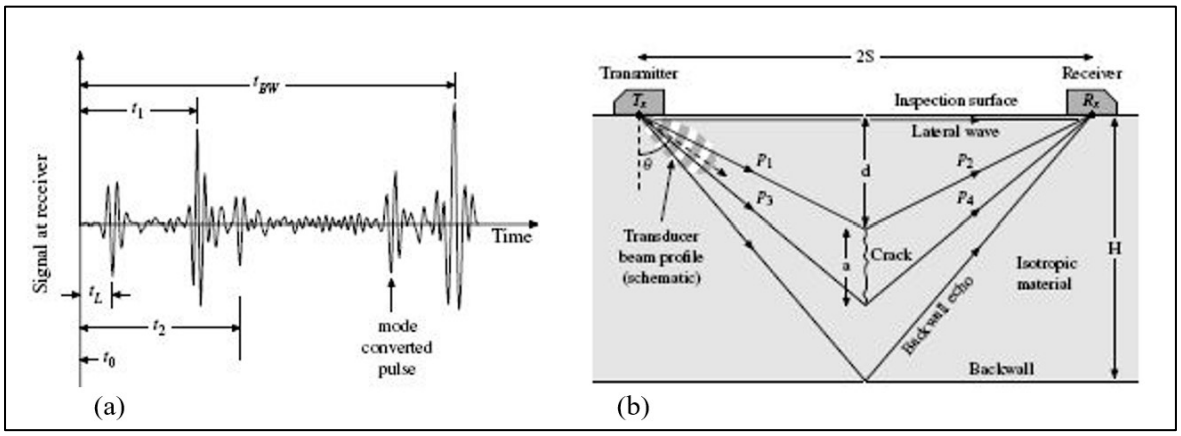

Figure 1.4 The two-probe basis of the Time-of-Flight Diffraction technique. The locations of the tips of the crack are determined from the time differences between the lateral wave and the pulses, which follow paths p_1+p_2 or p_3+p_4. These paths correspond to t_1 and t_2, respectively in the right figure
Taken from Charlesworth et al. (2001, p.21)

There are multiple advantages to using TOFD systems. The inspection speed of TOFD is high, and it has highly accurate defect sizing capability. Compared to conventional ultrasonic and radiography, the most important advantage of TOFD is a high POD. This method is easy to use and can be set up and operated quickly. Analysis can be performed immediately from the digital images and data are available for additional post-test reviews. TOFD has faster scanning times and is used for quantitative characterization with better accuracies. It does not depend on the orientation and surface features of the discontinuity (Manjula et al., 2012). The diffraction response from a flaw is much less angular dependent than the specular response from a flaw (Felice & Fan, 2018).

There are also several disadvantages to using TOFD systems. TOFD is only used for thick sections and very near-surface defects are more often overestimated; near-surface flaws are also often missed due to the dead zone created by the lateral wave ring time. To identify the echoes and to receive a meaningful signal for analysis, it needs manual or automated manipulation of the transducer to peak signals (Manjula et al., 2012).

TOFD seems to be the most favorable technique for life assessment models since it sizes the flaws more accurately and is based on signal timing, disregarding both wave amplitude and background noise. Considering the high thickness of turbine blades, amplitude-base techniques are expected to suffer from attenuation and noise. However, for complicated joints such as the Y-shape joint of runners, TOFD is challenging to apply, and further investigations are required (Boukani et al., 2014). The main problem with TOFD is configuring the probe to provide an accurate metal path. Y-shape is inappropriate because the Tx and Rx cannot face each other. According to Charlesworth, for complicated joints, the detection of flaws is a straightforward process. However, a good knowledge of the technique, the physics of sound waves, and the joints' geometry are needed to locate and size the indications (Charlesworth et al., 2001).

1.3.3 Total focusing method (TFM)

The industry is always looking for improved and reliable non-destructive evaluation methods. On the other hand, technology has continued to evolve. FMC and TFM are recent technological advancements in phased array testing which is proposed by Holmes (Holmes et al., 2004). Full Matrix Capture (FMC) is a UT data collection process and Total Focusing Method (TFM) is a data processing to produce an image (Richard et al., 2018). There are two approaches to applying delays when using ultrasonic arrays. Actual ‘physical’ delays can be applied to the elements, the approach referred to as ‘beamforming,’ with elements transmitting in parallel with different delays. Alternatively, data can be collected from an array without applying any delays, and the delays can be applied ‘synthetically’ during post-processing. The later requires the collection of raw A-scans for different transmitter-receiver combinations. If all the transmitter-receiver combinations are collected, this is referred to as Full Matrix Capture

(FMC) (Figure 1.5). Therefore, the Total Focusing Method (TFM) is a synthetic focusing technique that uses FMC for elementary ultrasonic signal recording. FMC consists of firing each element individually and receiving from all elements, as shown in Figure 1.5.

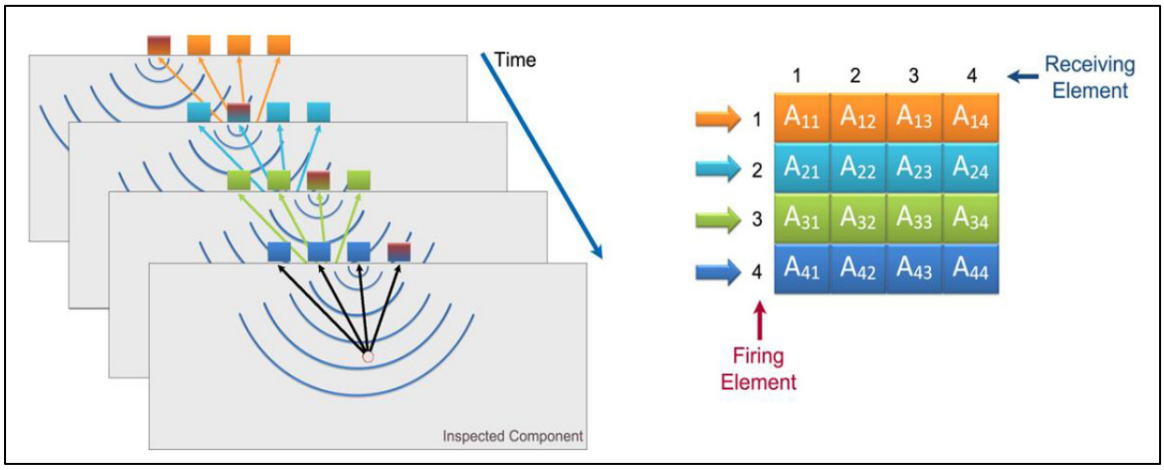

Figure 1.5 Full Matrix Capture
Taken from Tremblay et al. (2012, p.2)

The FMC matrix is an N×N matrix, N being the number of elements, with each matrix entry containing a raw signal. This creates a matrix of 4096 (64^2) elementary A-scans that is processed by the TFM algorithm. The TFM is essentially a delay and sum algorithm using the elementary A-scan matrix as an input, and the output is the time-delayed and sum amplitude map. The TFM is computed over a Region of Interest (ROI) divided into voxels with height and width smaller than 0.2 wavelength to avoid phase-related amplitude fluctuation. In our experiment, the voxels are 0.1mm x 0.1mm for a wavelength of 0.64 mm. The amplitude of each voxel is the sum of all A-scan's amplitude at the position corresponding to each emitter-receiver sound path. The algorithm is equivalent to focusing the 64-element array at each voxel to achieve the maximum acoustic resolution given the aperture, wave mode, and frequency. TFM imaging technique provides intuitive, interpretable results and a high signal-to-noise ratio. Applying the FMC-TFM method is very computationally intensive. For each acquisition cycle, the array is fired 64 times, 4096 A-scans are collected, and the resulting image is the processing of all 4096 A-scan to extract and sum the amplitude on each voxel. Specially

designed instruments using graphic card computation (in CUDA) are needed to perform the FMC acquisition efficiently and real-time display of the TFM image.

TFM calculation is based on the wave velocity, the wave interaction with flaws, and the specimen back wall. The TFM algorithm calculates the TFM image based on the selected wave mode and path. A direct TFM mode, either shear or compression, uses a single wave type for the incident and reflected paths. Indirect TFM modes use either reflection from the back wall or mode conversion on the back wall and the flaw. It may require two or more modes to inspect a weld and obtain accurate results for crack-like flaws. Indeed, in this case, the best practice is to validate the inspection setup on a mock-up. Typically, the direct shear mode is more sensitive to reflection from a volumetric flaw, whereas the indirect shear mode is better for a planar vertical flaw.

One of the uniqueness of TFM is that it requires the user to specify the interaction with the flaw and the sample back wall. TFM is implemented in the TOPAZ 64 device and offers different commonly used imaging modes which include direct (LL or TT), corner (L-LL or T-TT), indirect imaging (LL-LL or TT-TT), and mode conversion LL-T. Various imaging modes enable the obtaining of complementary information related to a defect. The “L” refers to the longitudinal wave, whereas the "T" refers to the transverse wave. For direct TFM, the first letter corresponds to the transmitter's path to the voxel position and the second is the reflected path between the voxel position and receiver. On the other hand, for corner echo and mode conversion, the first letter corresponds to the path between the transmitter and the back wall, the second path is between the back wall and the voxel point. On the contrary, the third is the path between the voxel point and the receiver (BS ISO 23864, 2021; BS ISO 23865, 2021; Reverdy et al., 2016).

There have been many instances where benefits of using full matrix capture and TFM have been reported. Some researchers observed a better opportunity for accurate flaw sizing sensitivity towards small flaws by using different TFM modes (Felice & Fan, 2018; Spencer et al., 2018; Rioux et al., 2018; Caulder et al., 2018). For inspection of highly attenuative

materials, highly improved signal-to-noise ratio was observed by (Deutsch et al., 2016; Rioux et al., 2018; Caulder et al., 2018). It has also been observed that full matrix capture with TFM allows for a fast high-resolution, and real-time inspection with ease of setup as no complicated focal laws are involved allowing ease of interpretation (Richard et al., 2018). (Richard et al., 2018) also reported that the inspection coverage in various applications is increased using full matrix capture and TFM. (Berke et al., 2016) has also observed that full matrix capture and TFM reduces dead zone, improving the Signal-to-Noise ratio and delivering a higher POD for inclined defects.

Advantages of FMC/TFM for flaw size determination:

- Focusing: TFM algorithm is a synthetic focusing process that effectively focuses the array on each voxel. Adding focusing on the passive axis increases the response from flaws and improves length sizing accuracy.
- Spatial resolution: TFM offers optimal vertical plane resolution and provides the best ultrasound accuracy for fitness-for-purpose analysis.

Disadvantages for FMC/TFM:

- Inspection speed: TFM requires a huge number of A-scans and real-time processing; this takes a toll in terms of inspection speed. More rapid acquisition algorithms are available such as plane-wave imaging, but they were not evaluated during this research.
- Operator training/certification: No certified training is currently available.
- Instrumentation: TFM requires a special instrument with dedicated hardware for acquiring and processing large amounts of data (Berke et al., 2016; Caulder,2018; Jobst et al., 2010; Deutsch et al., 2016; Felice et al., 2018; Iakovleva et al., 2014; Richard et al., 2018; Rioux et al., 2018; Spencer et al., 2018).

1.4 Probability of detection

As mentioned earlier, a proven NDT detection size is typically used as the initial crack size for life estimation (damage tolerance) calculations. Generally, this initial value is considered to be a size of the flaw that is almost always detected using a particular NDT method. In order to characterize this size, quantitative studies are carried out on the reliability of the applied NDT methods leading to the generation of Probability Of Detection (POD) curves. POD is usually expressed as a function of flaw size (length or height) but, in reality, it is a function of more: factors related to the material (microstructure, geometry), to the flaw itself (flaw type, orientation, shape, and density), and the inspection system (NDT method, testing conditions, and NDT personnel) (Georgiou et al., 2006). Figure 1.6 shows (in blue) a typical POD curve. In the lower zone of a curve, the POD is about zero for small flaw sizes, that is, no flaws of these sizes are detected. In the upper zone of a curve, it is about 1 for large sizes of flaws, i.e., all the flaws of these sizes are detected. In the intermediate zone, the POD curve increases from 0 to 1 (called a transition zone) in the form of “S” and is generally for flaw sizes of industrial interest. With an appropriate approximation, most of the experimental observations in the majority of situations are placed in this zone. For determining the POD curve, this methodology recommends using a model where supposedly the POD curve has a functional form (of “S” shape).

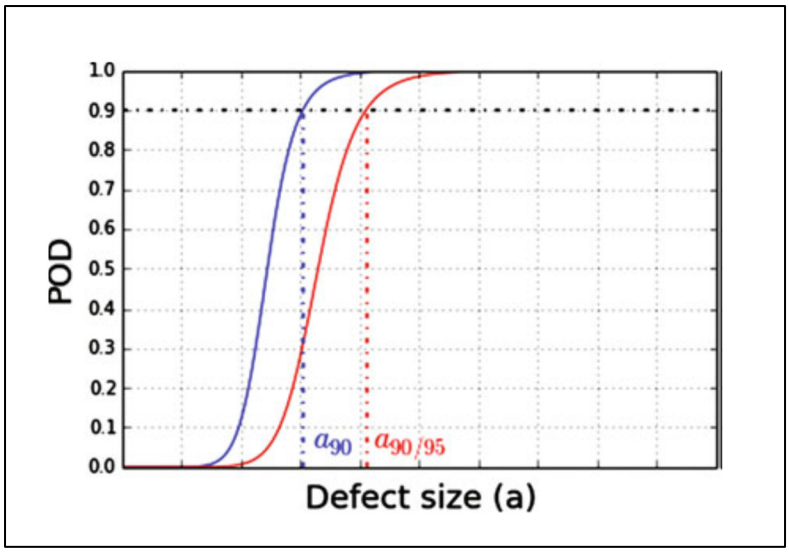

Figure 1.6 Typical POD curve (in blue) and 95% confidence limit (in red)
Taken from Chapuis et al. (2017, p.26)

POD curves can be built for two forms of data:

1. Binary response: It gives the outcome of an experiment as either hit or miss. A level of response is defined; data below this level is not detectable (called miss), and information above this level can be detected called hit (Figure 1.7(a)).
2. Signal response: For any set of experiments, if flaw size is taken as (a) and the response of the inspection system is measured as ($\hat{a}$), POD curve is evaluated as a function of ($\hat{a}$) from 0 % to 100 % vs. flaw size (a) (Figure 1.7(b)) (Malik, 2016; Annis, 2009).

The POD methodology currently adopted by the aircraft industry is described in the Military Handbook 1823A (Annis, 2009). It is based on a parametric estimation of the POD following Berens models (Foucher et al., 2018), which is also adopted in some ASTM standards;

1. ASTM E2862-18: Standard practice for the probability of detection analysis for hit/miss data (ASTM E2862-18, 2018).
2. ASTM E3023-15: Standard practices the probability of detection analysis for ($\hat{a}$) versus (a) data (ASTM E3023-15, 2015).

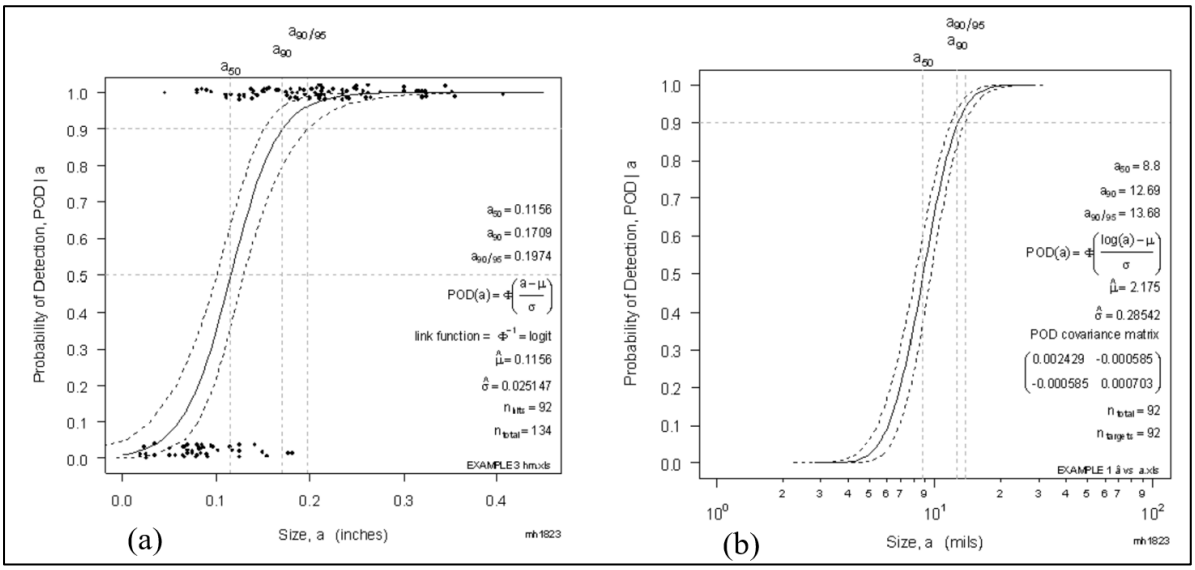

Figure 1.7 (a) POD curves for hit/miss data, (b) POD curves for signal response data
Taken from Annis (2009, p. 94 &123)

The Relative Operating Characteristics (ROC) curves or the Probabilities of False Alarm (PFA) curves are probabilistic criteria other than the POD curve. They are essential to determine the performance of an NDT inspection system. PFA is the probability that detection threshold is exceeded when no flaw is present (for example, due to strong background noise). An excessive PFA can lead to unacceptable rejection rates in the inspection process. An agreement is therefore necessary during the description of the inspection process between PFA and POD. Appropriate information about the noise characteristics is required to estimate the PFA and fix a sufficient threshold. Noise has two sources in the ultrasonic inspection; (a) Electronic noise due to the acquisition chain, generally of low level, indicating that the system works correctly, and (b) Ultrasonic backscattering noise due to material microstructure (Chapuis et al.,2017).

For building a typical POD curve, a large set of specimens is required having a range of defect sizes. For any NDT method very small defect sizes are considered not detectable, and very large defect sizes are considered as detectable in most of the experiments done in a wide range of defect sizes. Therefore, POD curve is critically studied for intermediate size range for given

settings where they can either be detected or not detected with varying probability. If we assume prior knowledge of such an intermediate range, a large set of specimens in this range is required to have a precise POD curve. One of the best works in experimental POD (Kurz et al., 2013) worked on various materials commonly used in nuclear facilities. They created 128 artificial and realistic defects; intact samples were also included. Intentionally induced intergranular stress corrosion cracking and fatigue cracking were used to create realistic defects. The sizes of defects were distributed asymmetrically with 3 mm as the most frequent size. The defects were validated through radiography and destructive testing. The inspections were carried out using phased array and TFM, subsequently the results were analysed using both hit/miss and ($\hat{a}$) versus (a) approaches. Based on the represented diagrams, $a_{90/95}$ for the hit/miss analysis is much larger compared to that of signal response analysis. In addition, POD curves of two different ultrasonic methods showed better capability of TFM in sizing the defects.

1.5 Review of previous research on advanced ultrasonic testing

(Ginzel et al., 2011) Evaluated the capability of TOFD and phased array UT techniques on T-shaped welds. The study stated that EDM notches could closely simulate surface-initiated fatigue cracks, but more natural processes should be employed for subsurface defects. Considering the DNV RP-F118 standard ((DNV), 2010), they suggested using welding parameter adjustments and welded-in flaws instead of ceramic inserts. In this study, rubber replicas were used to characterize surface crack dimensions. Furthermore, the accessibility of both sides of the T-joints helps to inspect each defect in two different conditions, which leads to more statistical data on detection and sizing. Each test was repeated at least two times to check the repeatability of the NDT techniques. Destructive tests using saw-cuts were carried out to find the actual size of the induced defects. According to DNV RP F-118 ((DNV), 2010), if the data shows a high dispersion rate, it is recommended to divide the defects into several classes based on their type and location; POD curves would be created for each class separately.

(Zhang et al., 2011) Studied the PAUT modeling of defects in the weld of turbine runners. Several typical defects were set in the weld joint to simulate all defects. The parameters of defects were the thickness (T) of defects location (ranges of 20 to 50 mm) and the tilt angle (θ) of crack (0 to 50 degrees). All cracks' width were 5 mm, and each type of crack has ten different sizes (1 to 10 mm in length). The detection rate of cracks near to edge (thickness of the blade is 20 mm) is high and cracks whose length is more than 1mm can be fully detected. However, the detection rate of cracks far from the edge (the thickness of the blade is 50 mm) is lower. All defects over 2 mm in length can be 100 percent detected; only vertical crack is hard to find.

(Xiao et al., 2013) Studied ultrasonic system for quality testing of weld joints in turbine runner. The distribution of defects depends on the thickness of the testing section, and main types of defects consist of (1) the lack of penetration on flange side, (2) the lack of fusion on the side wall, and (3) cracks around weld toe. All cracks were 5 mm in length along the axis of the welded joint, and 1 to 10 mm in length along the direction of their deflection angle. They found that the system has high testing accuracy, and the measuring error of defects in length can be held with 5 mm.

(Zhang et al., 2014) Studied the phased array ultrasonic testing of hydropower turbine runner welds. Y-type Blocks including artificial defects were made and used to demonstrate the capability of detection. The size and the position of each intended defect in the Y-type block and their horizontal distance and depth in PAUT are seen in Table 1.1. All intended defects in the zone covered, were detected and identified. However, an inspection using a small element straight beam probe is also needed for the defects at the near surface of the weld.

Table 1.1 Intended defects

Row	**Defect type**	**Defect position**	**Defect size (mm × mm)**
1	LOF	B-flange side, A and B web side	10×30
2	LOF	Near-surface	5×5
3	LOP	Middle	2×3
4	Crack	Weld toe, HAZ	10×30

(Boukani et al., 2018) Studied the abilities of different NDT techniques in hydro turbine runner joints to detect and characterize welding flaws. They investigated some T- joint samples in martensitic stainless steel manufactured according to the requirements of turbine runners. They studied the occurrence of one defect, which was slag inclusion at the toe of the weld. Because of size, position, orientation, the calibration process, and the NDT method limitations, there is a possibility that any of the NDT techniques in hydro turbine runner joints may not be able to detect some flaws. The results showed that PAUT is one of the most efficient methods due to the better access to the weld joint, the lower time amount required for the calibration and inspection (no wedge change), and its capability to characterize the flaw better.

(Ginzel et al., 2015) Describe how the FMC and TFM have advanced to provide superior displays and analysis tools for production pipeline weld inspections. They compared the TOFD, pulse-echo, and TFM methods. Pulse-echo imaging cannot resolve three separate indications. However, TOFD can detect three main arcs associated with the indications; the lower tips cannot be resolved for useful vertical sizing. The TFM image can be used to estimate flaws heights and ligaments. They demonstrated several advantages of using the new FMC/TFM AUT system: easy setup, simplicity of analysis, improved detection, sizing capabilities, and improved resolution for subsurface and ligament indications.

(Chatillon et al., 2015) In the 2014 Benchmark trials used TFM modeling implemented in CIVA simulation software. Their work aimed to evaluate the ability of CIVA UT module to reproduce the FMC acquisitions and multimode TFM images. The simulations and measurements were carried out on two steel blocks, one in carbon steel and another in stainless steel 302. Samples contain several embedded and back wall breaking notches of different heights. Also, each mock-up contained a 2 mm diameter side drilled hole to provide a reference echo. An excellent agreement between the experimental TFM images and the simulated images was observed in all the cases.

(Ewen et al., 2017) Compared TFM, PAUT and destructive testing (Macrograph) on pipeline girth welds. There were no tip echoes in their data set of TFM images. They simply used the -6dB beam boundary method on the TFM images. Overall, the sizing results from TFM (flaw, depth, and height) proved to be more precise than the conventional PAUT, and PAUT tends to oversize compared to TFM and destructive testing results.

(Reverdy et al., 2018) Present the application of the TFM inspection of samples containing hydrogen damages (HIC and HTHA). Until recently, it has been challenging to detect HTHA damages with the available NDT technology. However, irrespective of the size of HTHA damage, high sensitivity to the detection of microcracking with a good Signal-to-Noise ratio has been observed using TFM techniques.

(Hollette et al., 2018) Illustrated application of TFM to detect cracks around fastener holes. In complex shape assemblies currently used in aeronautics, it can be tricky to be able to detect cracks around fastener holes. TFM allowed a straightforward interpretation. Entirely all the defects are very well detected and sized with SNR similar to the previous setup in phased array. Also, they used different propagation modes (TT, TTT, TTTT).

1.6 Example of TFM sizing and accuracy for POD study

Upon an extensive search of different codes (MIL-HDBK 1823A, 2009; DNV-GL ST F101; 2017; ASME Art. 14; E2862-18, 2018; ASTM E2862,2015; ENIQ Recommended Practice #5), we found that for PODs, there are no rules to determine flaw size except for DNVGL-ST-F101, which requires cross-sectioning samples to determine flaw size by metallographic analysis. In accordance with POD standards, there is an assumption that the size given by the manufacturer is usually taken as the true value. However, flaws offered by flaw sample manufacturers have sizing uncertainties.

Recent developments in ultrasonic TFM have indicated that it can provide good accuracy in flaw sizing, which could improve the reliability of POD and save time and expense involved

in destructive tests or micro-CT X-ray verification of flaw sizes. As we discussed before, the TFM has been demonstrated to provide reasonable accuracy in many cases (Ginzel et al., 2022). When the NDT test method is being evaluated for reliability (and the test method being evaluated is not TFM), it may be feasible to use a TFM-determined flaw size as the truth value for POD purposes. Several studies have been carried out suggesting that the flaw size estimated by TFM is accurate.

(Spencer et al., 2018) Investigated the effectiveness of PAUT, TFM, and advanced focusing method (AFM) techniques for detecting and sizing both planar and volumetric flaw types. TFM experimental data compared to typical ultrasonic phased-array results and TFM inspection simulations. They used two carbon steel plates, first with intentionally welding flaws and the second sample un-welded containing EDM notches with vertically oriented (Wide:0.41mm and various deep). Following, Metallographic cross-section information was then compared to the ultrasonic scan data. The results comparison of the actual scan data and modeling data for the LOF flaw was very good. Also, technique comparison was conducted on the EDM notch samples to determine how each technique would perform on planar vertical flaws. Results revealed that the shear wave modes provided the best overall imaging for the notches, and the AFM technique provided better imaging of the notch tip than the standard FMC/TFM technique. The notch tip and notch corner trap can be seen in the results, but the notch face is not imaged by either PAUT or AFM. They reported that PAUT provided good flaw detection due to a larger beam. However, the larger beam made flaws appear larger than the actual size reducing resolution. They suggested PAUT for flaw detection and localized FMC/TFM to obtain accurate sizing. The smooth fracture face of vertical flaws such as EDM notches was not detected with the TFM and AFM.

(Rachev et al., 2018) sized notches over a range of 1 mm to 8 mm in height. By suitable selection of aperture (larger was better) and using a Plane Wave Imaging (PWI) acquisition, they achieved better than 0.5 mm accuracy for all but the largest notch.

(Peng et al., 2018) ran a similar test of TFM on a fatigue crack in aluminum. They also found an apparent error between the optical image of the crack on the surface and the TFM image attributable to the curved crack profile. This test demonstrated sizing errors less than 11% for surface breaking fatigue cracks 1.95 to 2.81 λ at 5 MHz (i.e., 2.50–3.6 mm) and 2.81–7.34 λ at 10 MHz (i.e., 1.80 – 4.70 mm). So, 11% of 3.6 mm for the 5MHz condition would be 0.39 mm, and 11% of 4.7 mm for the 10MHz condition is 0.52 mm.

(Volf et al., 2020) used TFM imaging to monitor crack growth in a fatigue test and compared the TFM depth of the crack to the values indicated by the clip gauge. During the test, TFM appeared to oversize the crack by 1-2 mm compared to the clip gauge. However, after the test was completed and the sample opened to expose the crack profile along the length, the final depth estimate from TFM was seen to be within 0.06 mm of the physical measurement. What appeared to be overestimated was due to a curved crack front where the crack tip had propagated deeper than was indicated by the clip gauge.

(Holloway&Ginzel, 2021) implemented the summation of TFM images using a commercialized software package which was used to overcome the limitations identified by (Sy et al., 2018), where certain combinations of modes improved flaws depending on the flaw location and orientation. Using this technique, the standard deviation of the sizing error on the real crack was 0.22 mm, and a maximum oversizing error of 0.6 mm.

When it comes to estimating the life of a structure, fracture mechanics experts deal with three types of uncertainty (material properties, stress field condition, and flaw detection and sizing capability of the inspection system) upon which life assessment calculations are converted into a probabilistic process (Ginzel et al., 2011; Thibault et al., 2014). Loading conditions and fatigue-related material properties have been studied in detail previously as two inputs of life estimation models while flaw characteristics are fed into the developed models as assumptive values as the third input (Gagnon et al., 2012; Gagnon et al., 2014).

In conclusion, due to the tendency of the hydro-turbine industry to move toward the damage tolerance approach, despite all the previous studies, there is an essential need to extend the knowledge on the characteristics and detectability of the welding flaws in runner joints. In addition, the knowledge of the POD curves required by fitness-for-service assessments is mostly absent for structures such as the hydroelectric turbine industry. This research aims to improve flaw detection and sizing using UT technology for hydraulic turbine runners welded joints. Then, evaluate the reliability of NDT methods for the inspection of welded joints in turbine runners. Furthermore, the three array configurations showing the highest POD during our trials with a mock-up T-joint have been applied to a real turbine runner that is kept in a facility as a training component. In addition, we propose an inspection strategy that would provide a high POD with good flaw sizing capability for real turbines. Finally, this research considers using TFM as a tool to provide accurate flaw sizing for POD determinations. The outcome of this research is an important source for preparing the input data for future POD studies and fatigue models.

CHAPTER 2

CAPABILITY OF ADVANCED ULTRASONIC INSPECTION TECHNOLOGIES FOR HYDRAULIC TURBINE RUNNERS

M. E. Bajgholi [a], G. Rousseau [b], M. Viens [c] and D.Thibault [d]

[a, c] Department of Mechanical Engineering, École de Technologie Supérieure, 1100 Notre-Dame West, Montreal, Quebec, Canada H3C 1K3
[b, d] Hydro-Québec's Research Institute, Varennes, Quebec, Canada, J3X 1S1

Paper published in *Applied Sciences*, May 2021

Abstract

This paper presents the results of a project aimed at evaluating the performance of ultrasonic techniques for detecting flaws in Francis turbine runners. This work is the first phase of a more ambitious program aimed at improving the reliability of inspection of critical areas in turbine runners. Francis runners may be utilized to supply power during peak periods, which means that they experience additional load stress associated with start and stop sequences. Inspection during manufacturing is then of paramount importance to remove as much as feasible all flaw initiation sites before the heat treatment. This phase one objective is to collect initial data on a simplified mock-up and then to compare the experimental ultrasonic data with the results of simulations performed by CIVA, a computer simulation package. The area of interest is the region with the highest stress between the blade and the web. A welded T-joint coupon made of UNS S41500 was manufactured to represent this high-stress area. During the FCAW welding process, ceramic beads were embedded in the weld to create discontinuities whose size is in the critical range to initiate a crack. Inspection of the material was carried out by various non-destructive testing (NDT) methods namely conventional pulse-echo, phased array, total focusing method (TFM). With these results, detection rates were obtained in order to compare the effectiveness of each method.

Keywords: non-destructive testing; defect detection; ultrasonic testing; phased-array ultrasonic testing; detection of rate; hydroelectric turbine runner

2.1 Introduction

In the province of Quebec, hydraulic turbines produce the vast majority of the electrical power (Huertas-Hernando et al., 2017). Multi-pass flux-cored arc welding (FCAW), used for turbine runner joints, naturally generates certain discontinuities such as slag inclusions, lack of penetration, macro shrinkage, and thermal stress cracking. Welding discontinuities and dynamic stress concentration result in a higher failure probability in Francis turbine runners (Boukani et al., 2014; Boukani et al., 2018). In the runner, the maximum stresses are located along the welds near the trailing edge of the blades. The critical weld region extends to approximately 300 mm from the trailing edge for both blade-to-crown and blade-to-web welds.

The Hydro-Quebec Research Institute (IREQ) has developed a life estimation model based on the distribution and size of structural discontinuities in turbines to ensure equipment reliability and control production costs. In this model, the probability of a cracking event at any given point in time depends on the joint probability of stress and defect being above the limit defined by the material properties (Gagnon et al., 2013). Indeed, if discontinuities remain undetected, they might initiate fatigue cracks under dynamic, in-service stresses, leading to unplanned failure, which itself results in high repair costs and long downtime. It is desirable to supply the life estimation model with accurate data regarding the distribution and size of discontinuities present in the turbine to reduce the unplanned outage costs. This type of data is typically determined using NDT methods to detect, locate, and size flaws (Boukani et al., 2018).

NDT is the development and application of technical methods to examine materials or components such that the pieces are not destroyed and their future usefulness and serviceability remain (Bray & Stanley, 1996). There is a wide range of NDT methods based on the physical principles of electromagnetic radiation, sound, and other inherent properties of the materials. The techniques selected should consider safety, economic, efficiency, and time factors (ASTM

E1316-13, 2004). Ultrasonic testing (UT) is a suitable method for detecting and sizing flaws embedded within or growing from inaccessible surfaces. Ultrasonic waves can propagate through thick solid parts (Cheeke, 2017). Therefore, UT is suitable for flaws far beneath the inspection surface, unlike methods that can only detect defects on, or very close to, the inspection surface, e.g., Eddy current testing or methods that detect flaws connected to the inspection surface, such as visual methods and penetrant testing (Shull, 2002). When defect assessment calculations require a value for how deep the defect has grown, ultrasonic testing is the primary desired method. It is used to detect various types of flaws, such as cracks and inclusions in a wide range of materials, compared to magnetic particle testing methods, which require the component to be ferromagnetic. Ultrasonic waves are inherently safe compared to radiography methods, which use ionizing radiation and thus require multiple protection types (Ahmad & Bond, 2018; Felice & Fan, 2018).

The basic NDT methods, such as visual testing (VT), ultrasonic testing (UT), penetrant testing (PT), and radiography (RT), are usually used to inspect hydraulic turbine runners. However, there are difficulties involved in detecting internal flaws in complex geometries, such as the runner's weld joints. Thus, hydraulic turbine runners are generally inspected using different ultrasonic inspection methods (Boukani et al., 2018; Katchadjian, 2004; Xiao et al., 2013; Yicheng et al., 2011; Zhang et al., 2014). Few studies have been performed on the inspection of hydraulic turbine runners with ultrasonic phased array. However, the published studies did not focus on the high-stress area, used artificial flaws embedded in a weld mock-up, and did not consider the material's properties (Xiao et al., 2013; Yicheng et al., 2011; Zhang et al., 2014; Boukani et al., 2018) worked on the capability of different NDT methods and the effect of microstructure on the acoustic properties of steel grades widely used for the manufacturing of hydroelectric turbine runners, these studies concluded that phased array is a very effective technique.

The current study goes further by including the total focusing method (TFM), and compares conventional, phased array and TFM techniques in order to assess their performance in detecting flaws in the trailing edge of a runner blade. The work focuses on ultrasonic inspection

techniques applied directly to the blade because they conform to current fabrication and in-service inspection methods. Simulations and experiments are used to identify the best practices to reliably inspect the blade high-stress regions.

This research, as part of a large project, focuses on the detection and characterization of flaws in the welded joints of hydroelectric turbine runners, as they are located in the most critical zones in terms of fatigue failure. Loading conditions and fatigue-related material properties have been previously studied in detail as two inputs of life estimation models (Gagnon et al., 2013, Gagnon et al., 2014), while flaw characteristics are still fed into the developed models as assumptive third input values. The current research aims at providing IREQ with a flaw data reliability index (both measured and simulated) for the life estimation model.

2.2 Experimental procedure

2.2.1 Manufacturing process description

Inspection of turbine runner welds is an essential aspect of electric-generator units' in-service reliability (Gagnon et al., 2013). In-service inspection data from installed runners show that fabrication flaws are found in the weld joint near the blade's trailing edge. Flaws were discovered by applying a phased array ultrasonic technique using a small wedge to provide suitable contact on a curved surface and good volumetric coverage with an azimuthal focal law type. Typically, flaws are within 30 mm of the trailing edge and in the weld reinforcement that smooths the stresses at the blade's end. Some flaws were found isolated, but clusters of up to 7 indications were also observed. The presence of flaws at the edge of the blade in the area of high service stress is considered in the current investigation. This area is where the start and stop of welding occurs, and thus it is not surprising to observe in-situ point-like reflectors in

the weld reinforcement. A T-joint sample was manufactured in martensitic stainless steel (UNS S41500) in accordance with the manufacturing requirements of turbine runners. The T-joint geometry often mimics a turbine runner's trailing edge, with both edges being 25 mm in thickness. The base plate is 60 mm thick and provides the same ultrasonic path for an inspection performed from the turbine web. The weld cap and blade ends are ground to obtain a smooth finish with a curved radius of 25 mm. The preparation is a J-shape grove with a 3 mm gap between the web and blade. Welding was carried out using a multi-pass FCAW process and EC410NiMo electrodes (same ultrasonic properties as UNS S41500). The study selected the dimensions of the joint to match a typical turbine runner assembly. Typically, 34 passes are required to fill the joint.

2.2.2 Flaw size and distribution

For technical manufacturing constraints imposed by the small size of the flaws examined by the current study (e.g., size of flaws between 1 mm and 5 mm), the scope is limited to inclusion flaws. Inclusions designate the incorporation, in the weld bead, of a foreign compound. Besides, the case of metal inclusions is studied to control the size of the flaws and the repeatability that are defined by the imprisonment of a foreign particle in the metal's mass. These flaws were relatively present in welded joints in laboratory samples that made inclusion a representative flaw for the current study. Spherical beads of a specific size are integrated into the weld fusion to simulate an inclusion. The choice of spherical shape is justified by limiting the external error factors that are linked to the defects' positioning and orientation.

To conduct the study, the requirement for precision on the defects' size, the obligation to respect an acceptable level of repeatability, and the flaws spherical shape guided in choosing ball bearings as the defect to be included. The extreme thermal conditions and the electric arc passage, during welding, close to the balls, forced the researchers to choose ceramic balls that were more resistant to extreme temperatures. This is because they interfered less with the heat-welding arc because of their non-conductive electrical properties.

The study considered three types of ceramic balls; alumina oxide balls (Al_2O_3), zirconia balls (ZrO_2), and silicon nitride balls (Si_3N_4). In this regard, all three types of balls were tried to determine the best ones for the study. After a series of tests, the study found that the alumina oxide (Al_2O_3) balls were to be avoided. This is because, despite the fact they offer a higher operating temperature compared to silicon nitride (Si_3N_4), they did not resist the electric arc passage and exploded (Zhang et al., 2019). Therefore, the study chose the silicon nitride balls because they were stronger and kept their original shape.

During welding, holes have been drilled in the weld pass to implement artificial flaws at known locations, as shown in Figure 2.1. Ceramic beads are inserted into these holes, and the holes are filled by welding. Thirty ceramic beads are distributed in the weld of the T-joint sample. They were of either 1, 2, 3, 4, or 5 mm in diameter (6 beads of each size). This range of discontinuity sizes reflects the critical range to initiate a fatigue crack. A three-millimeter diameter flaw has the critical size to develop a fatigue crack under cyclic loading from stress calculation. Beads are located within 75 mm from the edges of the sample in order to mimic the situation observed on in-service runners.

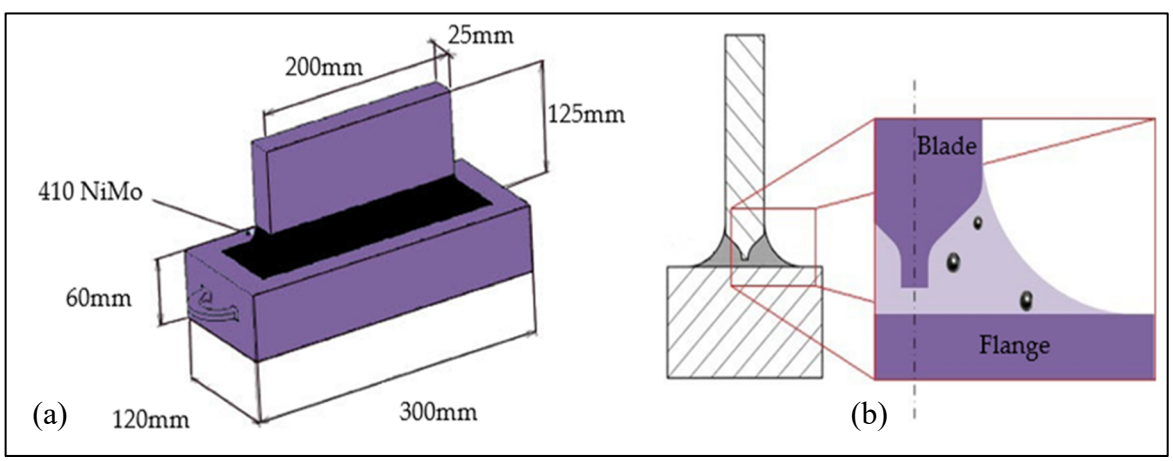

Figure 2.1 The experiment setup overview (a) Dimension of T-joint sample, and (b) Flaws implementation

2.2.3 Conventional ultrasonic testing (UT)

Four experienced UT practitioners with CGSB (Canadian General Standards Board) level 2 or 3 certification in Ultrasonic Testing did inspect the T-joint sample. The study performed inspections as per the Canadian Standards Association (CSA) W59, Welded steel construction (CSA W59-13, 2013). The study used a flat, 2.25 MHz 1/2 in round transducer mounted on a refracting wedge to produce a refracted shear wave beam at either 60° or 70° from normal. The conventional ultrasonic testing inspection was carried out using Olympus Epoch 600 and Krautkramer USN 58L Ultrasonic Flaw Detectors, as shown in Figure 2.2. All indications, rejectable or not, were to be reported.

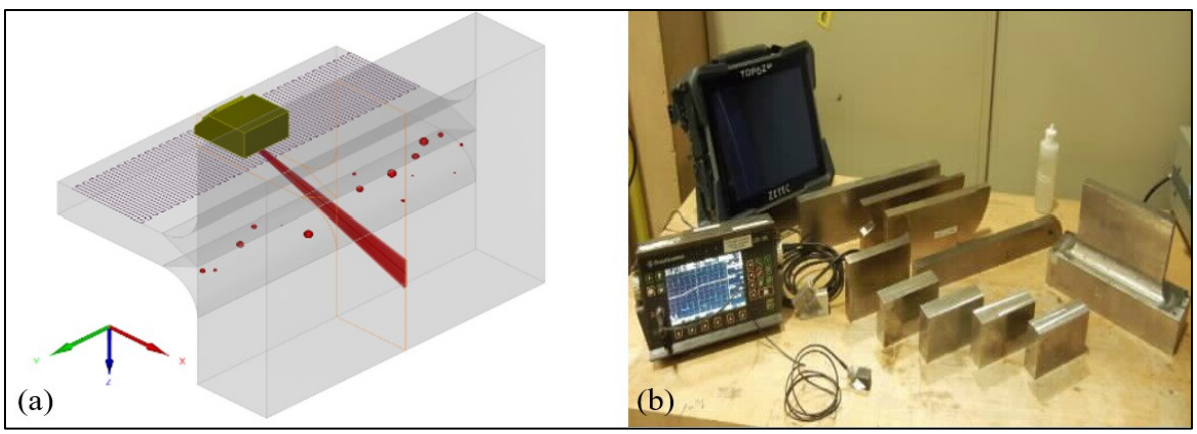

Figure 2.2 Simulation and experimental setup (a) Raster scanning from both blade surfaces, and (b) Ultrasonic Testing Equipment

2.2.4 Phased array ultrasonic testing (PAUT)

The scan plans prepared to inspect the regions of interest were devised according to standards. These scan plans indicate the required refracted beam angle and the probe standoff positions to ensure appropriate volume coverage. Wherever possible, welds shall be inspected from both sides of the blade (ASTM E2700, 2014; BS EN ISO 17640-2018; ISO 13588, 2019). The ultrasonic system was calibrated using standard blocks to ensure the repeatability and reliability of experimental data (ASTM E2700, 2014; CSA W59-13, 2013). Phased Array (PA)

transducers can be referred to as multiple small conventional transducers (elements) that are housed within a single unit (Drinkwater & Wilcox, 2006). Each transducer can be pulsed individually; by varying the delay between elements, the individual waves' constructive interference will occur at the desired angle, which enables the focus to be achieved. The phased array technique is a beamforming method that relies on emission delay to shape the beam in terms of refracted angle and position of the near field. A set of delays required to create a specific beam angle and focus point is called a focal law (Ginzel & Johnson, 2008; ISO 19675, 2017; PAUT, Basic Theory for Industrial Applications, 2010; TWI PAUT, 2017). By electronically changing the delays rapidly, the focal law group can produce an azimuthal scan with a starting angle, a final angle, and an angle step. For example, a focus group can use the following set of angles: starting at 40°, an increment of 1°, and stop at 70°. A phased array probe has limits for beam formation; hence, both wave physics and array limitation must be taken into account. In the experiment, the wedge nominal refracted angle is 55 shear wave and the array of 5MHz, with 0.6 mm element spacing, produces an acceptable beam profile in the range of 40° to 70° shear wave (Ditchburn & Ibrahim, 2009; Ginzel, 2013; Richard et al,.2018). The PAUT inspection was carried out using TOPAZ 64, as shown in Figure 2.2. The transducers were all linear Phased Array Ultrasonic probes operating at a center frequency of 5 MHz. The three models used in these inspections differ mainly in terms of the number of elements in the array, namely 12, 16, and 64 (Table 2.1). They were all used to perform manual or linear-encoded sectorial (Azimuthal) scans ranging from 40° to 70° from normal incidence, as shown in Figure 2.3. Data acquired along two different scan indexes (probe standoff positions) were combined to cover the whole volume of interest in a single file to analyze.

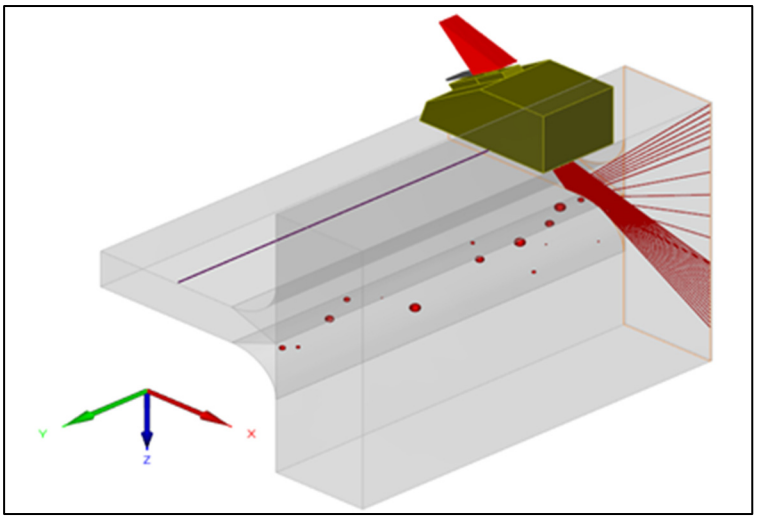

Figure 2.3 Sectorial scanning from both blade surfaces

Table 2.1 Used PAUT probes

Probe	**Frequency (MHz)**	**# Element**	**Aperture (mm)**	**Elevation (mm)**	**Wedge Angle (°)**
5L12-51S	5	12	7.2	10	51SW
AM5M-55S	5	16	9.6	10	55SW
LM5M-55S	5	64	38.4	10	55SW

The study developed an inspection configuration in accordance with the number of transducer elements and the focal group's capability to insonify the whole weld volume on the opposite face. The inspection strategy involves inspecting the direct skip to prevent beam spread and avoid ghost echoes caused by reflection from the weld cap's curved radius. With a direct skip inspection, the ultrasonic configuration is simpler by mainly focusing the beam for a metal path range of 10 to 50 mm. These permit the use of 16 elements per focal law and use small footprint wedges or a 64-element transducer's front elements to minimize the standoff distance. With these configurations, the focal group's high angle can hit the T-joint center where it meets with the web, and the lower angles can probe most of the weld cap radius. Only a small hidden

area exists and cannot be covered with angle beam inspection from the blade. The only inspection technique that can provide 100% coverage of the weldment is from the web using a normal incidence wedge. Inspection from the web was not attempted because this surface is not accessible during an in-service inspection. The following conclusions can be drawn from the results obtained;

1. Flaw resolution increases with the number of active elements used in the array.
2. However, the use of 32-element does not improve inspection performance. This finding could be attributed to the impact of a larger active aperture on the generated ultrasonic beam's characteristics. Indeed, the beam's exit point is further away from the weld's edge in this case. Besides, the beam is larger, and its power is spread over a larger cross-section, thus reducing the echo reflected by a given flaw. Therefore, focusing has been added to this configuration to narrow down the beam size in the range of interest.
3. Linear-encoded PAUT scans can distinguish two closely spaced flaws more easily than manual inspection. You can see example of PAUT results in Figure 2.4.

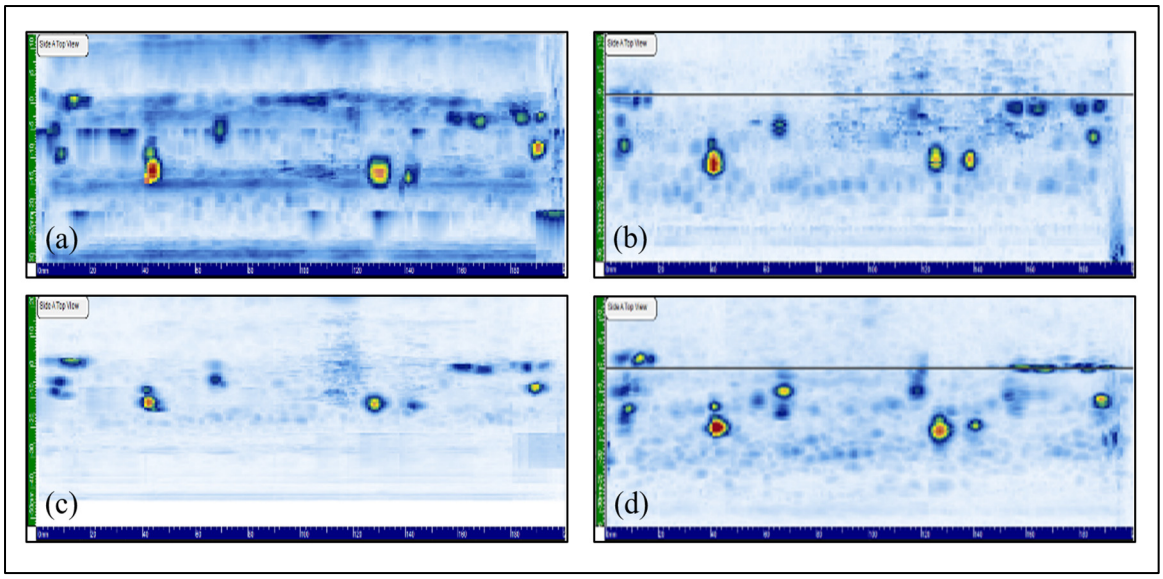

Figure 2.4 Example of PAUT results (Side A, Side view) (a) 5L12 (12-element): Merged data (-25 and -40 mm index), (b) LM5M (16-element): Compound scan (45-64) at -25 mm index, (c) AM5M (16-element): Merged data (-25 and -40 mm index),and (d) LM5M (32-element): Scan at -25 mm index with 22 mm deep focus

2.2.5 Total focusing method (TFM)

Total Focusing Method (TFM) is still part of the Ultrasonic Testing (UT). This is because it uses the same basic principles as PAUT as well as the conventional UT (Holmes et al., 2005; Richard et al., 2018). In this study, the new phased-array technique called the TFM is included in the test matrix. Unlike the sectorial scan described previously, this technique is not a beamforming method. The TFM is an imaging technique that processes elementary A-scan data to extract the amplitude for a determined path from a firing to a receiving element (Zhang et al., 2013). After multiplexing all elements as emitter and receiver and delaying and summing all the required amplitude, a data point in the region of interest is assigned an amplitude. The algorithm is simple, but the memory and processing burden increases geometrically with the increase in the number of elements of an array and the size of the area of interest. As a result, it is simple to achieve the configuration of TFM because once the transducer, the wedge, and the mode are defined, the user creates a rectangular area of interest, which is subdivided into a grid. In this regard, the grid spacing is the critical variable, which is normally smaller than one-

fifth of the wavelength. However, if the spacing is above this value, the measured amplitude fails to be within 2 dB of the true amplitude, hence, producing unreliable results. All experiments respected the wavelength criteria and opted for values that had a spacing of at most one-tenth of the wavelength (Ditchburn & Ibrahim, 2009; Principles FMC & TFM in Ultrasonic Inspections, 2017; Richard et al., 2018).

The TOPAZ 64 includes a beam simulation amplitude map function that helps to optimize all the parameters. Therefore, with the use of TFM, the region of interest covered the whole weld on the opposite side of the entry surface (Holmes et al., 2005). In this regard, the sample was to be tested from both sides of the blade in order to fully cover the weldment. The experimental work used a 64-element linear array probe at a nominal frequency of 5MHz. The study used two wedges, one for generating shear wave and one for generating compression wave and performed both manual and encoded scans. The linear encoder scan is done with the wedge's front abutting the weld cap, which produces a scan index of −25 mm. For manually delivered inspection, the technician has the freedom to make transversal, lateral, and skewing movements to locate discontinuities and peak them. The T-joint was examined using T-T and L-L direct modes with linear encoded scans and manual inspection. The T-T and L-L modes were used in the experiments because they produce a good amplitude response from a volumetric discontinuity. In this study, before starting the sample's inspection, the 3 mm SDH was used on the martensitic sample (same material properties) for TFM model calibration. From these results, we obtained the following conclusions:

1. TFM results appear clearer, with fewer spurious indications and better-defined flaw geometries.
2. The Longitudinal-Longitudinal reconstruction mode seems to give slightly better results than the Transverse-Transverse mode.
3. We obtained a slightly better detection rate with manual TFM as compared to the encoded one. We suspect that this is due to the operator's ability to minutely adjust the

probe's position to improve the signal to noise ratio on the testing unit display. An example of TFM results (with two different reconstruction modes) compare with 32-element PAUT result is observed in Figure 2.5.

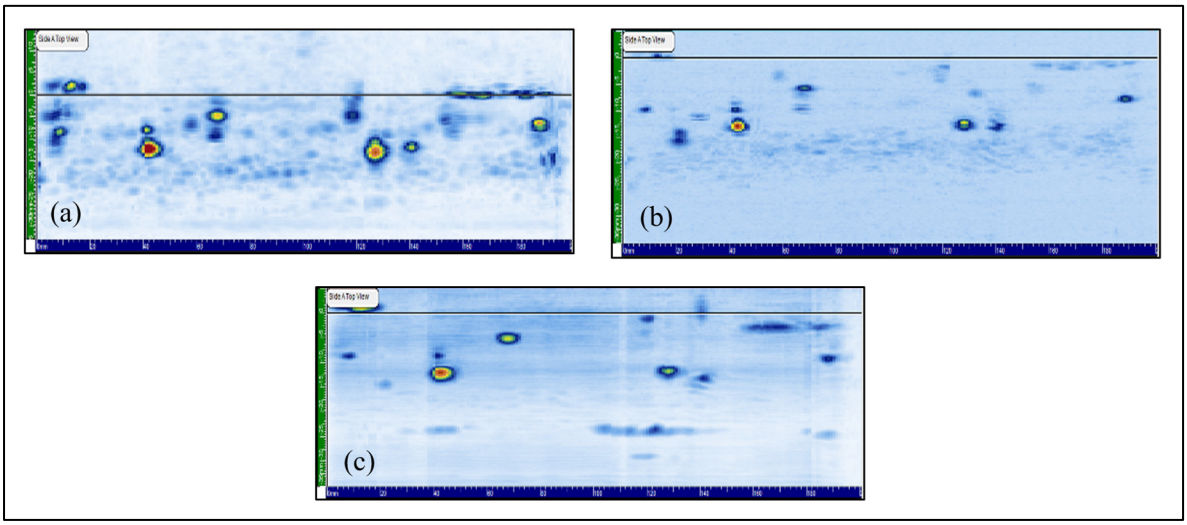

Figure 2.5 Example of TFM results (Side A, Side view) (a) LM5M (32 elements): Sectorial scan at -25 mm index with 22 mm deep focus, (b) LM5M (64 elements): FMC scan at -25 mm index with encoder, direct TFM T-T , and (c) LM5M (64 elements): FMC scan at -25 mm index with encoder, direct TFM L-L

2.2.6 Experimental detection rate

The performance of the different ultrasonic inspection techniques tested are compared in Figure 2.6. Obviously, among all these techniques, conventional UT results have the lowest detection rate. This could be because the fixed-angle beam can miss a flaw more easily than with ultrasounds impinging the flaw from different angles. Although the inspection is carried out to a well-defined standard, the detection rate is highly dependent on the operator. The certified practitioners reported between 7 to 16 flaws out of the 30 embedded in the weld, with an average reporting of 11 flaws.

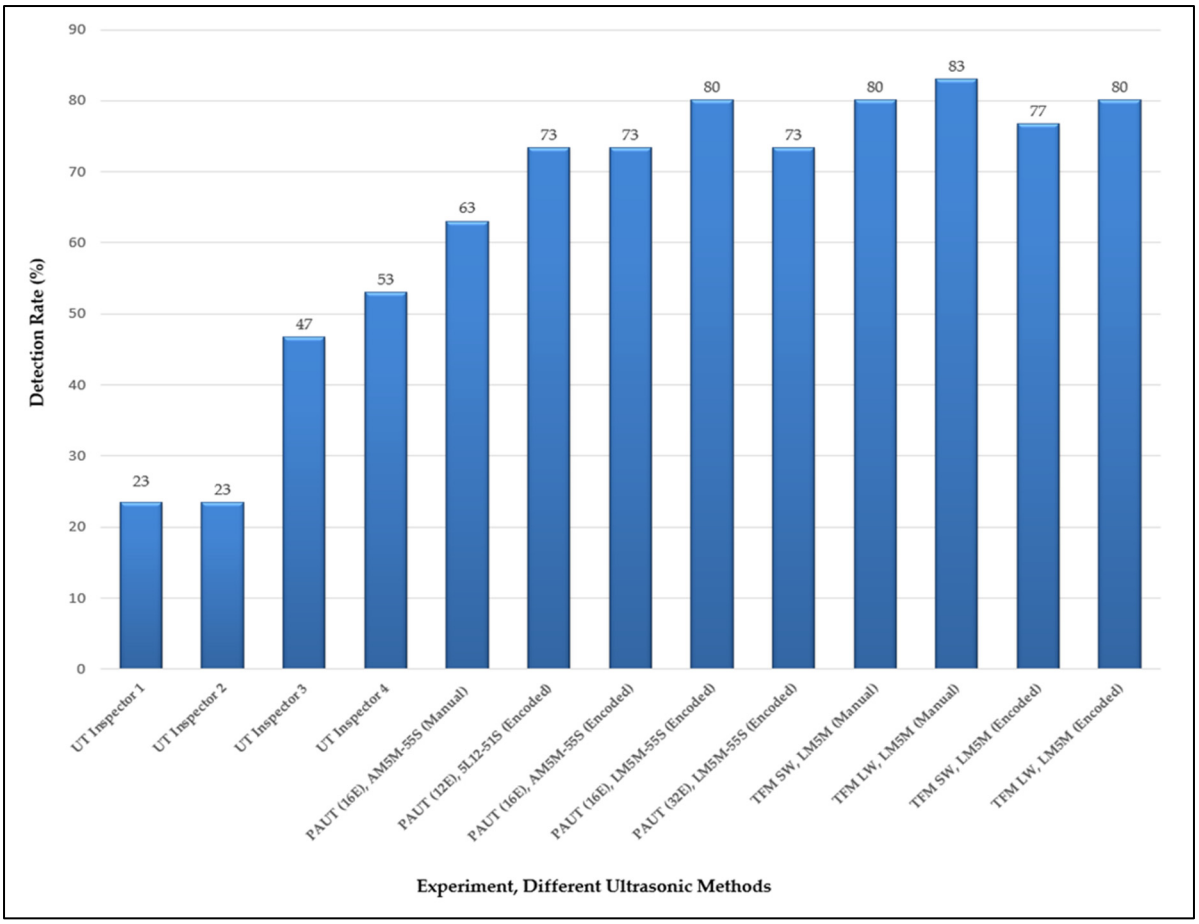

Figure 2.6 Experiment, different ultrasonic methods

Several difficulties were observed with manual testing; (a) Challenging to report a flaw nearby a larger reflector with all the attention on the large reflector, (b) Manual reporting of flaw position is cumbersome and leads to errors, (c) Low amplitude signal just above the rejection threshold is easily discarded, (d) the report's quality is directly related to the inspector's diligence in taking clear and precise notes. If the report is written several days after the test, the notes' quality is of paramount importance (Chaplin, 2017).

Manual phased array inspection suffers some of the limitations observed with a fixed-angle beam probe. The detection is done on the fly, and the flaw's information is written during the

inspection. If the sample has several flaws, the technician can get confused when measuring and reporting flaws. However, one of the advantages of manual PAUT inspection is the freedom the operator has to explore a suspected flaw by executing various probe motion; pivoting the transducer or orbital movement to reveal the target's volumetric features. The manual phased-array inspection provided the highest maximum amplitude measured and revealed flaws hidden in the trailing edge weld reinforcement. However, even if the manual phased-array found flaws hidden in the geometry, on average, it detected fewer flaws than the linear-encoded phased array.

The linear encoded inspection provides repeatable scans, and flaws with low amplitude are detected more readily by comparing the local base noise to check for any localized increase that would reveal a flaw. Close flaws may be separated, and when using the projection views, their location and separation can be measured. Generally, the aperture of 12 and 16 elements produced a reasonably good detection rate, and the small footprint of the 12-element transducer allows it to cover the center of the weld. As the aperture increases, the stand-of distance increases, and the weld's center is no longer covered. This explains why the 32-element tests did not perform better than the 12 or 16 element tests despite having a smaller beam diameter and a more extended working range covering the whole weld path.

The TFM method produced a higher detection rate, slightly better than a sectorial scan. One advantage noticed during the test is the operator can readily size the diameter of the flaw. This helped identify small beads from noise since the shape was maintained while probing the area. The TFM could also probe nearer to the surface and provided good coverage of the whole weldment. There is no dead zone compared to a 32-element sectorial scan. In our sample, the material has a low noise level suitable for a TFM inspection, which explains the high detection rate obtained with the study sample. Another advantage of the TFM is flaws could be categorized in apparent size or apparent reflective features. Small ceramic bead produces a specific round-shaped signal area proportional to their size, while larger beads showed either oriented facets or multiple facets surrounding the bead. TFM provided details about the reflective surface's nature, while a sectorial scan did not provide any hints about the flaw's

small features. A multi-element probe is, therefore, a better candidate in terms of detection rate. Although the difference is not huge, TFM seems to perform slightly better than standard PAUT sectorial scanning.

The optimum inspection strategy in order to reveal the most implanted flaws is to perform the inspection in two steps:
Step 1: linear encoded sectorial scan with an aperture of 16 elements or linear encoded TFM scan.
Step 2: manual inspection of the trailing edge and weld reinforcement using either a sectoral scan with an aperture of 16 elements or a 64-element TFM scan. In practice, because a real runner's trailing edge is not a flat surface, a small PAUT probe with a 12 or 16- element aperture is the only practical method for that region.

2.3 CIVA modeling and analysis

The current study used the ultrasonic module of CIVA to simulate the welded T-joint sample inspection considered previously. Models for the sample and the inspection system have been defined as accurately as possible. There is a wide range of input parameters available to the model (Figure 2.7) (Cinquin et al., 2006); only to give a few of the different parameters that need to be entered, we can mention:

- a CAD model describing the dimension of the sample.
- ultrasonic properties of the steel used to manufacture the sample.
- the location, the size, and the nature of the flaws distributed in the welded joints of the sample.
- ultrasonic probe geometry including a description of the array settings required for PAUT.
- the firing sequence of the elements as well as a description of the exciting impulse.

However, before embarking on a campaign of numerical simulations, it is necessary to validate the various parameters entered through measurements on real samples. This step was performed with a standard calibration block manufactured from the same steel alloy. The study carried out all the steps under the International Institute of Welding (Calmon. P, 2013; Iakovleva et al., 2014; Mahaut et al., 2009).

2.3.1 Simulation of conventional ultrasonic testing (UT)

A rectangular single element crystal assembled to simulate conventional ultrasonic testing to a flat refracting wedge was selected as the probe. Both beams refracting at 60° and 70° were tested, as shown in Figure 2.8. Two steel alloys with slightly different ultrasonic properties have been used for the T-joint sample model. Spherical voids, whose distribution and size mirror the manufactured T-joint sample, have been inserted into the model, as shown in Figure 2.9. In the real sample, the flaws were produced by silicon nitride balls whose ultrasonic impedance is very similar to that of steel. However, experimentally, we have noticed that ultrasonic reflection does not come from an impedance mismatch at the steel/ceramic interface but from a lack of wetting between the two. Therefore, for simulation purposes, we prefer to use voids. According to Hydro-Quebec's procedure, the numerical system's sensitivity was calibrated, namely, a side-drilled-hole with a diameter of 1.5 mm at a depth of 20 mm.

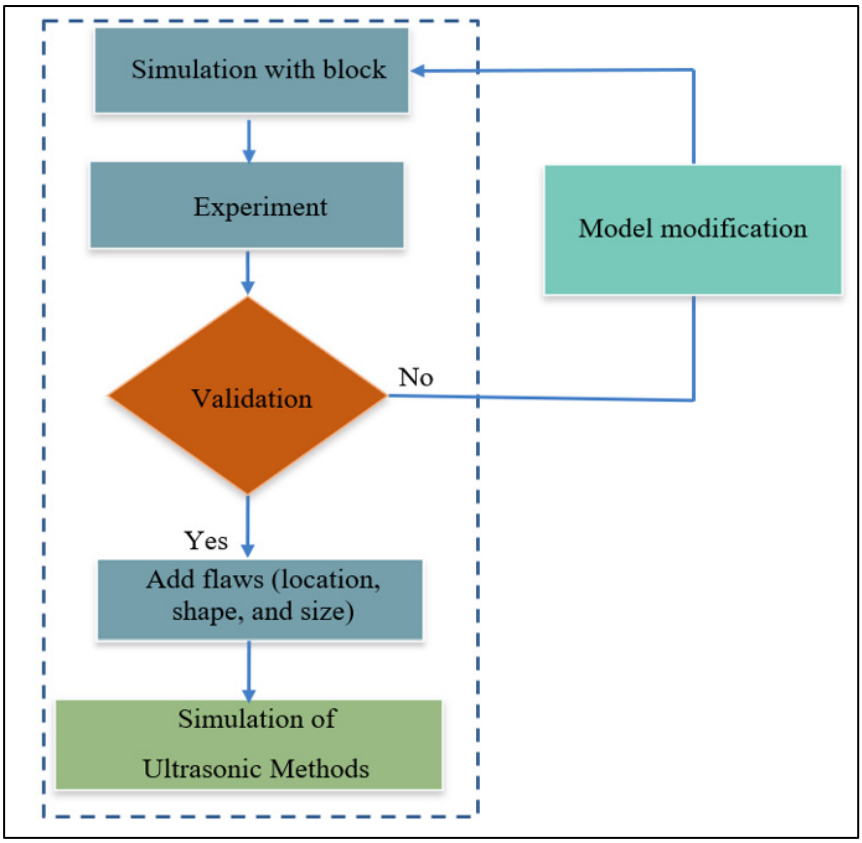

Figure 2.7 Configuring the CIVA model and input parameters

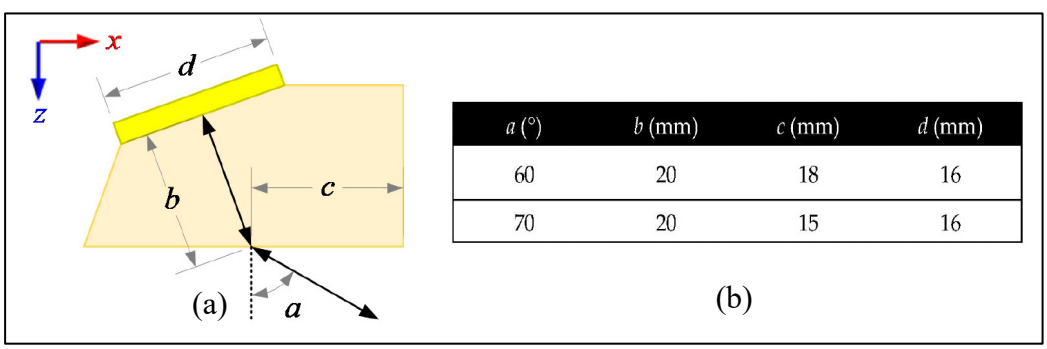

a (°)	*b* (mm)	*c* (mm)	*d* (mm)
60	20	18	16
70	20	15	16

Figure 2.8 Parameters of the ultrasonic probe (a) Conventional ultrasonic testing probe and (b) The dimension of the probe

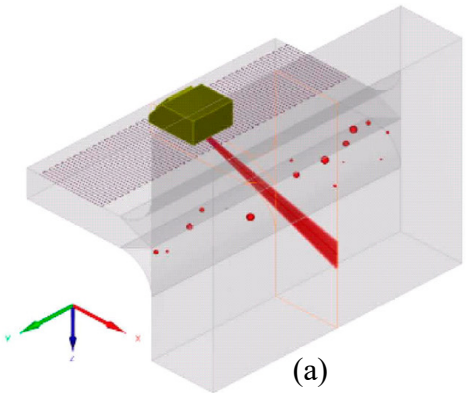

(a)

Velocity	UNS S41500	Alloy steel
Longitudinal wave (m.s $^{-1}$)	5880	5920
Transverse wave (m.s $^{-1}$)	3210	3255
Density (g.cm^{-3})	7.9	7.8

(b)

Figure 2.9 Scanning pattern and material properties (a) Raster scanning with water coupling, and (b) Material Properties

The following conclusions were obtained from the simulation results: Sample alloys appear to have little to no impact on the system's detection rate and could probably be attributed to the similarity between the two alloys' ultrasonic properties. Further work will consider the impact of steel microstructure on the ultrasonic beam's scattering, increasing its attenuation and producing a higher background noise level. Beam refracted at 70° gave a better detection rate than beam refracted at 60°. This result agrees with our experimental measurements and tends to prove our hypothesis; namely, this performance is due to the beam's larger divergence. However, we observe a significant difference between the simulated detection rate (Figure 2.10) compared to that obtained experimentally (Figure 2.6). The reasons for this difference are that the ceramic beads do not behave exactly like a void, and the simulation does not capture the operator's judgment.

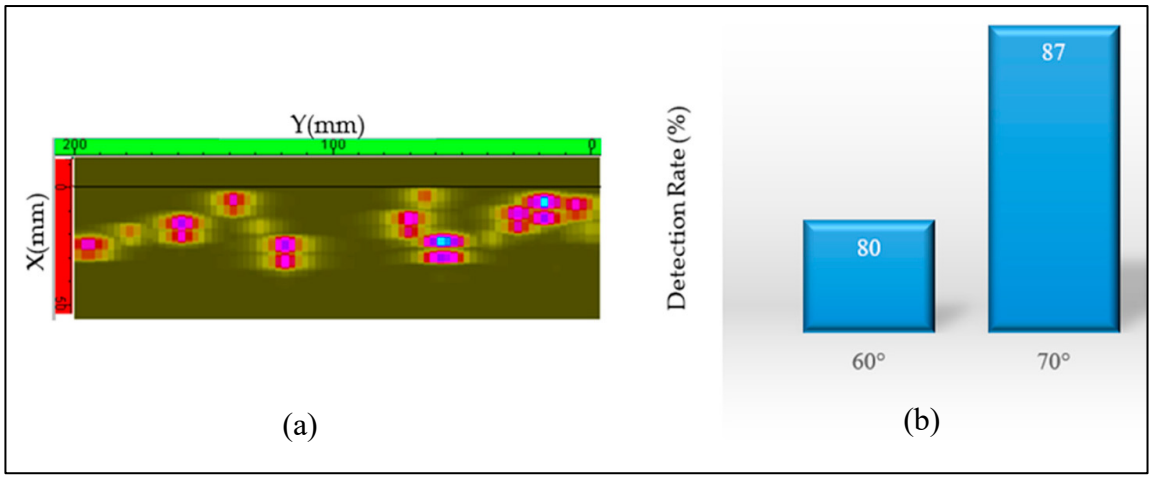

Figure 2.10 Simulation results from Conventional ultrasonic testing probe (a) 70° refracted beam, and (b) Simulated detection rate for Alloy steel and Martensitic stainless steel by probe 60° & 70°

2.3.2 Simulation of phased array ultrasonic testing (PAUT)

A linear array of 64 elements assembled to a flat refracting wedge was selected as the probe to simulate phased array ultrasonic testing. In all cases, this probe was used to sectorial scan the sample at angles ranging from 40° to 70° (with & without focusing) as shown in Figure 2.11. If there was focusing, the focal depth was either 22 or 50 mm. The electronic focusing enables optimizing the beam shape at the expected defect location and further optimizes the detection probability. Also, focusing at multiple depths improves the ability to size critical flaws for volumetric inspections.

The T-joint sample model was the same as the one used for conventional UT simulation; same material options, same flaws nature, size, and distribution. According to Hydro-Quebec's procedure, the numerical system's sensitivity was calibrated, namely three side-drilled-holes with a diameter of 1.5 mm at depths of 15, 30, and 45 mm, respectively. The study used the computed time corrected gain (TCG) in this calibration process.

The following conclusions were obtained from the simulation results: Sample alloys appear to have little to no impact on the detection rate of the system; A 16-element configuration has a better detection rate than a 32-element one (Figure 2.12). The result agrees with the experimental measurements and tends to prove our hypothesis, namely, the impact of the beam exit point and the width of the refracted beam on the sensitivity of these techniques; by phased-array sectorial scanning, we are sweeping the volume with a variety of angles. Even if the targets are not exactly aligned with the center ray as indicated by CIVA, there will be components of the wavefront that might hit the targets with a preferred reflection coefficient and directivity. Of course, the S-scan's fixed standoff is a limiting factor that could cause flaws at the extremes of the sectorial sweep to have a weaker response. This will be a factor in the way we set up the 16 element and 32 element apertures; for the same refracted angle, the 32-element aperture has an exit point farther back from the weld. So, we are approaching the targets from slightly different angles (and distances).

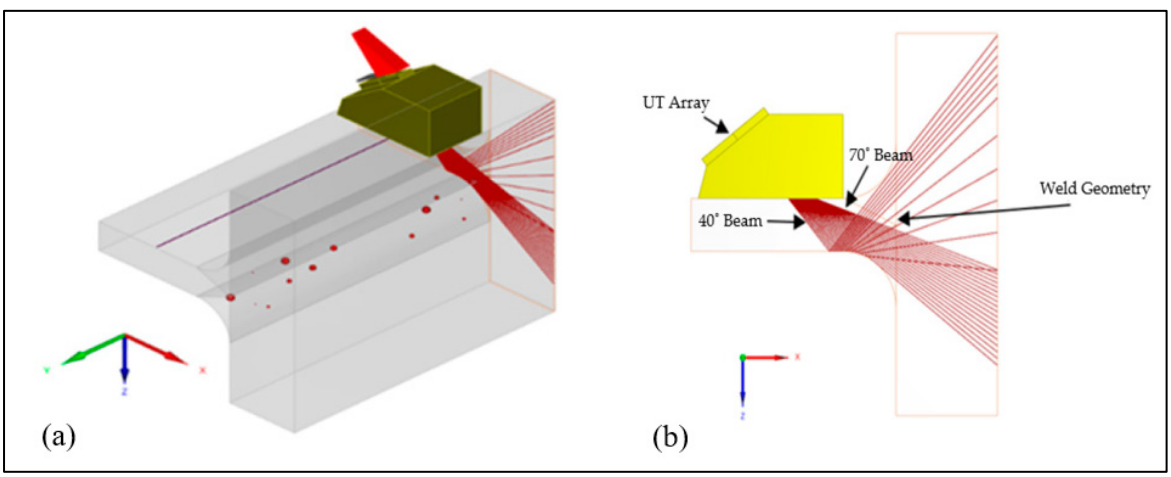

Figure 2.11 CIVA simulation configuration (a) Raster scanning with water coupling, and (b) Setup CIVA ray tracing with the selected sweep angles

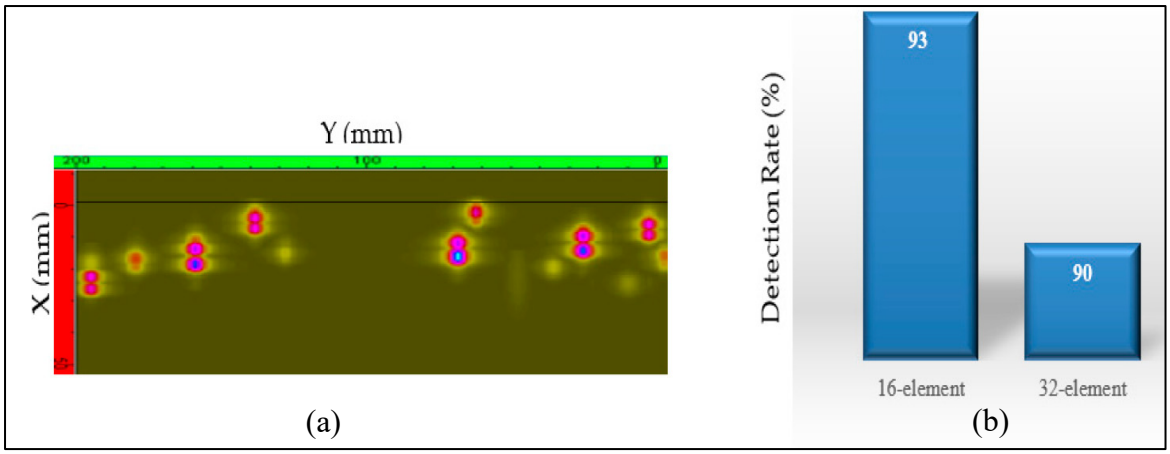

Figure 2.12 Simulation results from PAUT probe (a) 16-element, without focusing, and (b) Simulated detection rate for Alloy steel and Martensitic stainless steel by 16 & 32 element

PAUT simulated detection rate is significantly better than the conventional UT one. As mentioned previously, this could be because the fixed-angle beam can miss a flaw more easily than with ultrasounds impinging the flaw from different directions, as is the case with sectorial scans. Also, with a fixed angle and using a raster scan, detection will be a variable that can be a function of the wedge size (limiting the probe's access to the weld) and the beam divergence.

2.4 Finding and discussion

Our tests showed that conventional ultrasonic results in the lowest detection rate among the different ultrasonic testing methods evaluated. Although the inspection is carried out to a well-defined standard, the detection rate is highly dependent on the operator. Fixed angle conventional ultrasonic testing (UT) provides less information for accurate assessment of actual flaw conditions. Detection capability increases with the divergence of the beam of a single element probe. Because a beam refracted at 70° is more likely to show greater divergence than one refracted at 60°, the former has a better detection rate. PAUT allows one to use more angles and increases the probability of detection compared to conventional UT. PAUT sectorial scan is also well adapted to the T-joint sample's geometry. Low angles will be

tangent to the weld cap radius, while the high angles will probe the center of the blade to the web region.

The 16-element PAUT probe proves to be a good compromise for detection: Better resolution than the 12-element probe; Compared to the 32-element, a smaller wedge can be used, and for the same refracted angle, the beam exit point is closer to the edge of the weld; The size of the beam is adapted to the range of interest. With 32-element, focusing is needed to narrow down the beam emitted from a larger active aperture but did not lead to a better detection rate. Linear-encoded PAUT scans can distinguish two closely spaced flaws more easily than manual inspection.

Among the different ultrasonic testing methods evaluated, manual TFM resulted in the highest detection rate. It is slightly better than encoded TFM due to the operator's ability to adjust the probe's position to improve the signal to noise ratio on display. TFM L-L reconstruction mode seems to give slightly better results than the T-T reconstruction mode. TFM by nature has better coverage than beam-forming PAUT, and that could explain the slightly higher detection rate. TFM has the advantage of a clear display with appropriate information on the actual distribution and geometry of the flaws (faceted, multi-faceted, sphere-like). However, using the T-T mode did provide more details of the ceramic bead interface and better estimate of the diameter because of the shorter wavelength. TFM requires a transducer with a large number of elements. Thus, a large contact area and good coupling for all the ray paths are needed to produce consistent and repeatable results.

The best inspection strategy to inspect the trailing edge of a runner blade is to perform the inspection in two steps:
Step1: linear encoded scan with either PAUT sectorial scanning or TFM direct mode. PAUT shall use shear wave with the refracted angle from 40° to 70°. TFM could use either L-L or T-T direct mode.

Step 2: manual sectorial scanning with a 12 or 16-element aperture and a small wedge footprint to inspect the trailing edge and the weld reinforcement. The small footprint wedge is essential on a real turbine because of the trailing edge's curvature to maintain good contact while scanning.

2.5 Conclusion

The preliminary technical approach developed in phase I of this research was tested on a T-weld specimen. When developing the scan plans and the preliminary data analysis, the ray path analysis indicated the need to carry out a minimum of two scans at different index points to enable complete volume coverage of the weld, particularly for thick weld specimens. This study aimed to collect initial data on a simplified mock-up and then compare the experimental ultrasonic data with the results of simulations performed by CIVA. Experimental studies in a laboratory setup showed that, among the different ultrasonic testing methods evaluated, TFM appears to be the best ultrasonic inspection technique to provide reliable flaw data to the IREQ's life estimation model. In addition to this technique's ability to detect flaw distribution, the algorithm allows a better definition of flaw geometry and highlights its different facets. CIVA model could be used to simulate ultrasonic inspection of a weld. However, to obtain reliable data, the sample and the inspection system's models must be defined with a high accuracy level. To do this, we need to adjust model parameters through validation loops based on precise measurements on real calibration samples. While defining accurate numerical models seems like a tedious task, it ultimately drastically reduces the costs of developing a reliable inspection strategy.

Our future work uses such models to estimate the probability of detection (POD) of certain ultrasonic techniques applied to hydroelectric turbine runners' inspection.

Acknowledgments

We would like to deeply thank IREQ for their kind support. We are also grateful to Quebec Metallurgy Center (CMQ) for their valuable advice and support during experiments, in particular Mr. Jeremy Carignan. The authors also wish to acknowledge Edward Ginzel, Martin Gagnon, and Hamid Habibzadeh Boukani for many discussions and their technical assistance.

CHAPTER 3

RELIABILITY ASSESSMENT OF NON-DESTRUCTIVE TESTING (NDT) FOR THE INSPECTION OF WELD JOINTS IN THE HYDROELECTRIC TURBINE INDUSTRY

M. E. Bajgholi [a], G. Rousseau [b], M.Viens [c], M. Gagnon [d] and D. Thibault [e]

[a, c] Department of Mechanical Engineering, École de Technologie Supérieure,
1100 Notre-Dame West, Montreal, Quebec, Canada H3C 1K3
[b, d, e] Hydro-Québec's Research Institute, Varennes, Québec, Canada J3X 1S1

Paper submitted to the *Journal of Non-destructive Testing and Evaluation*, December 2022

Abstract

Due to the importance of energy production, it is critical to reduce unnecessary or unpredicted power generation equipment outages. As a major power generation company, Hydro-Québec uses models to estimate the service life of turbine runners in order to avoid such outages. The influential inputs for these models include the characteristics of flaws present in the runners. Since Non-destructive testing (NDT) methods are used to detect and characterize these flaws, this study aims to evaluate the reliability of NDT methods for inspection of weld joints in hydraulic turbine runners. Conventional ultrasonic testing (UT), radiography testing (RT), phased array ultrasonic testing (PAUT) and PAUT using total focusing method (TFM) were compared. The NDT tests were conducted on a T-joint specimen manufactured with embedded flaws. This specimen was used to determine the probability of detection (POD) curves for volumetric flaw sizes. The results showed that array technology, PAUT or TFM, has demonstrated a detection capability (a_{90}) around 2.5 mm, which is similar to the commonly used equivalent critical flaw size for such structure.

Keywords: Non-destructive testing (NDT); phased array ultrasonic technique (PAUT); total focusing method (TFM); flaws; probability of detection (POD); reliability

3.1 Introduction

Energy transition is changing the role of hydroelectric power generation in the global energy market. The flexibility and resilience of hydraulic power generating assets are becoming key factors. To meet these new requirements, the assets must be able to operate under a broader spectrum of operating conditions and must be able to do so with minimal maintenance. In the case of turbines, this means being able to sustain degradation mechanisms such as fatigue, cavitation and corrosion.

When it comes to turbine runners fatigue, one of the main factors to consider is the initial integrity of the runner. To ensure this integrity, non-destructive testing (NDT) is used during fabrication to detect flaws in the castings and in the welds. Historically - and still nowadays - acceptance criteria detailed in the manufacturing standards that are based on "good workmanship" have been used (e.g., ASME Boiler and Pressure Vessel Code) (Boukani et al., 2018; Paoliello, 2005). To move toward a damage tolerant approach that enables fitness-for-service evaluation and that facilitates digital twin deployment, acceptance criteria must be tailored to the application. To do this rigorously, we must be able to define tolerable defects and detect the deleterious defect with a high level of confidence. The first task - i.e. define tolerable defects - is the domain of fracture mechanics. The second task - i.e. detect deleterious defect - is the domain of non-destructive testing. A reasonable assessment of uncertainties associated with the different inspection methods in usage is therefore essential to assess the level of confidence (Bajgholi et al., 2021; Gagnon et al., 2013; Thibault et al., 2015). Hydro-Québec uses a unified approach integrating fracture mechanics to evaluate the risk of cracking during the life of the runners. The model inputs need to be defined as accurately as possible to obtain reliable estimations. Initial flaw size is one of the inputs whose uncertainty substantially impacts the reliability assessment modeling (Gagnon et al., 2013; Boukani et al., 2018). As shown in Figure 3.1, uncertainty in defect size can significantly impact the probability of crossing the propagation threshold described by the Kitagawa diagram used in this unified approach (Morin et al., 2021). Therefore, any improvement in the definition of defect size and

its uncertainty could significantly enhance the accuracy of the estimated risk of failure related to fatigue (Boukani et al., 2014)

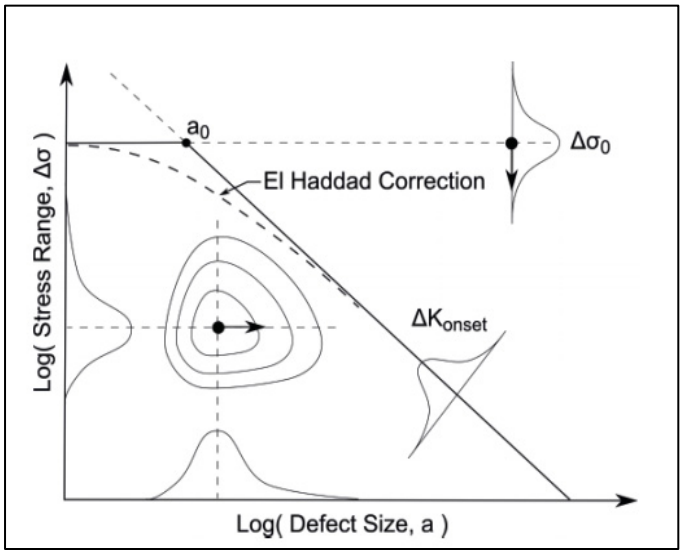

Figure 3.1 Fatigue risk assessment,
Kitagawa diagram
Taken from Gagnon et al. (2013, p. 3)

Previous researchers have investigated the POD of ultrasonic inspection applied to hydraulic turbine runner welds. However, they mostly investigated sectorial scanning (S-scan) and dynamic depth focusing (DDF) using PAUT transducers. Moreover, they only considered large flat defects (either artificial or simulated), which are not representative of real weld flaws that have been found in hydraulic turbine runners (J. Zhang et al., 2014; Y. Zhang et al., 2011).

The knowledge of the probability of detection (POD) curves, required by fitness-for-service (FFS) assessments, is mostly absent for structure such as hydroelectric turbine industry. The main goal of the study reported in this paper is to evaluate the reliability of NDT methods for the inspection of welded joints in turbine runners. It focuses on the determination of POD curves from different NDT inspections of a T-joint sample representative of a trailing edge of a turbine runner with artificially induced flaws.

3.2 Experimental Procedure

3.2.1 Specimen

A Francis turbine runner can be considered as a series of weld joint sections with different web thicknesses and angles (Bajgholi et al., 2021; J. Zhang et al., 2014). To investigate the performance of the different inspection methods, a mock-up T-joint sample very similar to real turbine runners was manufactured with ceramic beads inserted in the weld to create flaws.

The T-joint sample was made from martensitic stainless steel (UNS S41500) in accordance with the manufacturing requirements of turbine runners (Figure 3.2). The T-joint geometry mimicked a turbine runner's trailing edge, with both edges being 25 mm in thickness. The base plate was 60 mm thick and provided the same ultrasonic path for an inspection performed from the turbine web. The weld cap and blade ends were ground to obtain a smooth finish with a curved radius of 25 mm. A double J weld preparation with a 3 mm gap between the web and blade was used as shown in Figure 3.3. Welding was carried out using a multi-pass FCAW process and EC410NiMo electrodes (same ultrasonic properties as UNS S41500). 34 passes were required to fill the joint. Ceramic beads were positioned during welding at three different zones: near the flange, in the center of the weld, and near the blade. A total of 30 ceramic beads (artificial flaws) were inserted, ranging from 1 to 5 mm (6 of each size). The ceramic beads were distributed to cover the critical stress area, which runs up to about 75 mm from the trailing edge.

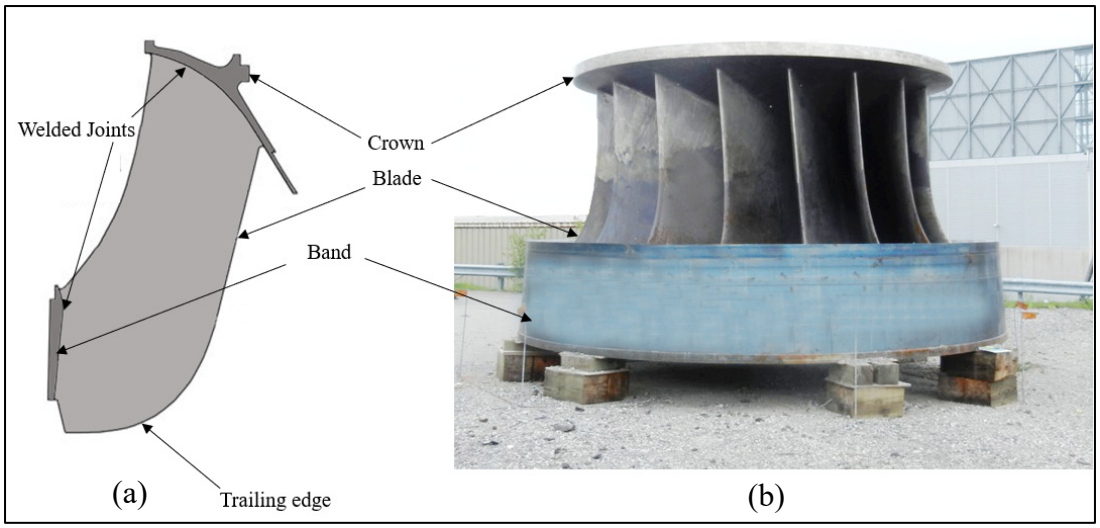

Figure 3.2 Francis turbine runner: (a) Schematic of the runner blade and (b) Overall overview of Francis turbine runner

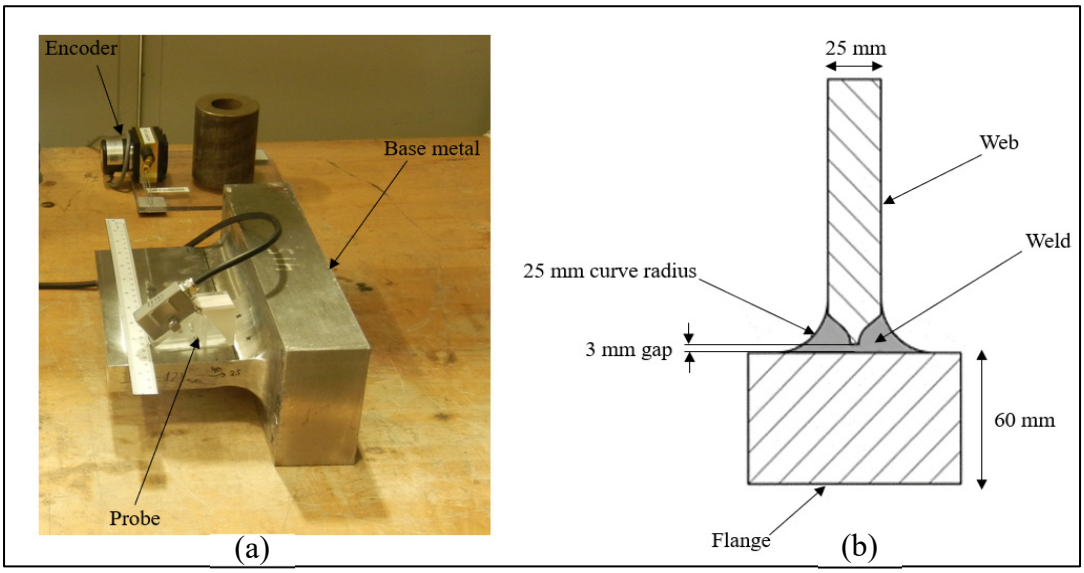

Figure 3.3 T-joint sample: (a) Mock-up T-joint sample and (b) Manufacturing drawing of T- joint sample

The central region of the joint was free from intentional flaws and provided a small region to assess the occurrence of unintentional welding flaws. No unintentional welding flaws were observed with the various NDT methods used to evaluate the quality of the sample. In fact, a

high-resolution ultrasonic inspection performed from the web face confirmed the presence of the 30 beads in the vicinity of the insertion location as per the fabrication report.

3.2.2 NDT procedures and tests

The investigation covers the application of ultrasonic techniques and radiography as a reference method. The instrument utilized for all array inspection was the Topaz 64 manufactured by Zetec Company with the high-resolution full matrix capture (FMC) option. Manual UT testing was performed with different commercially available flaw detectors (Olympus Epoch 600 and Krautkramer USN 58L Ultrasonic Flaw Detectors), but all were digital instruments with time-corrected gain (TCG) capability. All UT inspections used angle beam probes and scanning was performed from the surface of the blade. The T-weld sample geometry provided good access from both sides of the blade with no dead zone caused by the connection angle between the blade and the web (Bajgholi et al., 2019).

In this research, all NDT inspections were performed with procedures developed according to accepted standards. Conventional UT and PAUT testing followed the Canadian CSA W59 code, which is well suited for these techniques (CSA W59, 2013). However, to meet specific requirements, small amendments have been adopted such as probe movement for encoded scans and a lower acceptance threshold (-20 dB) to consider the small reflective surface of the target geometry as compared to the calibration side-drilled holes (SDH) (Bajgholi et al., 2020). The AWS PACS 1018 steel calibration block with wide spacing SDH (Davis NDE Inc.) has been used to allow PAUT TCG calibration without interference between holes (1.5 mm diam.) of different depths. Velocity and attenuation of the calibration block were very close to the sample materials (ISO 19675, 2017).

Full matrix capture (FMC) with the total focusing method (TFM) algorithm was utilized to generate real-time TFM volumetric images of the weld area (Holmes et al., 2008).The CSA W59 code does not mention TFM and TFM procedures are not well established in codes. ASME BPVC-V, Section V, Article 4 Appendix XI, ISO 23864, and 23865 (2021) were used

as guides for developing an adequate procedure (ASME, Section V Art. 4, 2021; ISO 23864, 2021; ISO 23865, 2021). The reconstruction algorithm must be a direct hit (L-L or T-T) because the geometry of the blade-web joint did not offer a back-wall surface for a reflected path. The calibration block, TCG, and scan plan were similar to the PAUT procedure, so data generated between techniques would have the same calibration artifacts and amplitude reference level (Ginzel, 2013). Four commercially available array transducers from Zetec Company (Table 3.1) were utilized for this study (Probes & Wedges, Zetec Company, 2016).

Table 3.1 PAUT probes used for the POD study

No.	**Probe**	**Frequency (MHz)**	**Elements**	**Pitch (mm)**	**Height (mm)**	**Focusing on passive axis**
1	LM5M-55S Standard linear array	5	64	0.6	10	No
2	AM5M-55S Standard linear array	5	16	0.6	10	No
3	5L12-51S Standard linear array	5	12	0.6	7.2	No
4	Focused linear array (Probe AL5-DF15)	5	64	0.3	15	Yes

UT inspectors were all certified to ISO 9172 UT/PAUT method level two or three (no certification scheme exists for TFM). The inspectors did not have a time limit and they produced written reports (ISO 9712, 2012).

Radiography was performed at the Quebec Metallurgy Center (CMQ) with a 450 kV generator and a Carestream HPX-1 CR general purpose plate. Film type, source to film distance and focal spot size were selected to achieve sufficient image definition and energy was selected to achieve proper contrast. The image quality indicator (IQI) and target density consideration suggested that a 2.64 mm ceramic ball should be detectable (Industrial Radiography Image Forming Techniques, 2006).

3.3 Reliability assessment

3.3.1 POD in NDT Techniques

The reliability of NDT methods, in other words, their ability to detect flaws in a certain size range under certain testing conditions, is generally quantified in terms of probability of detection (POD). POD is usually expressed as a function of flaw size (length or height). Nevertheless, POD is a function of more factors related to the material (microstructure, geometry), the flaw itself (flaw type, orientation, shape, and density), and the inspection system (NDT method, procedure, testing conditions, and operator) (Boukani et al, 2018; Georgiou, 2007; Zolfaghari et al., 2017). The POD methodology currently adopted by the aircraft industry is described in the United States military handbook 1823 (MIL-HDBK-1823). It is based on a parametric estimation of the POD following Berens models (Foucher et al., 2018; MIL-HDBK-1823A, 2009); The approach is also adopted in ASTM standards (ASTM E3023 ,2015; ASTM E2862, 2018). POD curves can be built for two forms of data:

1- Binary response: It gives the outcome of an experiment as either hit or miss. A level of response is defined; data below this level are not detectable (miss) and information above this level can be detected (hit).
2- Signal response: For any set of experiments, for flaw size (a) and amplitude response of the inspection system ($\hat{a}$), the POD curve may be evaluated as a function of ($\hat{a}$) from 0 % to 100 % vs. flaw size (a) (Chapuis et al., 2017; Malik, 2016).

3.3.2 POD determination

The POD model applied to analyze our data is the Berens Logit hit/miss (MIL-HDBK-1823A, 2009). Our signal response amplitude was not lognormal with respect to the flaw size, so the $\hat{a}$ vs. a POD model did not give consistent results. The mathematical packages utilized were the POD module that comes with CIVA and MH-1823 software. The CIVA-POD uses the

same mathematical tools as detailed in MIL-HDBK-1823. Verification was made with data sets to compare CIVA-POD with the software MH1823 supplied by Statistical Engineering (version 5.4.5) and the same statistical values were reported (CIVA, 2021; Annis, 2022). An example of CIVA and MH1823 software side by side in the case of our radiography results is shown in Figure 3.6. CIVA plot shows the POD curve and the lower 95% confidence limit. MH1823 plot shows the POD curve, upper and lower 95% confidence limits, a_{50}, a_{90}, $a_{90/95}$, number of hits and total number of samples.

Our primary goal was to compare inspection methods to find small volumetric flaws at the edge of a runner blade. Data were collected by experienced level two or three PAUT practitioners, and repeated scans were performed (typically three scans for encoded techniques). Our methodology focused on comparing NDT techniques and not on capturing, except for the conventional UT, the operator effect on measurement reliability. The results reported below show flaw size with 50 % POD (a_{50}) and flaw size with 90 % POD (a_{90}) within a confidence interval of 95 % ($a_{90/95}$). In some cases, the $a_{90/95}$ was not computed because the lower confidence bound at 95% is not reached with the Hit/Miss POD parametric model. Thus, this study focused on the 90 % POD (a_{90}) as the relevant indicator to compare techniques in our study (Safizadeh et al., 2004; Harding et al., 2011; Kurz et al., 2013).

3.4 Results and discussion

3.4.1 Ultrasonic testing response

Assuming the wetting of the ceramic beads with the weld metal, simulation and calculation using Ermolov's equations would result in reflected signal amplitude in the range of -48 dB with respect to a 1.5 mm side-drilled hole (SDH) used for calibration (Ermolov, 1972; Ginzel, 2011). Actual ultrasonic testing produced much stronger amplitude, with the weakest measure from a 2 mm bead being -17 dB. This finding demonstrates that the interface between the weld material and the ceramic bead was not smooth. While no air gap was observed during the radiographic examination, the acoustic impedance mismatch at the beads' interface acted as if

an air gap was present. It was possible to point out some features of the ceramic bead response using ultrasonic and metallographic examinations. Small beads behaved like point reflectors in the 1 to 2 mm diameter range (Figure 3.4). These targets were omnidirectional reflectors, and they provided a relatively constant amplitude while orbiting the probe at a constant metal path. Larger beads, between 3 and 5 mm in diameter, tended to show one or more facets. A peaked amplitude is a characteristic feature of a facet with a specific angle of incidence and direction. These beads may produce a strong signal, not necessarily in a direction perpendicular to the weld axis. This may lead to differences in results between techniques using a linear encoder scan versus a manual on-the-fly inspection. The latter usually reports higher peaked amplitudes. Examples of encoded responses with a high-resolution TFM examination method are shown in Figure 3.4.

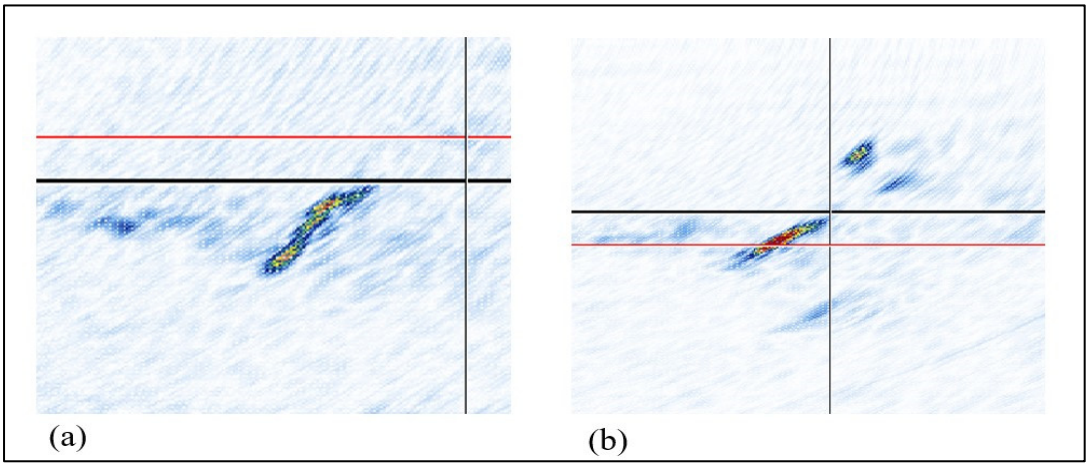

Figure 3.4 TFM results from different beads: (a) Ceramic ball with four facets and (b) 5 mm facet (bottom) and sphere type reflector (top) with a creeping wave

The following graph shows the maximum amplitude measured during a manual UT and phased array encoded linear scan during the project's development stage. Since there is no linear relation between measured amplitude and size of beads, any attempt to size a bead with amplitude leads to an erroneous evaluation of the flaw size. Figure 3.5 shows the complexity of the interaction between sound amplitude and ceramic bead implants. Furthermore, we observe a lower number of flaws detected with manual UT.

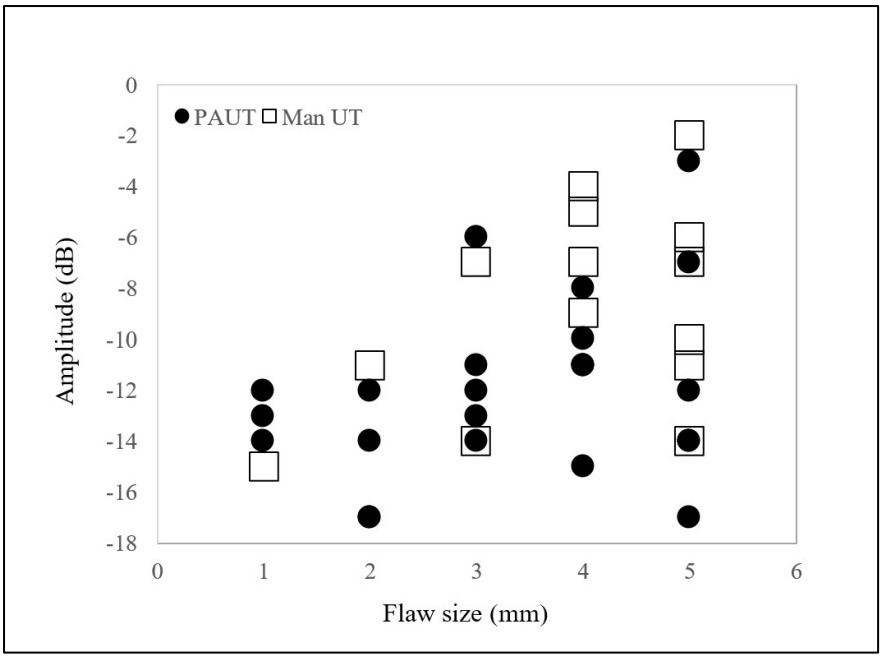

Figure 3.5 Amplitude map in dB with respect to
a 1.5 mm side-drilled hole (SDH)

3.4.2 POD analysis using conventional NDT method

Our main objective was to compare various NDT techniques to evaluate how they perform in terms of inspection reliability. Because our sample contained thirty flaws, combining inspection results for the same procedure/technique with data produced from different operators is advisable. Combining results adds the benefit of improving the confidence level (Annis et al., 2013). This was possible for manual UT, PAUT, and TFM inspections. However, for radiography testing, a single data set was generated. Overall POD Curves are shown in Figures 3.6-3.10. A detailed review follows.

Radiography is considered a reliable reference method. It is well suited for our study because the ceramic beads are volumetric, which is an optimum situation for radiographic testing. The radiographer was confident of finding all 3 mm beads and above. The results for radiography were a bit surprising because the evaluation of the contrast and sensitivity with an Image Quality Indicator (IQI) taking into account the density of the ceramic beads resulted in

a threshold of approximately 2.64 mm. The 90 % POD turned out to be a 3.94 mm bead, which is better than manual UT but less than any phased array techniques (Figure 3.6).

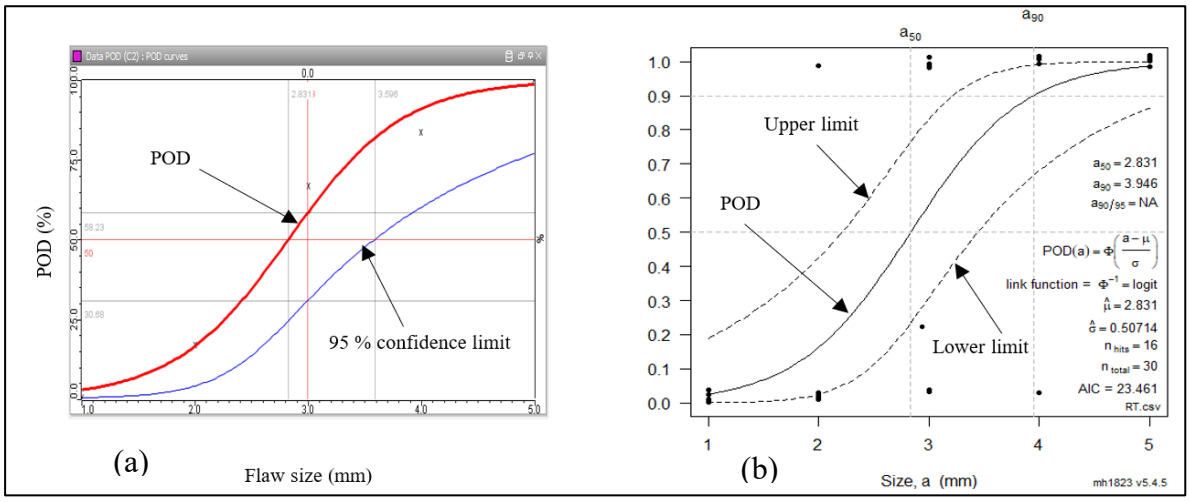

Figure 3.6 POD curves for radiography testing with CIVA and MH1823 software
(a) POD curve with CIVA simulation software and
(b) POD curve with MH1823 software

The ultrasonic method used during manufacturing turbine runners is manual inspection using conventional angle beam probes, so this technique is highly relevant for this study. Of all the ultrasonic inspection methods and techniques, conventional UT rated least reliable in our study. Conventional UT means a single crystal transducer with a fixed refracted angle of 70°. A lower refracted angle, although required by ASME Volume V Article 4, did not improve the results (ASME, Section V Art. 4, 2021). The average results of four inspectors did not reach a 90 % POD for the 5 mm bead. Two inspectors did fairly well with thirteen and fifteen beads detected, while the other two operators reported seven beads. The latter operators missed three 5 mm beads. As a result, the POD curve shifts slightly towards the right-hand side of the 5 mm size. When the data sets of the two best operators are considered separately, the POD curve produces a 90 % POD at approximately 4.41 mm bead diameter, as shown in Figure 3.7.

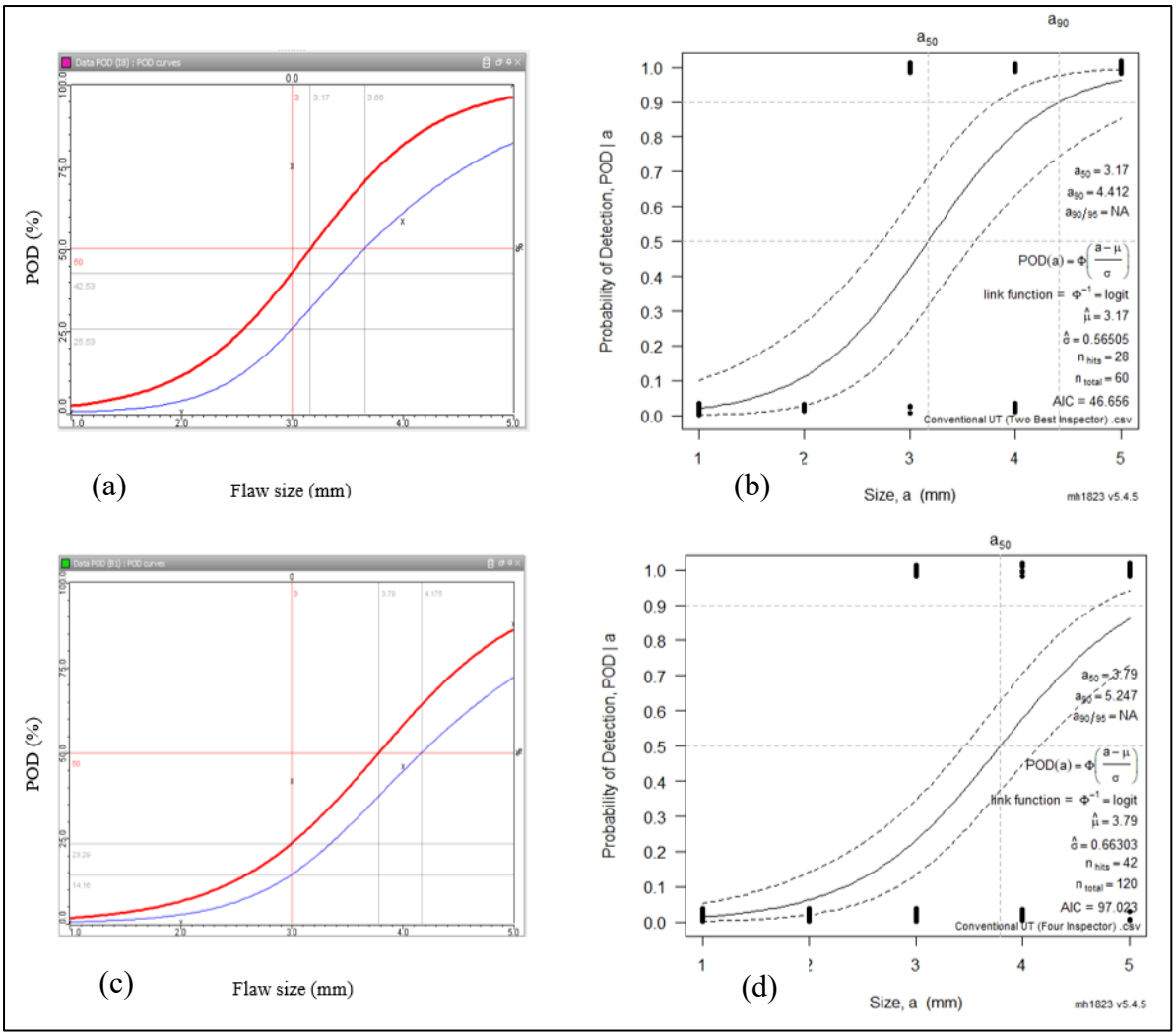

Figure 3.7 POD curves for conventional ultrasonic testing (UT) (a) POD curve with CIVA simulation software (two best inspectors), (b) POD curve with MH1823 software (two best inspectors), (c) POD curve with CIVA simulation software (four inspectors), and (d) POD curve with MH1823 software (four inspectors)

3.4.3 POD analysis on PAUT methods

This section presents the results obtained with several phased-array ultrasonic configurations to verify if the array size or the vibration mode could impact the results.

The configurations used different numbers of active elements; shear waves or longitudinal waves; and different array geometries. Our first approach was to apply an encoded technique

where the data capture was synchronized with a wire draw encoder and the array probe was kept perpendicular to the weld axis. Our results found that any encoded PAUT technique produced a 90 % POD in the 3.09 - 3.89 mm bead size range.

Combining the five array configurations results using the shear wave mode, the encoded PAUT demonstrates a 90 % POD of 3.41 mm. Optimal results were obtained with the small 12-element array (probe 5L12) in shear wave mode with a 90 % POD of 3.09 mm. However, this was at the expense of a small coverage that required two scans to cover the whole weld area. The 12-element transducer also suffers from limited steering capability. We noticed the presence of a grating lobe for refracted angle near 70° with an azimuthal range of 40°-70°. The correct steering range, either (40°-65°) or (45°-70°), must be selected depending on the nominal angle of the wedge.

A manual PAUT (non-encoded and hand-free) was then tested with various apertures and probe sizes in the shear wave mode. It was expected to produce slightly better results because some flaws were located at the extremity of the weld and were too close to the edge to be detectable using a linear encoded scan where the probe axis was maintained perpendicular to the weld axis. With the manual PAUT technique, the operator was instructed to perform additional scans at the sample extremities (Additional scans included orbital and radial motion to cover the trailing edge). Because manual PAUT reports slightly more flaws near the extremities than encoded PAUT, it was expected that this would be reflected in the POD curve. Our data showed a 90 % POD of 3.72 mm for manual PAUT, which is not better than most encoded PAUT configurations tested (Figure 3.8). The manually delivered PAUT technique and detection of flaws in real time have detrimental effects on the performance of the inspection. Table 3.2 shows the results of the POD calculation based on different NDT techniques.

Table 3.2 Results of the POD calculation based on different NDT techniques

No.	NDT techniques	a_{50} (mm)	a_{90} (mm)	$a_{90/95}$ (mm)	Number of samples
1	Conventional UT (four inspectors)	3.79	5.24	N/A *	120
2	Conventional UT (two best inspectors)	3.17	4.41	N/A *	60
3	Radiography testing	2.83	3.94	N/A *	30
4	Manual PAUT	2.20	3.72	4.85	60
5	Encoder PAUT	2.26	3.41	3.75	300
6	Manual TFM	1.90	3.55	4.78	60
7	Encoder TFM	2.16	3	3.72	60

N/A * = Not Applicable

We observed that TFM produces a detailed image of an indication's reflective surface and effectively characterizes and sized indications. Testing on real runners and experiments on the T-joint yielded the best estimates of indication geometry by TFM method. Data sets were collected with a 64-element array with shear and longitudinal waves, with manual or encoded scans. In encoded TFM, the 90 % POD was approximately 3.0 mm and in manual TFM, it was 3.55 mm (Figure 3.9). Therefore, encoded TFM performed slightly better than encoded PAUT. Again, manual inspections produced less reliable results.

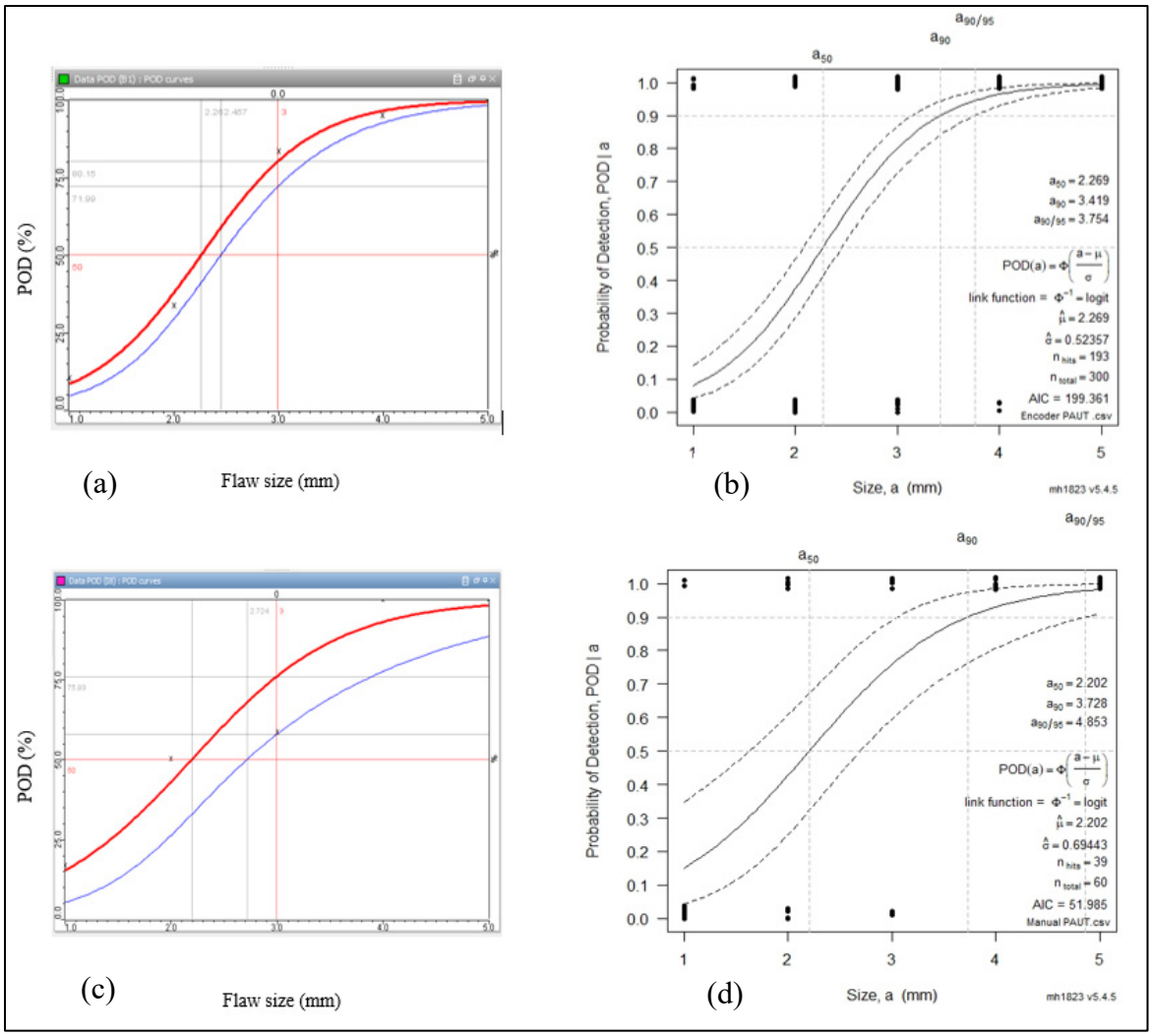

Figure 3.8 POD curves for PAUT (a) POD curve with CIVA simulation software for encoder PAUT, (b) POD curve with MH1823 software for encoder PAUT, (c) POD curve with CIVA simulation software for manual PAUT, (d) POD curve with MH1823 software for manual PAUT

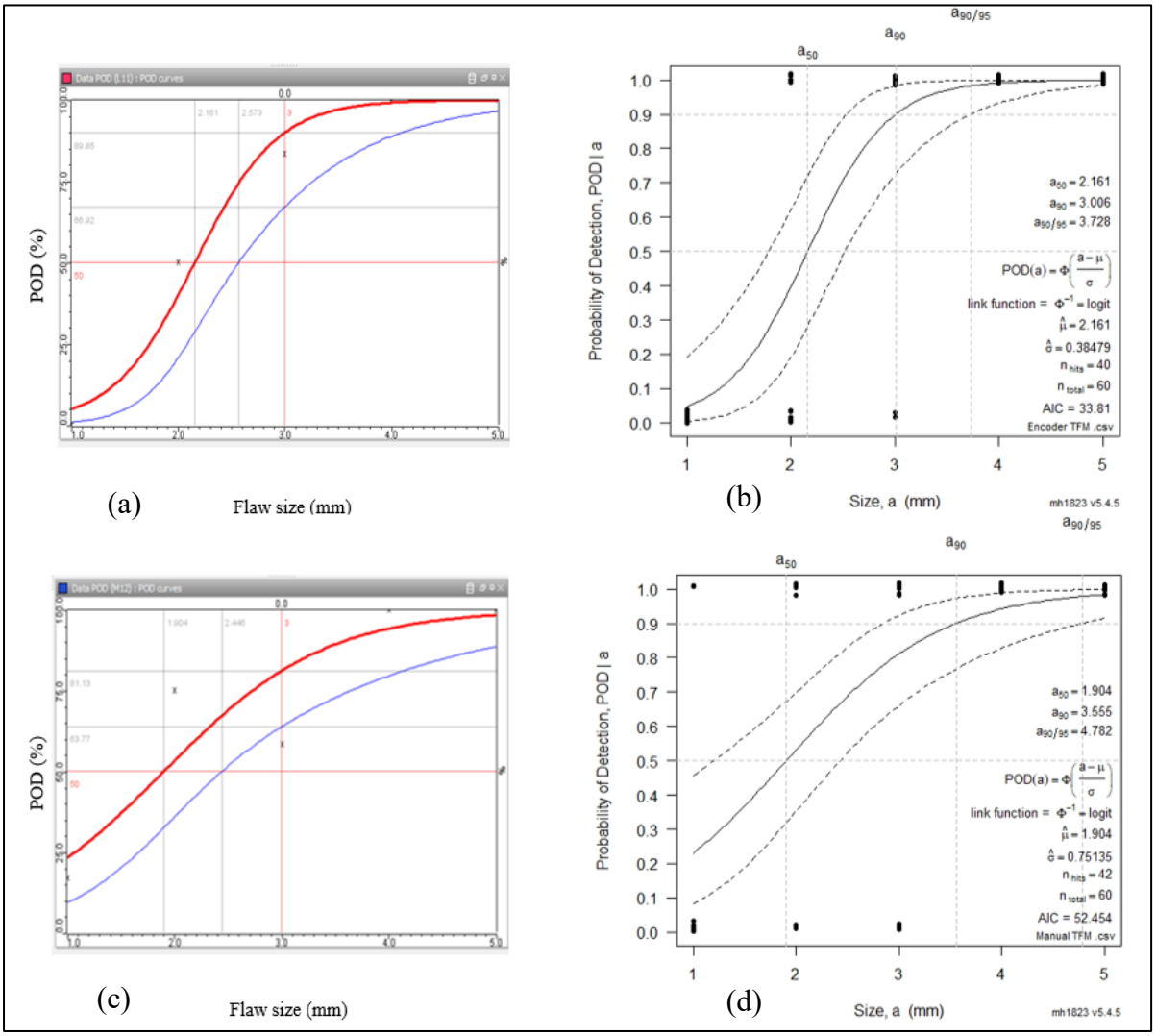

Figure 3.9 POD curves for TFM (a) POD curve with CIVA simulation software for encoder TFM, (b) POD curve with MH1823 software for encoder TFM, (c) POD curve with CIVA simulation software for manual TFM and (d) POD curve with MH1823 software for manual TFM

3.4.4 POD analysis with focused phased array probe

The last set of tests was conducted with an array probe designed explicitly for the TFM method. The transducer had a small element pitch of 0.3 mm and included a lens to focus the beam along the passive axis. The normal pitch for a 5 MHz transducer is typically 0.6 mm for angle beam application (Advanced PAUT Probes for TOPAZ64 Application Solution, 2020). The small dedicated TFM probe was used to perform azimuthal scanning and TFM imaging (Table 3.3). We chose a focal depth (passive axis) of 15 mm in the steel, slightly beyond the blade's center and providing a working depth range from approximately 5 to 35 mm. This TFM probe produced the best detection capability with a 90 % POD of 2.5 mm bead. Because the element pitch is small, this probe can effectively cover the whole weld joint since the small pitch makes the elementary beam more energetic at the high refracted angle needed to reach the center of the joint.

Table 3.3 Results of the POD calculation based on different configurations with focused probe in the passive axis (All scans done with AL5-DF-15 probe with encoder)

No.	Configuration with focused probe	a_{50} (mm)	a_{90} (mm)	$a_{90/95}$ (mm)	Number of Samples
1	PAUT-sectorial scan-16 element	2.30	5.38	NA*	60
2	PAUT-sectorial scan-24 element	1.88	3.68	NA*	60
3	PAUT-sectorial scan-32 element	1.79	2.99	3.92	60
4	PAUT-sectorial scan-48 element	1.61	2.78	3.694	60
5	PAUT-sectorial scan-64 element	1.44	2.50	3.382	60
6	TFM	1.44	2.50	3.382	60

NA* = Not Applicable

This probe acquired a clear and crisp image of the center of the weld and better resolution of the beads implanted at the tip of the J-preparation. Using the focused probe in PAUT method and varying the aperture from 16 to 64 elements makes it clear that a large aperture increases the POD under the same calibration conditions. With the full aperture of 64, we obtained

detection capability at 90% POD of 2.5 mm beads, which is identical to the result achieved in TFM mode (Figure 3.10).

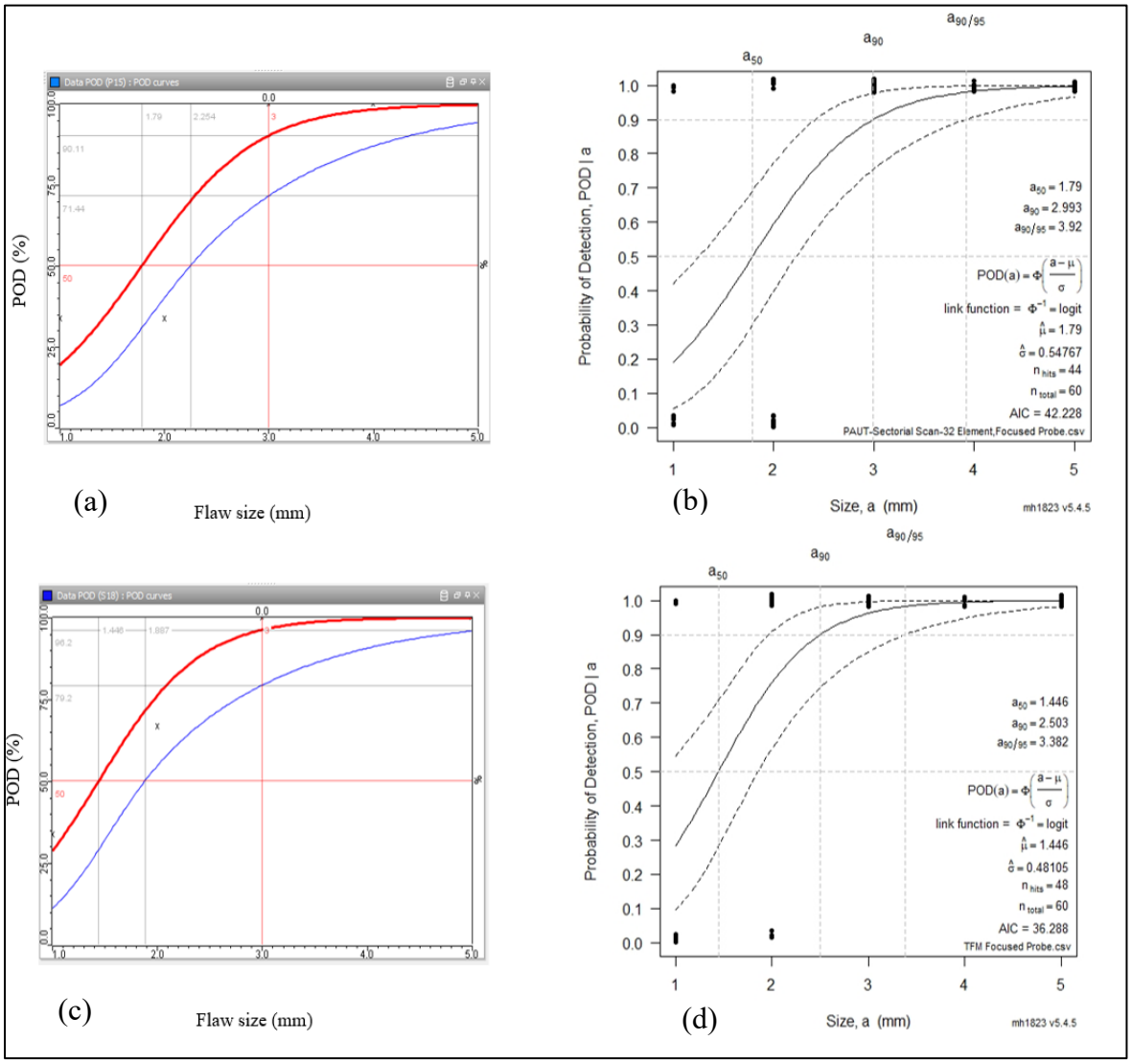

Figure 3.10 Examples of POD curves for the focused probe (a) POD curve with CIVA simulation software for PAUT-sectorial scan 32 elements, (b) POD curve with MH1823 software for PAUT-sectorial scan 32 elements, (c) POD curve with CIVA simulation software for TFM focused probe and (d) POD curve with MH1823 software for TFM focused probe

3.5 Assessment of fitness for service requirements

Manual UT testing and radiography testing did not demonstrate a POD that would meet the fitness for service requirement of 3 mm in size. It was found that conventional manual inspection was the least reliable method for inspecting the trailing edge of runners. We consider that this is because the operator has minimal information to judge by and because the indication is probed at a single refracted angle. That leads to many indications were missed and a higher rate of reporting errors. Selecting an ultrasonic technique using an array probe improved POD significantly when using manual inspection. In our experiment, 5 mm diameter beads were missed in conventional manual UT – either not reported or not seen. Using an array transducer allows the operator to monitor a weld section (pie sector for sectorial scan and a box for TFM). When an indication appears on display, the operator sees the indication in relation to the volume of the weld, which helps to interrogate the indication and determine if the signal is relevant. The A-scan display used with the conventional UT instrument supplies limited information (RF waveform), which is a major limiting factor in improving conventional UT.
To improve the outcome of manual inspection, an inspector qualification program should be implemented to select personnel with the best aptitude to perform the inspection. The fact that two manual conventional UT operators did not fair well indicates that proper training and evaluation would be a path to improve the performance of manually delivered inspection.

On the other hand, PAUT sectorial view or TFM view adds depth and position information that helps the operator identify suspicious reflectors. For encoded scans, a weld overlay was drawn on the sectorial scan view with matching offset position of the wedge. When the weld overlay is plotted on top of the data, the operator can see the interaction of the sound with the flaw and the specimen boundary, thus comforting his judgment.

Ultrasonic methods using an array transducer did provide the best detection performance. TFM performed slightly better than PAUT using a standard 64-element linear array and 0.6 mm element pitch. Using the standard 5 MHz array (0.6 mm pitch), TFM achieved 90 % POD flaw of 3 mm in size. The best results were obtained in terms of POD method with an array probe

having a small pitch (0.3 mm), focusing on the passive axis, and an encoded inspection. Experimentation with a special TFM array transducer demonstrated that a custom design can effectively improve sensitivity to smaller artifacts. Focusing on the passive axis and a smaller element pitch improves the detection rate and POD, while in our experiment, using TFM or PAUT did not result in significant differences in terms of detection. This custom configuration produced a 90 % POD for a 2.5 mm ceramic bead, while radiography testing produced a 90 % POD for approximately 4 mm. Manual UT did not achieve a 90 % POD for the 5 mm bead.
Two configurations achieved the best POD for our implanted ceramic beads:
a) TFM, shear wave, with focused probe (AL5-DF15) in the passive axis.
b) PAUT, shear wave, 64 element apertures with focusing (AL5-DF15) in the passive axis.

3.6 Conclusion

The reliability of different NDT methods in detecting flaws in welded components was investigated. The main conclusions, based on 90 % POD (a_{90}) measured experimentally, can be summarized as follows.

- Conventional ultrasonic testing has not demonstrated the capability to detection of the largest beads (5 mm) reliably.
- Encoded scans demonstrated a higher POD than manual inspections for all the NDT methods.
- Array technology applying an encoded PAUT configuration demonstrated a detection capability (a_{90}) around 3.4 mm.
- Array technology using the encoded TFM algorithm demonstrated a detection capability (a_{90}) around 3 mm.
- An array transducer, focusing on the passive axis demonstrated the best detection capability for a 2.5 mm diameter ball.

- TFM has the advantage of much richer images that help to characterize the nature of the reflector and it also showed the highest POD.

Acknowledgment

The authors would like to gratefully thank the Institute de recherche d'Hydro-Québec (IREQ), Quebec Metallurgy Center (CMQ), Mitacs Acceleration Program, oNDuTy Program and the École de technologie supérieure (ÉTS) for their support and financial contribution. Also, the authors wish to acknowledge Prof. Edward Ginzel for technical discussion.

CHAPTER 4

TOTAL FOCUSING METHOD APPLIED TO PROBABILITY OF DETECTION

M.E. Bajgholi [a], G. Rousseau [b], M.Viens [c], E. Ginzel [d], D. Thibault [e]

[a, c] Department of Mechanical Engineering, École de Technologie Supérieure,
1100 Notre-Dame West, Montreal, Quebec, Canada H3C 1K3
[b, e] Hydro-Québec's Research Institute, Varennes, Québec, Canada J3X 1S1
[d] Materials Research Institute, Waterloo, Ontario, Canada N2J 4G8

Paper submitted for *International Journal of Advanced Manufacturing Technology*,
December 2022

Abstract

Qualification of inspection processes is an integral part of the development methodology of existing and new inspection procedures. An essential aspect of demonstrating how the inspection method performs involves detection capability and discontinuity evaluation. Probability of detection (POD) determination is currently handled by manufacturing intentionally flawed coupons and by validating real flaw dimensions with destructive means. This destructive analysis is expensive to perform, but it also has the detrimental effect that the sample is no longer available for further testing. Novel non-destructive testing (NDT) technology, the total focusing method (TFM), can be considered to speed up and reduce the cost of the qualification process by avoiding destructive analysis. The destructive analysis aims to obtain the precise dimensions of the flaws. However, this permanent damage would be avoided if non-destructive process could be applied to generate the same information, i.e., provide flaw dimensions required to produce POD data sets. This paper presents the motivation and new methodology to generate POD curves based largely on TFM examinations to get the reference flaw size information. The result shows the feasibility of developing POD curves without destructive analysis and using the TFM to get flaw size data.

Keywords: Probability of detection (POD), Phased array ultrasonic technique (PAUT), Total focusing method (TFM), Flaws, Sizing.

4.1 Introduction

The methodology currently used to determine the POD of non-destructive method consists of fabricating coupons with range of flaw sizes and reporting the locations of flaws detected by the NDT procedure being evaluated for reliability. The number of coupons and flaws depends on the level of confidence set to meet the objective of the qualification. For procedure qualification, MIL HDBK 1823A recommends using a minimum of 60 flaws for a hit-miss binary set or 40 flaws for an amplitude-based set to demonstrate a POD of 90% with a confidence level of 95% ($a_{90/95}$) (Annis, 2009).

Determining the flaws dimensions in the coupons is a necessary step in carrying out the POD exercise and a variety of techniques can be used. In most cases, the size assumed/provided by the coupon manufacturer is used. However, for the POD to provide a valid indication of reliability, the flaw size should be accurate, and many factors can contribute to flaw sizes being different from those provided by the manufacturer (Safizadeh et al., 2004). The destructive analysis is expensive, and it also has the detrimental effect that the sample is no longer available for further usage (Ginzel et al., 2022). Although not required by most standards using POD to determine inspection reliability, other NDT methods can be used to estimate flaw sizes, for example, radiography for the length.

Upon an extensive search of different codes (MIL-HDBK 1823A, ASME Art. 14, ASTM E2862, ASTM E3023, DNV-GL ST F101, ENIQ Recommended Practice #5), the conclusion is that for PODs, there are no rules to determine flaw size except for DNVGL-ST-F101 which requires cross-sectioning samples to determine flaw size by metallographic analysis. In accordance with POD standards, there is an assumption that the size given by the manufacturer is usually taken as the true value. (Annis, 2009; DNVGL ST-F101, 2017; ASME Section V, Article 14, 2021; ASTM E3023, 2015; ASTM E2862, 2018). However, flaws offered by flaw

sample manufacturers have sizing uncertainties. Recent developments in Ultrasonic TFM have indicated that it can provide good accuracy in flaw sizing, which could improve the reliability of POD and save time and expense involved in destructive tests or micro-CT X-ray verification of flaw sizes (Bannouf et al., 2018; Carignan et al., 2019; Carter & Rogerson, 2013; Felice et al., 2014; Ginzel et al., 2015; Peng et al., 2018; Rachev et al., 2018; Volf et al., 2020; Carter et al., 2013). Since POD is highly dependent on accurately identifying a flaw size, there must be confidence in the sizing method. In this paper, TFM is used as a tool to provide accurate flaw sizing for POD determinations.

4.2 Methodology

The objective of the paper is to propose a methodology using NDT tools to get as accurate as technically feasible, flaw dimensions to plot POD curves. Due to the fact that NDT methods will be applied to quantify flaw size (horizontal axis of the POD curve), it is essential to ensure that the methodology described hereafter is independent of the procedure being qualified. It should use methods not involved in the technique under evaluation, i.e., for which the POD curve is being built. As an example, it would be inappropriate to use radiography to measure flaws length and then qualify a radiographic procedure. This would lead to a situation where the true flaw size is generated with the same method under evaluation.

4.2.1 Selection of NDT methods

Non-destructive evaluation of dimensions of indications is primarily influenced by the geometry of the coupons, their location, and their orientation. The methodology proposed hereafter uses NDT methods best suited to get flaws dimensions information to fully

characterize the affected volume inside the specimen. The NDT methods that can be used for sizing embedded indications are:

- Radiography, preferably Computed or Digital Radiography (CR & DR)
- Computed tomography (CT-Scan)
- Time-of-Flight Diffraction (TOFD)
- Phased array ultrasound (PAUT)
- Total Focusing Method (TFM)

4.2.1.1 Radiography testing

Radiography is a projection technique that makes it possible to obtain the real dimensions of a discontinuity if it is possible to orient the axis of the beam perpendicularly to the defect's axis to be measured. Radiography is a very useful tool for measuring the length of flaws, their axial position, and the height of volumetric flaws on an angled shot. However, radiography does not allow, in most cases, to position of the flaws in the thickness of the part. Two main drawbacks to accurate dimensions of the flaws in radiography are magnification and geometric distortion. Both these phenomena, combined with the uncertainty about the depth of the flaw will add up and cause inaccuracy of the reported dimension and location (Shull, 2002). In order to get accurate dimensions and position of flaws, a CT-Scan would be needed. CT Scan has some limitations. These can include the dimension of the specimen, its thickness, and the density of the material. Aluminum is more suitable for CT-scan imaging than steel, so steel components should be relatively thin for a successful flaw characterization. Also, the sample must be cut to allow rotation in the CT machine, limiting its application to samples of relatively small dimensions (Handbook of Advanced Non-destructive Evaluation, 2019; Kastner et al., 2019).

4.2.1.2 Time-of-flight diffraction (TOFD)

TOFD is a well-known ultrasonic method for height sizing and has been demonstrated to be accurate within approximately one wavelength for positioning and sizing in the thickness plane. Diffraction is a wave phenomenon occurring when the beam bends around the tip of a

flaw and generates an omnidirectional wave that irradiates in all directions (Al-Ataby et al., 2010). The technique uses forward scattering in a through-transmission configuration, and the time of arrival of diffracted waves permits the calculation of the depth of the diffraction point. TOFD is adequate to measure the height and position of an embedded volumetric or vertical planar flaw. The height sizing accuracy is typically the wavelength, so increasing the frequency improves height sizing measurements. TOFD suffers from dead zones near the surface boundaries, and sizing accuracy reduces as flaws approach the test surface (ASTM E2373, 2014).

4.2.1.3 Phased array ultrasonic method (PAUT)

An array transducer is a monoblock piezo composite cut at regular intervals in order that each element's width is in the order of the wavelength. Each element has its own electrical connection and can be pulsed independently of its neighbors. A phased array transducer is thus an ultrasonic probe that is controlled electronically by applying emission and reception time delays to produce focusing and steering. A phased array system is thus equivalent to an array of individual transducers with varying focusing lenses and incident angles.

Focusing is an intrinsic property of phased-array configuration. Time delay focusing is only possible along the active axis, i.e., in a plane parallel to the array. The beam spread in the passive axis is a function of the element length. So, it is common to describe two near-field values for a phased-array configuration: one along the active axis (which can focus) and one along the passive axis (which cannot focus) (ASTM E2700, 2014; Ginzel, 2013).

Sizing with PAUT can be done using back scattering tip diffraction. This method efficiently uses a shear wave, and the diffraction wave's amplitude can be improved using time delay focusing. For volumetric flaws, sizing is based on analysing the amplitude received as a function of probe displacement. It is a beam boundary method, and the accuracy is thus

dependent on the beam size. While focusing will improve sizing in the array plane, the sizing accuracy along the passive axis is fixed by the element length. Several techniques can be applied to reduce the beam boundary uncertainty: among them using focussing on the passive axis or pivoting the array by 90° to measure the flaw length with the array plane parallel to the scan axis.

4.2.1.4 Total focusing method (TFM)

TFM is a synthetic focusing technique that uses Full Matrix Capture (FMC) for elementary ultrasonic signal recording. The TFM algorithm is a delay and sum processing that enhances coherent signals produced at the boundary of a flaw and otherwise attenuate non-correlated artifacts. The algorithm produces an image equivalent to focusing all array elements over the region of interest (ROI) and getting the maximum acoustic resolution achievable given the aperture, wave mode, and frequency. TFM sizing is classified as a beam boundary method, but the algorithm provides improved spatial resolution, and the boundary of a flaw can be delineated. TFM imaging technique provides intuitive, interpretable results and a high signal-to-noise ratio. Also, its calculation is based on the knowledge of the wave velocity and the wave interaction with the specimen back wall and flaw. In this regard, the TFM algorithm calculates the TFM image based on the selected wave mode and path (BS ISO 23865, 2021; ASME Sec 5 Article 4, 2019).

A complete flaw characterization is feasible with TFM. If multiple configurations are applied to the sample, and the data is merged into a single volume, then the data set is equivalent to an ultrasonic CT scan. Producing such an ultrasonic pseudo CT-scan requires adequate hardware and software that permit accurate encoded data acquisition and processing of the data from various contact surfaces and TFM modes to image flaws from various observation points. The sample used in case study #1 is illustrated in Figure 4.1.

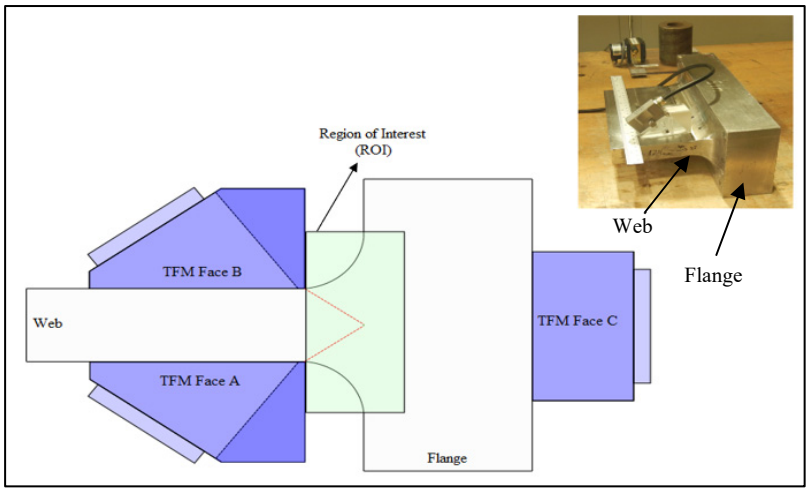

Figure 4.1 Schematic view for TFM of the T-joint sample
in the first case study by Beam Tool software

4.2.2 Sizing process

As a first step, the methodology to size flaws requires an analysis of the specimen geometry to determine which inspection surfaces are available to collect flaw data. For a butt weld, there are four possible contact surfaces for ultrasonic inspection, while a T-joints has three surfaces. Then the flaw geometry and location in the weld must be considered to select the best NDT methods and configurations to extract the dimension required for the POD. As an example, if the length sizing of volumetric flaws (e.g., slag inclusion) is the qualification goal, radiography would be a recommended method for measurement. RT has adequate sensitivity to such types of flaws, and the projection on the detector will represent the flaw length with a known geometric error. To ensure that RT sizing is accurate, a supplementary inspection using TFM would be advisable to confirm that RT did not undersize the indication due to portions of the slag thinning and presenting no RT evidence. During the development phase of a qualification program, an essential aspect to consider is quantifying the sizing measurement error and assessing if it is suitable for the qualification goal. The POD flaw size range shall be known in order to select an NDT sizing method suitable for that range (Annis, 2009; BS 7910, 2019). For example, in RT and UT, the sizing error can be easily estimated by calculating the geometric projection or beam width. The error can be verified using a calibration block

covering the flaw size range of interest. A practical case that was dealt with is the divergence of a phased array transducer in the passive axis. Using a calibration block, we verified that the TFM height measurement error was equivalent to the wavelength along the active aperture. However, the sizing measurement was systematically overestimated along the passive axis by approximately the beam width (-6dB). In order to reduce the passive axis error, a phased array transducer with a lens focussing on the passive axis reduced this error to approximately 1 mm. Validation of the sizing methodology should be verified using calibration blocks and preferably with a coupon. If a coupon is produced, it should be destructively analysed using the salami cutting method to ascertain that the NDT sizing strategy finds all the relevant defects and that the sizing error is within an acceptable tolerance band. The proposed methodology for sizing process is shown in Figure 4.2.

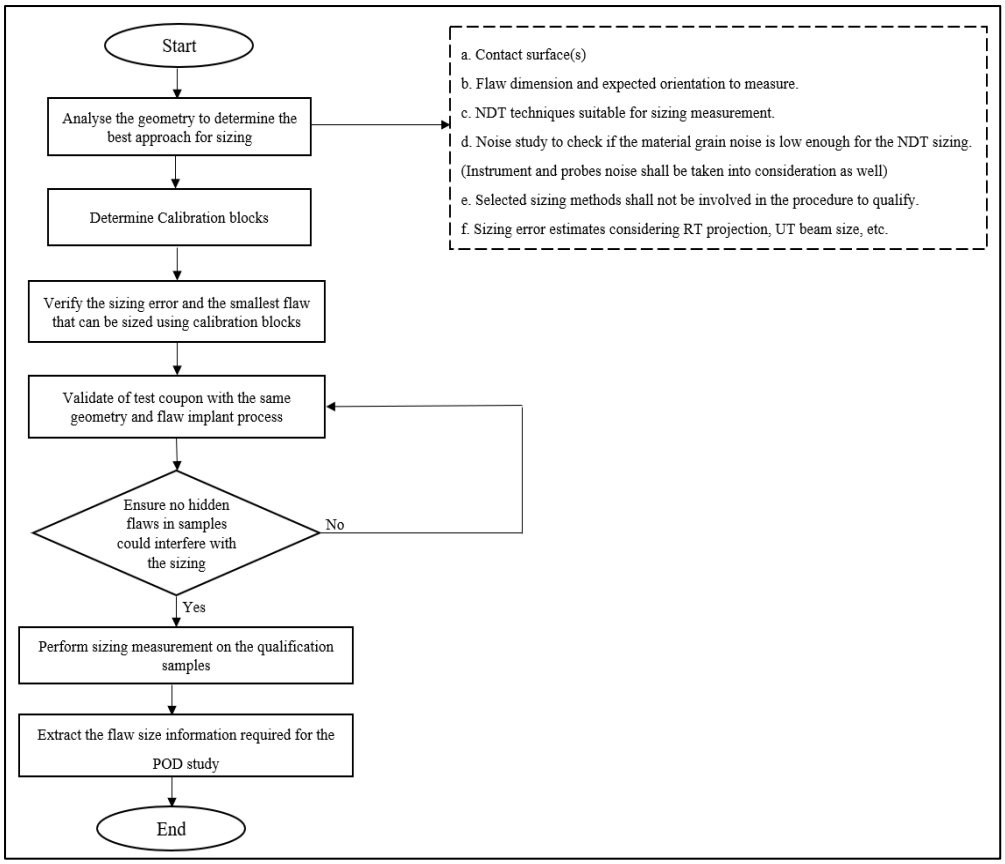

Figure 4.2 Proposed method for sizing process

4.3 Results and discussion

The proposed methodology was applied to two case studies, and both cases concern the demonstration of ultrasonic procedures for inspecting the trailing edge of hydraulic turbine runners. A volumetric flaw size height of 3 mm and length of 6 mm is proposed as a target value to evaluate the proficiency of NDT methods. Critical flaw size was obtained from fatigue stress analysis based on Kitagawa diagrams and finite element analysis. There is a consensus that the critical flaw size is a good candidate to demonstrate NDT methods proficiency (Gagnon et al., 2013).

4.3.1 Case study 1: T-joint mock-up sample

The first case study is a mock-up T-joint sample that was manufactured to investigate the performance of NDT methods. It is made from martensitic stainless steel and is representative of the geometry of a Francis runner trailing edge weld. Ceramic beads were inserted (30 beads, ranging from 1 to 5 mm) to create volumetric flaws of known size. The qualification exercise aims to produce POD curves for conventional ultrasonic and PAUT techniques.

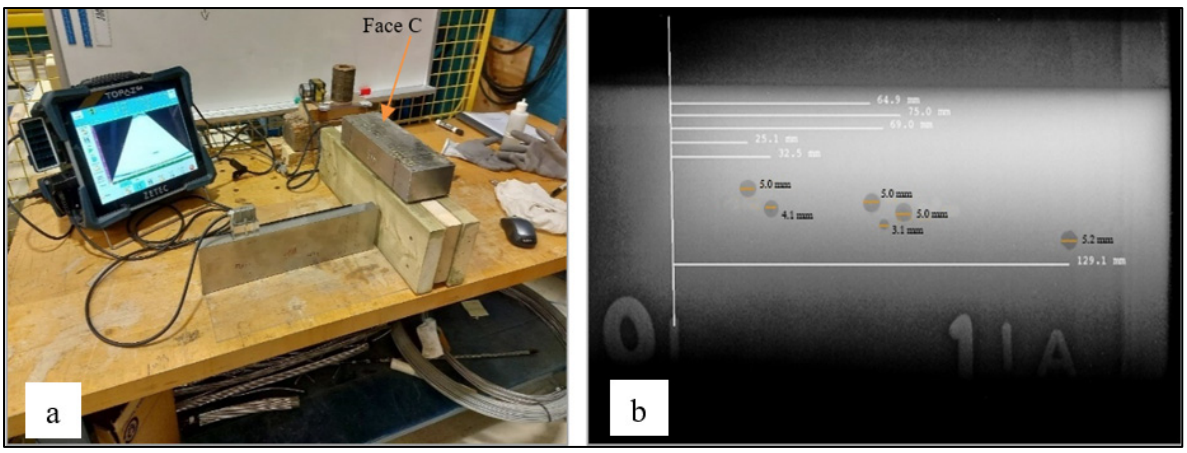

Figure 4.3 NDT tests (a) T-joint examination from Face C by TFM
(The sample is inserted into wooden support and only the flange is visible), and
(b) digital radiography was applied to locate and size ceramic beads

Ultrasonic testing was performed on the sample according to the procedures used for qualification, and the results could not be matched with the fabrication report. A problem reported by the supplier is that small beads did float and flow to some extent in the weld puddle. The location stated in the fabrication report is thus the intended position of beads and not the actual location. The sample was investigated using digital radiography and encoded TFM from the blade (Face A and B, as shown in Figures 4.1 and 4.3b). RT revealed that the approximate location of artificial flaws (ceramic beads) did not correspond with the fabrication report. Only 16 out of 30 detected beads with RT, could have their size confirmed or corrected. Investigation of the coupon was expanded to include high-resolution ultrasonic inspection from Face C (flange), which is not accessible during an in-service inspection, to locate precisely every bead.

Two techniques were applied, normal incidence PAUT with focussing on the area of interest, and contact TFM (5MHz 64-element transducer). Both techniques produced very similar results, i.e., locating 30 discontinuities in the weldment and confirming the absence of unintentional flaws. The final flaw table used for the qualification exercise was updated using RT flaw size when available and PAUT/TFM position information (Face C inspection) to produce the final flaw table. There are 14 beads not observed by RT, and their size was deduced from a combination of factors based on the ultrasonic reflective energy (PAUT from Face C), the TFM indication size, and the proximity from the intended location (fabrication report). Good knowledge of NDT methods was a key factor in determining the location and most probable size of the flaws with high confidence to produce a reliable final flaw table to assemble the POD data set.

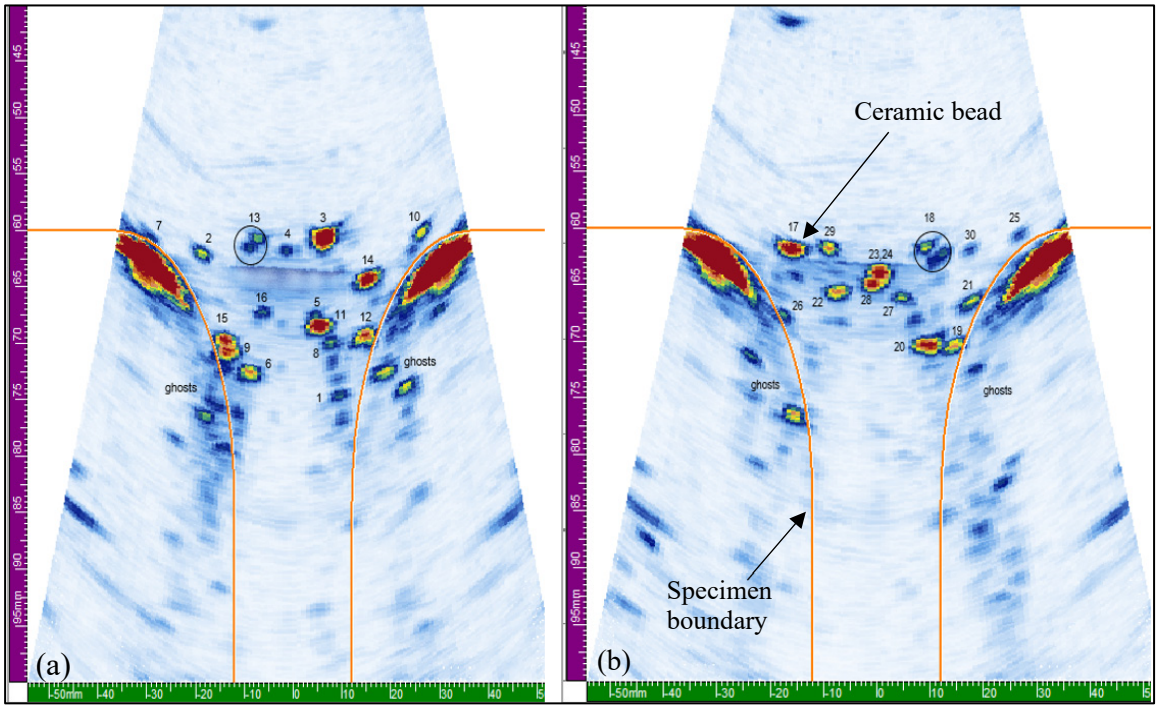

Figure 4.4 Inspection results from Face C by Ultravision software 3. End view with projection along the weld axial direction to show discontinuities. All 30 ceramic beads are detected from Face C. Ghost echoes are produced from paths reflecting from the sample's boundary or a creeping wave. (a) PAUT results from Face C (axial distance 0 - 100 mm) and (b) PAUT results from Face C (axial distance 100 - 200 mm)

In this experiment, the NDT methods used to size and locate flaws were independent of the procedures to be qualified (RT, TFM, and large aperture normal incidence PAUT from the flange). The methods for which a POD curve was built are manual fixed angle beam, manual PAUT, and encoded PAUT. All methods to qualify are applied from the blade and the procedures tested have nothing in common with the ultrasonic techniques applied on Face C as shown in Figure 4.3a. Therefore, the image in Figure 4.4 is only possible in the NDT lab because that Face C is not accessible once the component is installed in the turbine well enclosure.

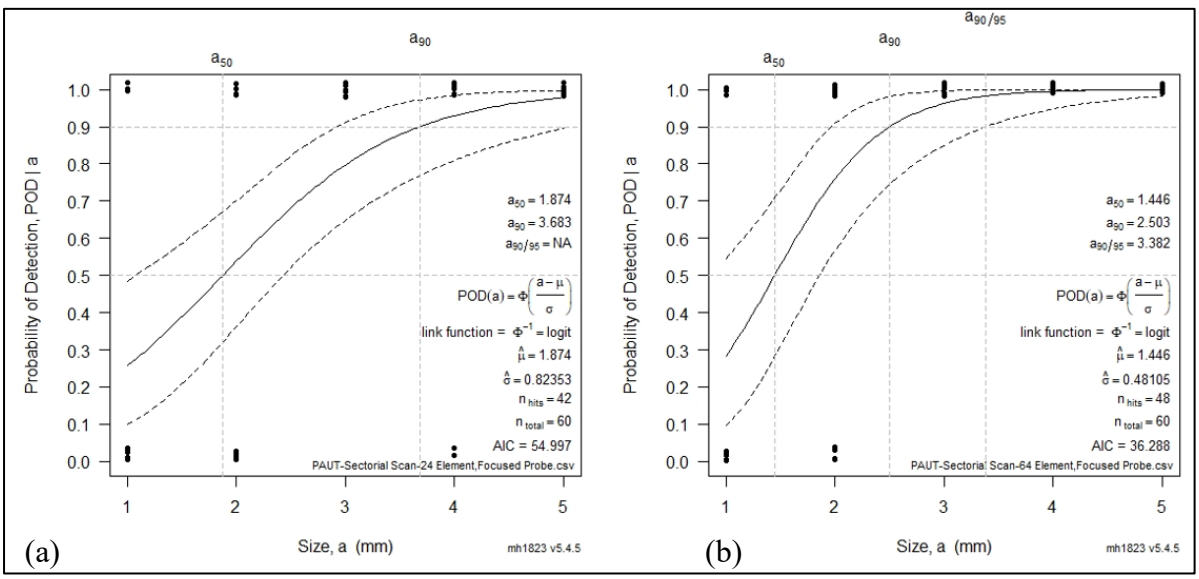

Figure 4.5 Examples of POD curves by mh1823 Software for encoded PAUT inspection from the blade on Face A&B (a) POD Curve for PAUT Sectorial Scan by 24 Element and (b) POD Curve for PAUT Sectorial Scan by 64 Element

Figure 4.5 shows some of the resulting POD curves using a corrected flaw table built from RT, TFM, and PAUT on Face C. Inspecting the sample using various PAUT procedures and probes produced a 90% POD (a_{90}) between 2.50 and 3.73 mm for the bead diameter. This experiment demonstrates the benefits of PAUT as a more reliable NDT method for runner weld joint inspection. These POD curves were obtained after correcting the manufacture-supplied flaw table using the high-resolution phased array (TFM and large aperture PAUT) and digital radiography.

4.3.2 Case study 2: Real turbine runner

The POD methodology explained in Figure 4.2 was tested on a real Francis turbine runner. For this project, a 17-blade martensite steel (CA6NM) runner fabricated around 2014 was available. The runner never experienced service and is kept in an outside facility for non-destructive testing techniques development. The welds were inspected during fabrication and met the acceptance criteria based on ASME standards (ASME Sec 8, appendix 12). The blade-to-band weld joint of the runner with an example of TFM indications is shown in Figure 4.6.

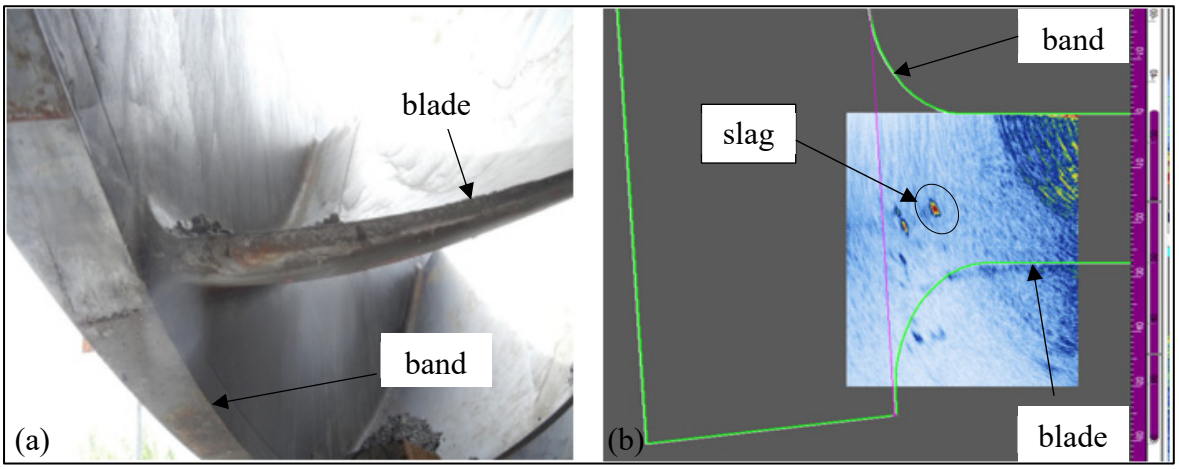

Figure 4.6 Blade-to-band weld joint of the runner with an example of TFM indications

A review of the geometry and NDT methods with good capability to identify flaws led to the application of angle-beam TFM performed directly from the blade. A transducer with nominal frequency of 5MHz, 64 elements with a pitch of 0.6 mm was selected (Advanced PAUT Probes for TOPAZ64 Application Solution, 2020), and several tests were made to optimize the configuration. The TFM configuration offers a large aperture for improved flaw height sizing in the weldment. The gain setting is a crucial variable that must be set to find small flaws but not trigger false calls. The overall sensitivity of the procedure is -26 dB compared to our calibration block made of SS415 (same composition as CA6NM but hot rolled) and containing 3 mm side-drilled holes (SDH) (ISO 19675, 2003). The TFM configuration also includes a Time Corrected Gain (TCG) to normalize the amplitude response over the region of interest (ROI). This configuration is very sensitive to small volumetric flaws such as porosity in the

parent material, with a vertical sizing accuracy of the order of the wavelength based on calibration blocks with SDHs. The only drawback with this procedure, which is fundamental for the qualification exercise, is the sizing accuracy in the horizontal plane, the plane perpendicular to the array axis, which is of the order to 2.2 mm. Considering that the objective of the qualification is to demonstrate if procedures can meet an axial size (slag length) of 6 mm or better, the axial sizing error is thus of critical importance.

In order to improve detection and sizing accuracy, a second array transducer was selected. Transducer #2 is a 5MHz 64-element array designed specifically for high-temperature hydrogen attack (HTHA). It has two distinct features: a small element pitch of 0.3 mm and focusing on the passive axis at a depth of 15 mm in the component (Advanced PAUT Probes for TOPAZ64, 2020). The small element pitch increases the array effectiveness at high refracted angles and focusing on the passive axis reduces the beam spread in the horizontal plane. The active axis is the transducer array axis where elements are stacked at regular spacing, and the passive axis is perpendicular to the transducer array axis, and beam width is fixed by the element width, as shown in Figure 4.7. These two features produce a small concentric beam and improve spatial resolution. The TFM-AF (AF is for passive axis focusing) configuration uses the exact same settings as for the regular TFM probe, the only difference being the construction of the array where a lens is added to focus along the passive axis and an element pitch of 0.3 mm.

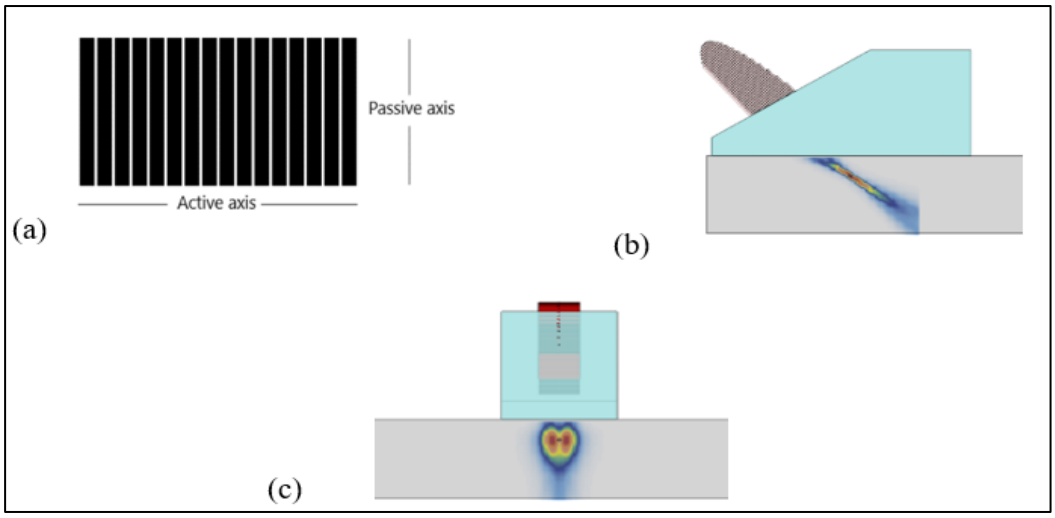

Figure 4.7 Illustration of the passive and active axis by Ultravison 3 simulation software (a) Dimensions of phased array probe, (b) Transducer array by Active axis and (c) Transducer array by Passive axis

Height sizing accuracy was verified on calibration blocks. As seen in Table 4.1, PAUT tends to oversize by an amount proportional to the beam width (Ewen et al., 2017) . TFM has a better sizing accuracy (0.55 mm for TFM and 0.88 mm for TFM-DF) because the sum and delay algorithm emphasize coherent signals diffracted from the flaw's contour and otherwise attenuates noncorrelated signals. On the other hand, the length sizing error correlates with the passive axis's beam size. Transducer #2 produced an oversizing error of 1 mm, which is in line with a beam width of 0.95 mm computed using the focussing factor to produce a focal point depth of 15 mm in steel.

Table 4.1 UT Sizing measurements on calibration block

Hole Diameter (mm)				
SDH diam.	0.75	1.5	3	**Mean error (mm)**
PAUT	2.8	3.8	5.3	2.22
TFM	1.4	1.8	2.3	0.55
TFM-DF	1.9	2.5	3.5	0.88

The two TFM configurations were applied to the accessible blade-to-band welds, as shown in Figure 4.8. Encoded inspections were performed with an axial resolution of 1 mm. All indications from the welds (casting inclusions were filtered out) were mapped and sized down to a relative intensity of -26 dB. The TFM configuration detected 51 indications, while the TFM-DF configuration detected 90 indications. The higher number of indications with the focused probe results from its array design: the small pitch makes the probe more effective at a high incidence angle, and the focusing on the passive axis makes this probe more sensitive to minute flaws.

Flaw characterization proceeded as follows; the TFM configuration data are used for height sizing because it proved most accurate on calibration blocks (larger aperture). If the TFM configuration misses an indication, height sizing reverts to the TFM-DF measurement. We used for length sizing the TFM-DF configuration because focusing on the passive axis provides a better resolution in the horizontal plane. The final sizing of all 90 discontinues produces results ranging between 1 and 14 mm for length and from 1 to 6 mm for height.

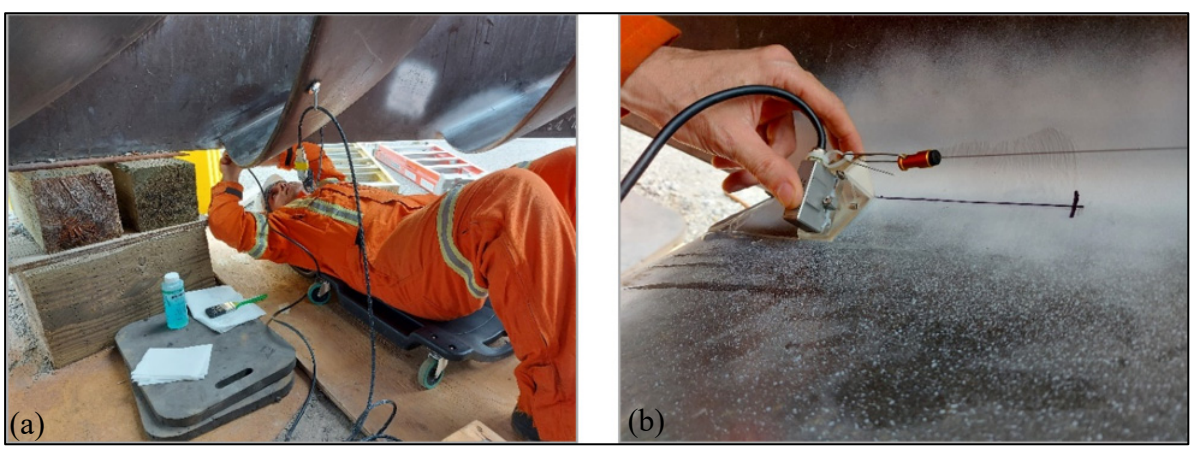

Figure 4.8 TFM inspection (a) with angled-beam TFM on the extrados surface and (b) intrados surface. The probe shown is the standard array, 5MHz 64-element with 0.6 mm pitch

The welds were then tested with the PAUT procedure to qualify. The procedure uses a standard 5 MHz 64-element transducer with a pitch of 0.6 mm. The aperture is set to 24-element with a

focal law strategy based on a compound scan, 40° to 70° shear wave. This configuration provides a good compromise in terms of sensitivity to small SDH and good coverage of the weldment for a single pass encoded scan. The overall analysis sensitivity was set to -26 dB from an IIW steel block containing 3 mm SDH (ISO 19675, 2003). A total of 60 discontinues were reported. A comparison between the TFM sizing table and the PAUT results revealed that five discontinues were observed with PAUT and not with any TFM configurations. An investigation found that these five discontinues were lack of fusion (LOF), i.e., planar in nature (narrow-angle reflective range). The qualification is for volumetric type flaws (slag inclusion), so those five LOF were not included in the POD analysis.

MH1823 software was used to calculate the probability of detection from the data (Annis, C, 2018, Version 5.4.5). What is determined here is the detection capability of a conventional array transducer using a PAUT compound configuration using reference values obtained with the high-resolution TFM/TFM-DF configurations. The TFM/TFM-DF configurations were selected to get the flaw size data because they demonstrated excellent detection (number of indications) and sizing capability on calibration blocks and T-joint sample used in case study #1. Numerous publications also support this choice, which reports that TFM is very sensitive and more precise in characterizing volumetric embedded flaws (Ginzel et al., 2022). All our experiments are in agreement that TFM is the right NDT method, if applied with proper NDT engineering analysis, to get flaw data that is as valid as a destructive method would provide.

MH1823 graph for PAUT hit/miss versus length sizing (Figure 4.9a) shows a well-defined POD curve (black line). The 90% POD (a_{90}) is estimated at a length of 6.77 mm, and the 50% POD (a_{50}) is estimated at 2.68 mm flaw length. However, the confidence bands (dashed lines) are not symmetrical along the POD curve and provide a hint that the data set does not have a linear distribution along the size axis. The main reasons for the asymmetrical confidence bands are (a) that significant flaws were repaired after NDT inspection during fabrication and (b) that the TFM-AF configuration has limited capability to find very short flaws (less than 1mm). So, the data set is mainly built around flaw size *(a)* in the range between 2 and 6 mm in length.

The second MH1823 graph (Figure 4.9b), where the flaw height is correlated to the PAUT hit/miss results, shows a well-defined knee with a 90% POD (a_{90}) estimated at 3.76 mm and a 50% POD (a_{50}) estimated at 2.25 mm. The confidence band is more balanced for the height because the population of flaws is more linearly distributed in the 1 to 5 mm range (very similar to case study #1). A closer look at the distribution of hit/miss data points in Figure 4.9b reveals that 89 out of 90 indications were height-sized to be 5 mm or less. This means that most of the flaws left after fabrication are 5 mm or less in height. Most larger flaws, i.e., height greater than 5 mm, were removed during in-shop inspection and repair. This directly implies that the inspection methodology used during fabrication leaves undetected flaws of 5 mm or less in height (again, this observation is in line with case study #1). If the PAUT procedure under qualification had been applied during fabrication, 51 flaws with heights equal to or greater than 3 mm would have been reported for repair (depending on the rejection threshold, calibration block, etc.). That still leaves a certain quantity of flaws in the 1- 3.4 mm range, 39 to be precise, left after PAUT inspection but with a vertical height below the critical size (except for 2 flaws) and located predominantly in the weld root region (band to blade interface where stress is low). The benefit of using the PAUT configuration during fabrication is quite significant; all flaws with a height greater than 3.5 mm would have been removed, and most of the remaining flaws would be located in the weld root region. Obtaining POD data from a real-life component inspection has, of course, intrinsic limitations, e.g., the real number of flaws is unknown, and flaw size distribution is not controlled. However, this methodology makes it possible to evaluate the capability of any NDT procedure on the actual component that is being non-destructively tested.

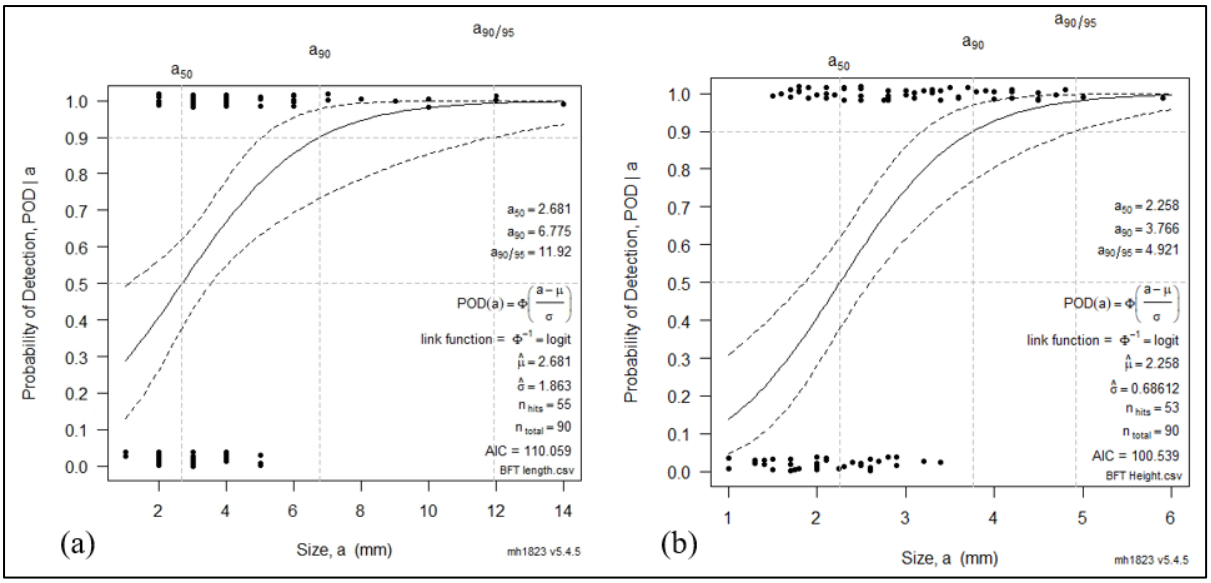

Figure 4.9 POD curves generated with the proposed methodology where TFM measures flaw size (a) POD curve for flaws length from PAUT method and (b) POD curve for flaws height from PAUT method

4.3.3 Comparison between case studies 1 and 2

The proposed methodology to build POD curves using a real component can be used to assess the risk of leaving a flaw after fabrication based on the ultrasonic technique and inspection procedure. We observe in our experiment (Case study #2) on the real component that the 90% POD (a_{90}) for an encoded conventional phased array inspection is 3.76 mm flaws height and 6.72 mm flaws length. These results align with our previous study (case study #1) using a mock-up T-joint and ceramic beads where 90% POD (a_{90}) for the same inspection configuration was reported to be 3.42 mm (1-dimensional analysis, only flaw diameter was considered) (Bajgholi et al., 2021). This implies that the measured POD for flaw height measured on the training runner is aligned with our experimental data generated with a mock-up. Realistically, conventional phased array inspection applied to a turbine runner blade-to-band joint should have a high probability of findings embedded flaws with a height (perpendicular to the stress axis) in the range of 3.42-3.76 mm based on our inspection methodology and the component geometry. This conclusion was achieved using a real

component and without requiring destructive analysis that would have destroyed the runner used for training.

4.4 Conclusion

The development of POD curves relies on the accurate knowledge of flaw size. Most of the current methodologies used to develop POD curves do not specify uncertainty requirements for the reference flaw size values but without any specific requirement, flaw size information is expected to be accurate and trustworthy. The only requirement found in the literature is the salami-cutting method recommended by DNVGL ST-F101. However, this approach inconveniences that the sample must be destroyed after NDT testing. Moreover, improvements in procedures cannot be compared using the same set of samples. Due to the manufacturer's misleading flaw table, our POD exercises based on the fabrication report did not provide consistent results (Case study #1). After thoroughly inspecting the T-joint sample using NDT methods, specifically RT and FMC-TFM, we realized a mismatch between the fabrication report flaw size and NDT measurements. When the flaw size table was corrected, we produced meaningful POD curves using reference flaw size obtained with advanced NDT methods. This approach, where the flaw dimensions are entirely measured by non-destructive means, allows the use of real components to develop POD curves. It also keeps the component available for further training and qualification of NDT personnel.

In our experience, using advanced NDT methods to ascertain flaws characteristics for the purpose of building POD curves is necessary to improve confidence in the data set. Sizing a flaw is not an easy task (Davis, 2001). However, using NDT methods, specifically the TFM, and a methodology to check the sizing error, reliable information on flaw size can be obtained with a higher degree of confidence than the ones supplied on a fabrication report. Confidence in the sizing data relies on a careful analysis of the qualification goals, applicable NDT methods, and a process that measures the sizing capability and accuracy.

In TFM analysis, sensitivity and sizing accuracy are functions of the inspection set-up. Probe positioning relative to the inspection volume, probe design, probe aperture, probe frequency, and the voxel grid size in the region of interest may have a bearing on the results. The nature of the measured flaw also affects the sensitivity and accuracy of a TFM configuration (vertical planar flaws are challenging). TFM imaging can improve tip diffractions' resolution, which is probably the most accurate sizing technique for planar flaws. TFM sizing resorts to a beam boundary technique when diffraction tips cannot be resolved. However, the TFM delay and sum algorithm improves spatial resolution for coherent signals and thus delineates the contour of a flaw.

In POD reliability analyses, flaw sizes determined using TFM can be used as “true” flaw sizes with adequate evidence. Codes prescribing POD analysis should provide guidelines on how to ascertain flaw size and allow for other means than metallographic cross-sectioning to get the flaw size data. A round-robin test should be conducted on one or more sets of samples in the future. Comparing the TFM reported sizes with destructive tests and micro-CT X-rays will then provide a better understanding of the limitations of TFM to provide accurate flaw size estimates.

Acknowledgment

The authors would like to thank the Hydro-Québec Research Institute (IREQ), Mitacs Acceleration program, and oNDuTy program for financial support of part of the present research work. The authors also wish to acknowledge Dr. Martin Gagnon and Mr. Jeremy Carignan for their discussions and technical assistance.

CONCLUSION

This thesis investigated the performance of different ultrasonic inspection technologies applied to hydraulic turbine runners. Hydro-Québec, as a major power generation company, uses fracture mechanic models to estimate the service life of turbine runners so as to avoid unpredicted halts of such critical equipment. For these models, the location, the orientation, and the size of welded joint flaws are some of the most influential inputs. This project aims to provide Hydro-Québec with a clear understanding of the performance of advanced ultrasonic inspection methods in detecting harmful flaws that could impact the service life of their turbine runners. In order to improve our knowledge of the integrity of the welded joints of hydraulic turbine runners and to investigate the reliability of NDT methods in picturing the aforementioned integrity, the following objectives should be answered:

- Evaluation of the capability of ultrasonic inspection methods to detect flaws in a T-joint mock-up mimicking a Francis runner trailing edge.
- Quantification of the inspection reliability (POD) of various NDT methods applied to a T-joint sample representative of a turbine runner trailing edge.
- Determination of the probability of detection of advanced ultrasonic inspection using TFM as an accurate non destructive sizing method.

Considering the aforementioned objectives, each chapter of the thesis answers the following:

- Chapter 2: What are the best NDT method(s) and technique(s) for inspection of the trailing edge of a turbine runner?
- Chapter 3: What is the POD for volumetric flaws located in the trailing edge of a turbine runner?
- Chapter 4: How to demonstrate the efficiency of NDT methods applied to a real turbine runner?

Contributions

Chapter 2 is devoted to the capability of advanced ultrasonic inspection technologies for hydraulic turbine runners. The goals were to find the best NDT method(s) and technique(s) for inspection of the trailing edge of a turbine runner. This work is the first phase of a more ambitious program aimed at improving the reliability of inspection of critical areas in turbine runners. This phase one objective is to collect initial data on a simplified mock-up and then to compare the experimental ultrasonic data with the results of simulations performed by CIVA, a computer simulation package. The material was inspected by various NDT methods, namely conventional pulse-echo, phased array, and TFM. Inspection procedures used either free probe movement (non-encoded) or linear-encoded scan. All inspections were carried out with certified personnel, scan plan preparation (ray tracing and coverage analysis), and Codes were compliant. With these inspection results, detection rates were obtained to compare each method's effectiveness. The result shows that TFM is the best ultrasonic inspection technique to provide reliable flaw data to the IREQ's life estimation model among the different ultrasonic testing methods evaluated. In addition to this technique's ability to detect small flaws, the algorithm allows a better definition of flaw geometry and highlights the nature of the target (facets, size). The CIVA model could be used to simulate ultrasonic inspection of a weld. However, the sample and the inspection system's models must be defined with high accuracy to obtain reliable data. To do this, we need to adjust model parameters through validation loops based on precise measurements on real calibration samples. While defining accurate numerical models seems like a tedious task, it ultimately drastically reduces the costs of developing a reliable inspection strategy. Therefore, our significant contribution was to show the effectiveness of each ultrasonic technique by measuring its detection rate from a representative coupon.

In chapter 3, we evaluate the reliability of NDT methods for the inspection of weld joints in hydraulic turbine runners. Conventional Ultrasonic Testing (UT), Phased Array Ultrasonic Testing (PAUT), and Total Focusing Method (TFM) and Radiography testing (RT) were compared. The knowledge of the probability of detection (POD) curves, required by fitness-

for-service assessments, is mostly absent for structure such as hydroelectric turbine industry. The main goal of the study reported in this paper is to evaluate the reliability of NDT methods for the inspection of welded joints in turbine runners. It focuses on the determination of POD curves for different inspection techniques of a T-joint sample representative of a turbine runner trailing edge with artificially induced flaws (ceramic beads inserted during welding). The result shows that, TFM performed slightly better than PAUT with a linear array and 0.6 mm element pitch (standard pitch for 5MHz). The encoded inspection did provide slightly better POD for all the techniques. Only TFM with a standard array did achieve a 90% POD (a_{90}) for a flaw size of 3 mm. In order to verify if detection improvements are possible, a special design array was added to the test matrix. The array has a smaller element pitch, 0.3 mm, and a focusing lens is added in the probe case to limit the beam spread in the passive axis. The specially designed array proved to be more effective in finding smaller ceramic beads with both PAUT and TFM methods. So, Two configurations achieved the best POD for our embedded ceramic flaws (TFM, shear wave, with a focused probe in the passive axis & PAUT, shear wave, 64 element apertures with focusing in the passive axis).

Afterward, chapter 4 presents our motivation and process to generate POD curves based largely on TFM examinations as the ground truth method to get the flaw size information. Two case studies are presented to demonstrate the NDT methodology for producing POD curves without relying on destructive analysis, and an application of NDT methods to a real turbine runner was demonstrated. The proposed methodology to build POD curves using a real component can be used to assess the real risk of leaving a flaw after fabrication based on the array geometry and the ultrasonic technique. We observe in our experiment (case study #2) on a real component that the 90% POD (a_{90}) for an encoded conventional phased array inspection is 3.77 mm flaws height, and 6.77 mm flaws length. These results align with our previous study (Chapter 3) using a mock-up T-joint and ceramic beads where 90% POD (a_{90}) for the same inspection configuration was reported to be 3.42 mm (1-dimensional analysis, only flaw diameter was considered). This implies that the measured POD for flaw height measured on the real runner is aligned with our experimental data generated with a mock-up.

Realistically, conventional phased array inspection applied to a turbine runner blade-to-band joint should have a high probability of findings embedded flaws with a height (perpendicular to stress axis) of 3.5 mm based on our inspection methodology and the component geometry. This conclusion was achieved using a real component without requiring a destructive analysis that would have destroyed the runner used for this work. In our experience, the POD exercises based on the fabrication report did not provide consistent results because the manufacturer's flaw table was misleading. Only once we interrogated the T-joint using advanced NDT methods, more specifically RT and TFM, did we understand that the problem was the fabrication report flaw's position and size were not aligned with NDT measurement. Once we corrected the flaw size table based on NDT methods, our data produced meaningful POD curves. This approach, where the flaw's dimension is entirely measured from non-destructive means, allows the use of real components to develop POD curves and keep the component for training and qualification of NDT personnel. In our experience, using advanced NDT methods to ascertain flaw's characteristics for the purpose of building POD curves is necessary to improve confidence in the data set. Sizing a flaw is not an easy task. However, using advanced NDT methods, specifically the TFM, and a methodology to check the sizing error, reliable information on flaw size can be obtained with a higher degree of confidence than the ones supplied on a fabrication report. Confidence in the sizing data relies on a careful analysis of the qualification goals, applicable NDT methods, and a process that measures the sizing capability and accuracy. The benefit is that the overall process is performed with NDT tools and does not require the destructive examination phase. The main advantage of this new approach is developing POD curves based on real components' inspection data. The value of this approach is that the overall process is performed with NDT tools for sizing, and the subject of the experimentation could be the real component that cannot always be sacrificed for destructive analysis.

Originality of the thesis

Due to the originality of the thesis, several publications related to the research work have been produced. The following part lists the aforementioned papers in chronological order:

- Mohammad E. Bajgholi, Martin Viens, Gilles Rousseau, H. Habibzadeh Boukani. 2019. « Evaluation of the dead zones in the welded joints of hydraulic turbine runners ». Presented as Conference Paper, NDT in Canada Conference, Edmonton, Canada, June 18-20, 2019.
- Mohammad E. Bajgholi, Gilles Rousseau, Martin Viens, Denis Thibault. « Performance of Ultrasonic Inspection on hydroelectric turbine runner». Virtual Presented as Conference Paper in 3rd International Symposium on Structural Health Monitoring and Non-destructive Testing, 25-26 Nov 2020, Quebec, Canada.
- Mohammad E. Bajgholi, Gilles Rousseau, Martin Viens, Denis Thibault. « Capability of advanced ultrasonic inspection technologies for hydraulic turbine runners ». Published in Applied Sciences , May 2021, vol. 11, nº 10.
- E. Ginzel, M. Bajgholi, M. Burrowes M. Guimarães, F. Foucher, Gilles Rousseau, Martin Viens « Total Focusing Method used for flaw sizing in probability of detection determination». Published in NDT.net Journal, July 2022, Vol. 27, nº 07.
- Mohammad E. Bajgholi, Gilles Rousseau, Martin Viens; Martin Gagnon, Denis Thibault. «Reliability Assessment of Non-destructive Testing (N.D.T) for Inspection of Weld Joints on Hydroelectric Turbine Industry». Submitted to Journal of Non-destructive Testing and Evaluation, December 2022. under Rev.
- Mohammad Ebrahim Bajgholi, Gilles Rousseau, Edward Ginzel, Martin Viens, Denis Thibault « Total Focusing Method Applied to Probability of Detection» Submitted to International Journal of Advanced Manufacturing Technology, December 2022. under Rev.
- Mohammad Ebrahim Bajgholi, Gilles Rousseau, Martin Viens, Denis Thibault. « Inspection of Real Turbine Runner by Advanced Ultrasonic Testing Methods for Fitness for Service Purpose». Technical report published in Institut de recherche d'Hydro-Québec (IREQ), July 2022.

RECOMMENDATIONS

The following paragraphs summarize some perspectives for continuing the current study and future research topics. These perspectives are classified into two categories, including short-term and long-term perspectives. Short-term plans could be summarized as follows:

- Inspection with a contact array probe applied to the weld fillet is new endeavor, and our results strongly support to keep developing of this method. It provides a different vantage point and may reveal planar flaws oriented parallel to the surface of the weld. Inspection at normal incidence on the weld fillet has several advantages, such as single isotropic material with low attenuation, complete weld volumetric access, and a shorter metal path.
- The Francis Turbine runner used in this investigation cannot be destroyed, so study for sizing accuracy should be considered using weld coupons to give a better understanding of the precision and reliability in measuring the ligament from the blade direct ligament measurement from the weld fillet would be an alternative to assess.
- The TFM algorithm used the direct reconstruction path. Other reconstruction paths (or modes) could be envisioned once the accurate opposite surface profile is determined. The method of delineating the opposite surface using the noise and dual-path flaw-echo is practical. However, the commercially available instrument does not offer a reconstruction path that applies to a profiled surface and not to a surface delineated from the raw data. This could be the subject of a future research project to investigate the tools necessary to accomplish a more complex TFM reconstruction with the surface information embedded in the data set.
- The only problem with post-reconstruction would be the data file size. Storing the raw TFM data would require much space because the matrix contains 4096 A-scan per acquisition position, for 1,024,000 A-scans per 250 mm long scan. So, post-processing FMC-TFM is burden to implement and needs dedicated computers, software, and lots of free time. This technology may become available for advanced image processing in the near future, and effort to reach this goal should be considered. Would it be possible to apply a compression algorithm to package A-scan in a smaller file? A review of

possible paths to compress raw A-scan data could be valuable for implementing TFM inspection using multi-mode analysis.

- Plane-wave imaging (PWI) is a hybrid technique between PAUT and TFM. Its performance in detection and sizing should be evaluated to measure its benefits for inspection reliability, speed, and sizing accuracy.
- TFM algorithm is a synthetic focusing process that effectively focuses the array on each voxel. Adding focusing on the passive axis increases the response from flaws and improves length sizing accuracy. Rules concerning the selection and depth of focusing should be analyzed using CIVA to maximize the benefits for a given thickness range.
- It is recommended to apply the dual configuration, the standard array with PAUT, and a specially designed array focussing on the passive axis for TFM. That strategy would produce the highest detection capability with high-resolution images for sizing.
- Ligament measurement with contact method applied directly on the weld fillet has excellent potential for ligament sizing and should be further developed. This is definitively suitable method to consider for characterizing defects and for the blade-to-roof joint (which was not in the scope of this study). It also has an excellent capability for inspection of Kaplan runners. The geometry of Kaplan runners is not compatible with angle beam inspection.

The subsequent paragraphs provide a summary of the long-term perspectives:

- The significant aspect is the sizing accuracy to minimize the error during weld assessment for fitness for service purposes. Usually, PAUT tends to oversize, which could be overcome by using TFM to improve sizing. Demonstrating how TFM has better sizing accuracy is key for implementing TFM on Hydraulic turbine runners.
- Future work should include a round-robin test on one or more sets of samples, comparing the TFM, PWI, and contact phased array reported sizes with destructive tests & CT X-rays will then provide a better understanding of the limitations of array techniques to provide accurate flaw size estimates.
- Future work should use a Model Assisted Probability of Detection (MAPOD) to estimate the POD of certain ultrasonic techniques applied to hydroelectric turbine

runners' inspection based on real flaws found in the real turbine by CIVA Simulation software. Data could then be processed with Status 5 software to better estimate the POD curves.

- Compare TFM with PWI for increasing the data acquisition speed. TFM is a slow acquisition process, which limits its application on a real turbine runner. Using PWI as the data acquisition instead of FMC as the acquisition technique could greatly increase data acquisition speed, the sensitivity and improves SNR because of how the wavefront is formed (it is at least twice the amplitude of particle displacement). A comparison between PWI and TFM should be considered to improve inspection proficiency.

APPENDIX I

EVALUATION OF THE DEAD ZONES IN THE WELDED JOINTS OF HYDRAULIC TURBINE RUNNERS

M. E. Bajgholi [a], M. Viens [b], G. Rousseau [c], H. Habibzadeh [d]

[a,b] Department of Mechanical Engineering, École de Technologie Supérieure,
1100 Notre-Dame West, Montreal, Quebec, Canada H3C 1K3
[c] Hydro-Québec's Research Institute, Varennes, Québec, Canada J3X 1S1
[d] Zetec Canada, Quebec, Canada G1N 2C9

Paper published in *NDT in Canada Conference*, June 2019

Abstract

Because of the presence of welding discontinuities and highly stressed area, the most critical parts of turbines are runner joints. NDT methods are crucial to investigate precisely the integrity of these zones. In order to evaluate the usefulness of phased array ultrasonic techniques in such cases, CIVA simulation software has been used. A 5 MHz, 64-elements transducer, a refracting wedge and a martensitic stainless steel (UNS S41500) T-joint sample have been modelled in this framework. By studying the simulation results, it was found that, due to some constraints imposed by the runner geometry and inspection limitations, there are dead zones where the welded joint is not accessible to ultrasonic inspection. Although dead zones could be roughly estimated using simple ray tracing method (first and second half skip), a more accurate and realistic estimation is provided using beam computation which also takes mode conversion and beam divergence into account. Existence of dead zones is a challenging issue for those involved in the assessment of the integrity of a welded joint; especially when these dead zones are in highly stressed areas. To circumvent this issue, complementary NDT methods will be proposed.

Keywords: Dead zones, Non-destructive testing, Ultrasonic testing, Phased-array ultrasonic testing, Welding defects

APPENDIX II

PERFORMANCE OF ULTRASONIC INSPECTION ON HYDROELECTRIC TURBINE RUNNER

M. E. Bajgholi [a], G. Rousseau [b], M. Viens [c], D.Thibault [d]

[a, c] Department of Mechanical Engineering, École de Technologie Supérieure, 1100 Notre-Dame West, Montreal, Quebec, Canada H3C 1K3
[b, d] Hydro-Québec's Research Institute, Varennes, Québec, Canada J3X 1S1

Paper published in *3rd International Symposium on Structural Health Monitoring and Non-destructive Testing (SHM-NDT 2020)*, November 2020

Abstract

This paper gives the results of a project aimed at evaluating the performance of ultrasonic techniques for detecting flaws in Francis turbine runners. This work is the first phase of a more ambitious program aimed at improving the inspection of critical areas of turbine runners. Francis runners may be utilized to supply power during peak periods which means that they experience additional load stress associated with start and stop sequences. Inspection during manufacturing is then of paramount importance to remove as much as feasible all flaw initiation sites before the heat treatment. This phase one objective is to collect initial data on a simplified mock-up and to compare experimental ultrasonic data with results provided by CIVA, a computer simulation package. The area of interest is the region with the highest stress between the blade and the web. A welded T-joint coupon made of UNS S41500 was manufactured to reproduce this high stress area. During the FCAW welding process, ceramic beads were embedded in the weld to create discontinuities whose size is in the critical range to initiate a crack. Inspection of the material was carried out by various Non-Destructive Testing methods namely conventional pulse echo, phased array, total focusing method (TFM), and other ultrasonic methods. With these results, probability of detection was computed in order to compare the effectiveness of each method.

Keywords: Defect detection, Non-Destructive Evaluation (NDE), Ultrasonic Testing, Total Focusing Methods (TFM), hydroelectric turbine runner

APPENDIX III

TOTAL FOCUSING METHOD USED FOR FLAW SIZING IN PROBABILITY OF DETECTION DETERMINATION

E. Ginzel [a], M. Bajgholi [b], M. Guimarães [c], F. Foucher [d],
G. Rousseau [e], M.Viens [f]

[a] Materials Research Institute, Waterloo, Ontario, Canada N2J 4G8
[b, f] Department of Mechanical Engineering, École de Technologie Supérieure,
1100 Notre-Dame West, Montreal, Quebec, Canada H3C 1K3
[c] Federal University of Rio de Janeiro, Brazil
[d] Extende S.A, Massy, France
[e] Hydro-Québec's Research Institute, Varennes, Québec, Canada J3X 1S1

Paper published in *e-Journal of Non-destructive Testing*, July 2022

Abstract

Probability of Detection (POD) is used as an indicator of an inspection procedure's reliability to detect flaws of concern. In non-destructive testing (NDT), POD is usually described using a cumulative distribution function that plots the random size variable on the horizontal axis against the probability or likelihood that a flaw of a given size will be detected. Standards describing the use of POD assume that the flaw size is known and no provision is made for sizing error. Test coupons made for inspection-procedure qualification using naturally occurring flaws (e.g., varying welding parameters to induce flaws) generally make unpredictably sized flaws; however, even intentionally fabricated flaws are often not the size and location that the manufacturer intended or documented them to be. This is particularly problematic for subsurface flaws that cannot be verified visually. NDT methods can be used to verify flaw sizes; however, this seems to be something of a conflict of interest when qualifying an inspection procedure by using another inspection method; e.g., verifying an ultrasonic weld inspection procedure by locating and sizing the same flaws with radiography. Such an approach seems to suggest that the verifying method (e.g., radiography) is trusted more than the method being qualified (e.g., ultrasound). When the purpose of the qualification is to establish reliability by POD, the apparent conflict can be lessened if the secondary NDT

method is used solely for sizing. Since POD is highly dependent on accurately identifying a flaw size, there must be confidence in the sizing method. This paper considers the use of Total Focussing Method (TFM) as a tool to provide accurate flaw sizing for POD determinations.

Keywords: NDT, POD, TFM, sizing, reliability, flaws

APPENDIX IV

INSPECTION OF WELD JOINTS OF FRANCIS TURBINE RUNNER BY ADVANCED ULTRASONIC TESTING METHODS BASED ON ASSESSMENT OF FITNESS-FOR-SERVICE

M. E. Bajgholi [a], G. Rousseau [b], M.Viens [c], D, Thibault [d]

[a, c] Department of Mechanical Engineering, École de Technologie Supérieure,
1100 Notre-Dame West, Montreal, Quebec, Canada H3C 1K3
[b,d] Hydro-Québec's Research Institute, Varennes, Québec, Canada J3X 1S1

Technical report published in *Institute de recherche d'Hydro-Québec (IREQ)*, May 2022

Abstract

This paper presents an ultrasonic inspection methodology to improve the fitness-for-service assessment of hydraulic turbine runners after manufacturing or during the in-service inspection. The improvement proposed here is to apply ultrasonic array inspection techniques with an emphasis on the Total focusing method (TFM), to produce data compatible with fitness-for-service methodologies. Conventional ultrasonic inspection methods based on good workmanship are mandatory for manufacturing, and in-service inspections are generally limited to surface methods such as penetrant or magnetic testing. Our previous work found serious limitations with conventional ultrasonic testing (UT) applied to the high-stress area located in the welded joint between the blade and the band. Undetected flaws will likely remain in a weld after fabrication, which can reduce the component's service life. Our work is centered on a real turbine runner using various ultrasonic array configurations to characterize detected flaws left after fabrication. According to an experimental evaluation of a Francis turbine runner, our results suggest that a dedicated TFM transducer with passive axis focusing and encoded inspection results in a higher detection rate, more accurate flaw definition, and more accurate sizing for the fitness-for-service assessment of hydraulic turbine runners.

LIST OF REFERENCE

Advanced PAUT Probes for TOPAZ64, Application Solution (2020), Zetec company, https://e2im0n5mz6-flywheel.netdna-ssl.com/wp-content/uploads/2020/03/.pdf.

Association, C. S. (2015). CSA W59-13 Welded Steel Construction (metal Arc Welding). Canadian Standards Association.

ASTM E3023, 15. (2015). Standard Practice for Probability of Detection Analysis for â Versus a Data. ASTM International, West Conshohocken, Pennsylvania.

ASTM E2373, 15. (2015). Standard terminology for non-destructive examinations. West Conshohocken, PA ASTM International.

ASTM E2862, 18. (2018). Standard practice for the probability of detection analysis for hit/miss data, West Conshohocken, Pennsylvania.

ASTM E1316-07. (2007). Standard terminology for nondestructive examinations. West Conshohocken, PA ASTM International.

ASTM E2700-14. (2014). ASTM Standard Practice for Contact Ultrasonic Testing of Welds Using Phased Arrays; ASTM International: West Conshohocken, PA, USA.

Ahmad, A., & Bond, L. J. (2018). Fundamentals of ultrasonic inspection. ASM Int, 17, 155-168. https://doi.org/10.31399/asm.hb.v17.a0006470

Al-Ataby, A., Al-Nuaimy, W., & Zahran, O. (2010). Towards automatic flaw sizing using ultrasonic time-of-flight diffraction. Insight: Non-Destructive Testing and Condition Monitoring, 52(7), 366–371. https://doi.org/10.1784/insi.2010.52.7.366.

Annis, C. (2009). Nondestructive evaluation system reliability assessment, MIL-HDBK-1823A. U.S. Department of Defense.

Annis, C. (2018), Statistical best-practices for building Probability of Detection (POD) models (Version 5.4.5). https://StatisticalEngineering.com/mh1823/.

Annis, C., Gandossi, L., & Martin, O. (2013). Optimal sample size for probability of detection curves. Nuclear Engineering and Design, 262, 98–105. https://doi.org/10.1016/j.nucengdes.2013.03.059.

ASME BPVC-V (2021). SEC V, Article 4, Article 4, Mandatory Appendix V, phased array e-scan and s-scan linear scanning examination techniques, The American Society of Mechanical Engineers, New York, USA.

ASME BPVC-V (2021). SEC V, Article 4, Mandatory Appendix XI Full Matrix Capture (FMC) and Nonmandatory Appendix F Examination of Welds Using Full Matrix Capture (FMC). The American Society of Mechanical Engineers, New York, USA.

ASME BPVC-V (2021). SEC V, Article 14, The American Society of Mechanical Engineers, New York, USA.

Bajgholi, M., Rousseau, G., Viens, M., & Thibault, D. (2021). Capability of advanced ultrasonic inspection technologies for hydraulic turbine runners. Applied Sciences, 11(10), 4681. http://dx.doi.org/10.3390/app11104681

Bajgholi, M., Rousseau, G., Viens, M., & Thibault, D. (2020). Performance of Ultrasonic Inspection Methods on Hydroelectric Turbine Runner. 3rd International Symposium on Structural Health Monitoring and Non-destructive Testing (SHM-NDT 2020), Quebec, Canada & E-Journal of Nondestructive Testing (NDT) vol. 25, no. 12 https://www.ndt.net/search/docs.php3?id=25561

Bajgholi, M. (2019). Evaluation of the dead zones in the welded joints of hydraulic turbine runners, NDT in Canada Conference, Edmonton, Canada. E-Journal of Nondestructive Testing(NDT)vol.24,no.10https://www.ndt.net/search/docs.php3?id=24715&file=article/ndt-canada2019/papers/Bajgholi_2019136-bajgholi-2019.pdf

Bannouf, S., Lonné, S., Gibert, C., & de Roumilly, L. (2018). Feasibility study of the characterization of planar defects in a circular weld with TFM. https://www.ndt.net/search/docs.php3?id=22811

Berke, M., Koralewski, S., Roye, W., Le Ber, L., Kaps, U., & Berke, I. (2016). Practical Application of Total Focusing for Sizing of Imperfections in Welded Joints. In 19th world Conference. https://www.ndt.net/article/wcndt2016/papers/th3a2.pdf

Boukani Habibzadeh, H. (2018). Evaluation of the reliability of nondestructive ultrasonic inspection methods for the detection and the characterization of defects in hydroelectric turbine welded joints (Doctoral dissertation, École de technologie supérieure).

Boukani, H. H., Viens, M., Tahan, S. A., & Gagnon, M. (2014). On the performance of nondestructive testing methods in the hydroelectric turbine industry. In IOP Conference Series: Earth and Environmental Science (Vol. 22, No. 1, p. 012018). IOP Publishing. http://dx.doi.org/10.1088/1755-1315/22/1/012018

Boukani, H. H., Viens, M., Tahan, S. A., & Gagnon, M. (2018). Case study on the integrity and nondestructive inspection of flux-cored arc welded joints of Francis turbine runners. The International Journal of Advanced Manufacturing Technology, 98(5), 2201-2211. https://doi.org/10.1007/s00170-018-2139-y

Bray, D. E., & Stanley, R. K. (2018). Nondestructive evaluation: a tool in design, manufacturing and service. CRC press. https://doi.org/10.1201/9781315272993

British Standards Institution. (2021). British Standards BS ISO 23864: Non-destructive testing. Ultrasonic testing, use of automated total focusing technique (TFM) and related technologies.

British Standards Institution. (2021). British Standards BS ISO 23865: Non-destructive testing. Ultrasonic testing, General use of full matrix capture / total focusing technique (FMC / TFM) and related technologies.

British Standards Institution. (2018). British Standards BS ISO 17640: Non-destructive testing.Ultrasonic testing, Techniques, testing levels, and assessment.

British Standard BS 7910. (2019). Guide to methods for assessing the acceptability of flaws in metallic structures, BSI Group, 2019.

Calmon, P. (2013). Recommendations for the use and validation of NDT simulation. V, IIW Best Practice Document, IIW, 2313–2363.

Carignan, J. C., Despaux, M.-P., Lachance, F., & Rioux, P. (2019). Sensitivity Response of Total Focusing Method (TFM) for Weld Inspection Versus Other Techniques FMC / TFM Glossary. NDT in Canada Conference, Edmonton, Canada.

Carter, L., & Rogerson, A. (2013). Advances in Ultrasonic Flaw Characterization.

Caulder, A. (2018). Full matrix capture and total focusing method: The next evolution in ultrasonic testing. Mater. Eval, 76(5), 591-597. http://dx.doi.org/10.12737/article_5dcc0a6eb5e9e1.26070131

Chaplin, R. (2017). Industrial Ultrasonic Inspection: Levels 1 and 2. Friesen Press.

Chapuis, B., Calmon, P., & Jenson, F. (2018). Best practices for the use of simulation in POD curves estimation (pp. 978-3). Springer International Publishing, Cham. https://doi.org/10.1007/978-3-319-62659-8

Temple, J. A. G. (2001). Engineering applications of ultrasonic time-of-flight diffraction (No. 2). Research Studies PressLtd.

Chatillon, S., Robert, S., Brédif, P., Calmon, P., Daniel, G., & Cartier, F. (2015, March). Results of the 2014 UT modeling benchmark obtained with models implemented in CIVA: Solution of the FMC-TFM ultrasonic benchmark problem using CIVA. In AIP Conference Proceedings (Vol. 1650, No. 1, pp. 1847-1855). American Institute of Physics.https://doi.org/10.1063/1.4914810.

Cheeke, J. D. N. (2017). Fundamentals and applications of ultrasonic waves. CRC press. https://doi.org/10.1201/b12260

Cinquin, M., Lonné, S., Raillon, R., Darmon, M., Mahaut, S., & Le Ber, L. (2006). Results of the 2005 UT Modelling Benchmark Obtained with the CIVA Software Developed at the CEA. In AIP Conference Proceedings (Vol. 820, No. 1, pp. 1828-1835). American Institute of Physics. https://doi.org/10.1063/1.2184742

Jobst, M., & Connolly, G. D. (2010). Demonstration of the application of the total focusing method to the inspection of steel welds. In 10th European conference on non-destructive testing. https://www.ndt.net/search/docs.php3?id=9054

DNVGL-ST-F101 Submarine pipeline systems. (2017). http://www.dnvgl.com.

Davis, J. M. (1998). Advanced ultrasonic flaw sizing handbook. Art Room Corporation.

Deutsch, K., ROYE, W., RAST, H., & BENOIST, P. (2016). High resolution phased array imaging using the total focusing method. In Proceedings of the 19th World Conference on Non-Destructive Testing. Munich, Germany (Vol. 8).

Ditchburn, R. J., & Ibrahim, M. E. (2009). Ultrasonic phased arrays for the inspection of thick-section welds. defense science and technology organization victoria (australia) maritime platforms div.

Drinkwater, B. W., & Wilcox, P. D. (2006). Ultrasonic arrays for non-destructive evaluation: A review. NDT & e International, 39(7), 525-541. https://doi.org/10.1016/j.ndteint.2006.03.006

Ermolov, I. N. (1972). The reflection of ultrasonic waves from targets of simple geometry. Non-destructive testing, 5(2), 87-91. https://doi.org/10.1016/0029-1021(72)90100-4

Ewen, Carcreff, Rémi, Lallement, Alan, Caulder, Larbi, Hallal, Dominique, & Braconnier. (2017). Total Focusing Method (TFM) for Automated Pipeline Girth Weld Inspections. NDT in Canada 2017 Conference.

Felice, M. V., & Fan, Z. (2018). Sizing of flaws using ultrasonic bulk wave testing: A review. Ultrasonics, 88, 26–42. https://doi.org/10.1016/j.ultras.2018.03.003

Felice, M. v., Velichko, A., & Wilcox, P. D. (2014). Accurate depth measurement of small surface-breaking cracks using an ultrasonic array post-processing technique. NDT and E International, 68, 105–112. https://doi.org/10.1016/j.ndteint.2014.08.004

Foucher, F., Fernandez, R., Leberre, S., & Calmon, P. (2018). New tools in CIVA for Model Assisted Probability of Detection (MAPOD) to support NDE reliability studies. In NDE of Aerospace Materials & Structures 2018 (pp. 32-43).

Gagnon, M., Tahan, A., Bocher, P., & Thibault, D. (2013). A probabilistic model for the onset of High Cycle Fatigue (HCF) crack propagation: Application to hydroelectric turbine runner. International Journal of Fatigue , 47,300-307. https://doi.org/10.1016/J.IJFATIGUE.2012.09.011

Gagnon, M., Tahan, A., Bocher, P., & Thibault, D. (2014). Influence of load spectrum assumptions on the expected reliability of hydroelectric turbines: A case study. Structural Safety, 50, 1–8. https://doi.org/10.1016/j.strusafe.2014.03.008

Gagnon, M., Tahan, S. A., Bocher, P., & Thibault, D. (2012, November). The role of high cycle fatigue (HCF) onset in Francis runner reliability. In IOP conference series: earth and environmental science (Vol. 15, No. 2, p. 022005). IOP Publishing.https://doi.org/10.1088/1755-1315/15/2/022005

Georgiou, G. A. (2007). POD curves, their derivation, applications and limitations. Insight-Non-Destructive Testing and Condition Monitoring, 49(7), 409-414. http://dx.doi.org/10.1784/insi.2007.49.7.409

Ginzel, E. (2011). Fun With Civa. NDT.Net – The e-Journal of Nondestructive Testing, 12

Ginzel, E. (2013). Phased Array Ultrasonic Technology. Eclipse Scientific Products Incorporated. https://books.google.com.my/books?id=qRh_rgEACAAJ

Ginzel, E. A., & Johnson, D. (2008). Phased-Array Resolution Assessment Techniques. NDT.Net – The e-Journal of Nondestructive Testing, July.

Ginzel, E. A., Thomson, R., & Ginzel, R. K. (2011). A Qualification Process for Phased-Array UT using DNV RP-F118 Guidelines. NDT. net, 1-12.

Ginzel, E., Bajgholi, M., Guimarães, M. B. M., Foucher, F., Rousseau, G., & Viens, M. (2022). Total Focusing Method used for flaw sizing in probability of detection determination. NDT.Net – The e-Journal of Nondestructive Testing, July. https://www.ndt.net/search/docs.php3?id=27128

Ginzel, E., Volf, O., & Brown, B. (2015). Next Generation Technology for Pipeline AUT TFM/FMC. The e-Journal of Nondestructive Testing, 20(8), 1-12. https://www.ndt.net/article/ndtnet/2015/7_Ginzel.pdf

Harding, C. A., & Hugo, G. R. (2011). Guidelines for interpretation of published data on probability of detection for nondestructive testing. defense science and technology organization victoria (australia) maritime platforms div. https://apps.dtic.mil/sti/pdfs/ADA563805.pdf

Hollette, M., Voillaume, H., & Guerid, J. (2018). Crack detection around fastener holes with Total Focusing Method ultrasonic system. 12th European Conference on Non-Destructive Testing (ECNDT 2018), Gothenburg, June 11-15 (ECNDT 2018) http://www.ndt.net/?id=22735

Holloway, P., & Ginzel, E. (2021). TFM[i] TM Part 2: Improved Imaging with 3D Rendering. http://www.ndt.net/?id=26388

Holloway, P., & Ginzel, E. (2021). TFM[i] TM Part 1: Using Intermodal Analysis to Improve TFM Imaging. http://www.ndt.net/?id=26036

Holmes, C., Drinkwater, B. W., & Wilcox, P. D. (2005). Post-processing of the full matrix of ultrasonic transmit–receive array data for non-destructive evaluation. NDT & e International, 38(8), 701-711.https://doi.org/10.1016/j.ndteint.2005.04.002

Holmes, C., Drinkwater, B. W., & Wilcox, P. D. (2008). Advanced post-processing for scanned ultrasonic arrays: Application to defect detection and classification in non-destructive evaluation. Ultrasonics, 48(6-7), 636-642. https://doi.org/10.1016/j.ultras.2008.07.019

Holmes, C., Drinkwater, B., & Wilcox, P. (2004). The post-processing of ultrasonic array data using the total focusing method. Insight-Non-Destructive Testing and Condition Monitoring, 46(11), 677-680.https://doi.org/10.1784/insi.46.11.677.52285

Huth, H. J. (2005). « Fatigue design of hydraulic turbine runners ». Norwegian University of Science and Technology. http://hdl.handle.net/11250/241313

Huertas-Hernando, D., Farahmand, H., Holttinen, H., Kiviluoma, J., Rinne, E., Söder, L., ... & Menemenlis, N. (2019). Hydropower Flexibility for Power Systems with Variable Renewable Energy Sources: An IEA Task 25 Collaboration. Advances in Energy Systems: The Large-scale Renewable Energy Integration Challenge, 385-405. https://doi.org/10.1002/9781119508311.ch23

Iakovleva, E., Chatillon, S., Bredif, P., & Mahaut, S. (2014). Multi-mode TFM imaging with artifacts filtering using CIVA UT forwards models. In AIP conference proceedings (Vol. 1581, No. 1, pp. 72-79). American Institute of Physics. https://doi.org/10.1063/1.4864804

Ida, N., & Meyendorf, N. (Eds.). (2019). Handbook of advanced nondestructive evaluation (pp. 235-251). Cham, Switzerland: Springer International Publishing. https://doi.org/10.1007/978-3-319-26553-7

ISO 19675. (2003). Ultrasonic Testing, Specification for a Calibration Block for Phased Array Testing (PAUT); International Organization for Standardization: Geneva, Switzerland.

Industrial Radiography Image forming techniques GE Inspection Technologies. (2006). www.geinspectiontechnologies.com/en. www.geinspectiontechnologies.com/en

Kastner, J., Heinzl, C., Plank, B., Salaberger, D., Gusenbauer, C., & Senck, S. (2017). New X-ray computed tomography methods for research and industry. In 7th Conference on Industrial Computed Tomography (iCT2017).http://www.ndt.net/?id=20884

Katchadjian, P. (2004). Practical applications of ultrasonic testing in nuclear and conventional industry. Insight-Non-Destructive Testing and Condition Monitoring, 46(12), 754-757. https://doi.org/10.1784/insi.46.12.754.54494

Kurz, J. H., Jüngert, A., Dugan, S., Dobmann, G., & Boller, C. (2013). Reliability considerations of NDT by probability of detection (POD) determination using ultrasound phased array. Engineering failure analysis, 35, 609-617.https://doi.org/10.1016/j.engfailanal.2013.06.008

Mahaut, S., Darmon, M., Chatillon, S., Jenson, F., & Calmon, P. (2009). Recent advances and current trends of ultrasonic modelling in CIVA. Insight-Non-Destructive Testing and Condition Monitoring, 51(2), 78-81. https://doi.org/10.1784/insi.2009.51.2.78

Malik, M. S. (2016). Model assisted POD of laser-ultrasonics NDT for train axles: A review. In 2016 International Conference on Electrical, Electronics, and Optimization Techniques (ICEEOT) (pp. 4645-4648). IEEE. https://doi.org/10.1109/ICEEOT.2016.7755600

Manjula, K., Vijayarekha, K., Venkatraman, B., & Karthik, D. (2012). Ultrasonic time of flight diffraction technique for weld defects: A review. Research Journal of Applied Sciences, Engineering and Technology, 4(24), 5525-5533.

Morin, O., Thibault, D., & Gagnon, M. (2021). On the Comparison of Hydroelectric Runner Fatigue Failure Risk Based on Site Measurements. In IOP Conference Series: Earth and Environmental Science (Vol. 774, No. 1, p. 012126). IOP Publishing. https://doi.org/10.1088/1755-1315/774/1/012126

Michael D. C. Moles. Olympus, N. D. T. (2010). Phased array testing: Basic theory for industrial applications. Olympus NDT, 2, 1.

Paoliello, F. A. (2005). Guidelines for integrity evaluation and remaining life assessment of recovery boilers–CENIBRA's experience. Tappi journal, 4(2), 17-22.

Peng, C., Bai, L., Zhang, J., & Drinkwater, B. W. (2018). The sizing of small surface-breaking fatigue cracks using ultrasonic arrays. NDT & E International, 99, 64-71. https://doi.org/10.1016/j.ndteint.2018.06.005

Principles of Full Matrix Capture (FMC) and Total Focusing Method (TFM) in Ultrasonic Inspections. (2017). Zetec company, Quebec City, Canada. Available online: https://www.slideshare.net/ZetecNDT/principles-of-full-matrix-capture-fmc-and-total-focusing-method-tfm-in-ultrasonicinspections.

Rachev, R. K., Wilcox, P. D., Velichko, A., McAughey, K., & Giese, J. (2018). Ultrasonic immersion testing for crack detection and depth sizing in large diameter pipes. In Proc. ECNDT (pp. 1-8). https://www.ndt.net/search/docs.php3?id=22708

Reverdy, F., Benoist, G., & Le Ber, L. (2016). Advantages and complementarity of phased-array technology and total focusing method. In 19th World Conference on Non-Destructive Testing, Munich. https://www.ndt.net/article/wcndt2016/papers/th3a4.pdf

Reverdy, F., Le Ber, L., Roy, O., & Benoist, G. (2018). Real-time Total Focusing Method on a portable unit, applications to hydrogen damage and other industrial cases. In 12th European Conference on Non-Destructive Testing (ECNDT 2018), Gothenburg, Sweden. https://www.ndt.net/search/docs.php3?id=22773

Richard, Daniel, Federico Zottig, and G. M. (2018). Richard. D; Zottig.F; Maes.G; "On the Use of Advanced Focusing Techniques for Enhanced PAUT Inspection Capability" 12th European Conference on Non-Destructive Testing, Gothenburg. https://www.ndt.net/search/docs.php3?id=22764

Rioux, P., Lachance, F., & Turcotte, J. (2018). Novel Imaging Techniques for Defects Characterisation in Phased Array Inspection. 1–10. https://www.ndt.net/search/docs.php3?id=23194

Safizadeh, M. S., Forsyth, D. S., & Fahr, A. (2004). The effect of flaw size distribution on the estimation of POD. Insight-Non-Destructive Testing and Condition Monitoring, 46(6), 355-359. https://doi.org/10.1784/INSI.46.6.355.55657

Shull, P. J. (2002). Nondestructive evaluation: theory, techniques, and applications. CRC press.

Spencer, R., Sunderman, R., & Todorov, E. (2018). FMC/TFM experimental comparisons. In AIP Conference Proceedings (Vol. 1949, No. 1, p. 020015). AIP Publishing LLC. https://doi.org/10.1063/1.5031512

Sy, K., Brédif, P., Iakovleva, E., Roy, O., & Lesselier, D. (2018). Development of methods for the analysis of multi-mode TFM images. In Journal of Physics: Conference Series (Vol. 1017, No. 1, p. 012005). IOP Publishing.https://doi.org/10.1088/1742-6596/1017/1/012005.

SÖDERSTRAND, H., MARTIN, O., & GANDOSSI, L. ENIQ Recommended Practice 5-Guidelines for the Design of Test Pieces and Conduct of Test Piece Trials-Issue 2. https://doi.org/10.2790/33727

Temple, J. A. G. (2001). Engineering applications of ultrasonic time-of-flight diffraction (No. 2). Research Studies Press Ltd.

Thibault, D., Gagnon, M., & Godin, S. (2015). The effect of materials properties on the reliability of hydraulic turbine runners. International Journal of Fluid Machinery and Systems, 8(4), 254-263.https://doi.org/10.5293/IJFMS.2015.8.4.254

Tremblay, P., Richard, D., & Ann, H. (2012). Development and validation of a full matrix capture solution. En 2012 KSNT Workshop (pp. 85-94). https://www.ndt.net/article/jrc-nde2012/papers/79.pdf

Volf, O. (2020). Crack Growth Monitoring with Phased-array Total Focusing Method (TFM). EWI, Columbus, OH USA, The e-Journal of Non-destructive Testing - ISSN 1435-4934. https://www.ndt.net/search/docs.php3?id=25542

Wedge, S., Carter, L., Rogerson, A., NDT, A., Zhang, U. K. J., & Drinkwater, B. (2013, October). Defect detection and sizing trials using the total focusing method and scattering coefficient matrix with a linear phased array. In 10th International Conference on NDE in Relation to Structural Integrity for Nuclear and Pressurized Components (pp. 1-3). https://www.ndt.net/search/docs.php3?id=18530

Xiao, K., Shi, Y. K., Ma, Q. Z., Zhang, J., & Li, X. H. (2013). The intelligent ultrasonic system for quality testing of weld connections in turbine runners. In Advanced Materials Research (Vol. 774, pp. 1543-1546). Trans Tech Publications Ltd. https://doi.org/10.4028/www.scientific.net/AMR.774-776.1543

Zhang, J., Drinkwater, B. W., & Wilcox, P. D. (2013). Comparison of ultrasonic array imaging algorithms for nondestructive evaluation. IEEE transactions on ultrasonics, ferroelectrics, and frequency control, 60(8), 1732-1745. https://doi.org/10.1109/tuffc.2013.2754

Zhang, J., Li, X. H., Shi, Y. K., & Liang, L. S. (2014). Phased array ultrasonic inspection of embedded defects in hydropower turbine runner welds. Insight-Non-Destructive Testing and Condition Monitoring, 56(7), 390-394. https://doi.org/10.1784/insi.2014.56.7.390

Zhang, X., Zhang, Y., Tian, B., An, J., Zhao, Z., Volinsky, A. A., ... & Song, K. (2019). Arc erosion behavior of the Al2O3-Cu/(W, Cr) electrical contacts. Composites Part B: Engineering, 160, 110-118. https://doi.org/10.1016/j.compositesb.2018.10.040

Yicheng, Z., Xiaohong, L., Jun, Z., & Hui, D. (2011). Model based reliability analysis of PA ultrasonic testing for weld of hydro turbine runner. Procedia Engineering, 16, 832-839. https://doi.org/10.1016/j.proeng.2011.08.1162

Zolfaghari, A., & Kolahan, F. (2017). Reliability and sensitivity of visible liquid penetrant NDT for inspection of welded components. Materials Testing, 59(3), 290-294. https://doi.org/10.3139/120.111000